9-23-2020 2:00 PM

The effect of free-stream turbulence on turbulent boundary layers and convective heat transfer from flat plates

Ivian Carolina Alfaia de Magalhaes, *The University of Western Ontario*

Supervisor: Savory, Eric, *The University of Western Ontario*

A thesis submitted in partial fulfillment of the requirements for the Master of Engineering Science degree in Mechanical and Materials Engineering

Abstract

The present work investigates the effect of free-stream turbulence (FST) on turbulent boundary layers and forced convective heat transfer from flat plates. High resolution, 2-D and 3-D, steady Reynolds-Averaged Navier-Stokes (RANS) simulations using Computational Fluid Dynamics (CFD) techniques were performed to analyze the influence of different free-stream conditions, such as turbulence intensity (*TI*), integral length scale (L_u) and free-stream velocity (U_o) on local and total skin friction and convective heat transfer coefficients (CHTC), as well as on turbulent boundary layer parameters (boundary layer thickness and momentum thickness). The present study shows that the Shear Stress Transport (SST) k-ω model with the low Reynolds number (*Re*) approach is the most suitable model for representing incident turbulent flow over isothermal flat plates, since it provides the correct skin friction and Nusselt number for turbulent boundary layers, along with the appropriate streamwise TI decay through the numerical domain. Using the results, a set of non-dimensional correlations for local and total skin friction, momentum thickness, local and total CHTC were developed. These are simple and useful tools for the prediction of skin friction and forced convective heat transfer from flat plates under FST, which can be helpful for many engineering applications such as photovoltaic systems.

Keywords

Turbulent boundary layers, Convective heat transfer, Reynolds-Averaged Navier-Stokes (RANS), Computational Fluid Dynamics (CFD), Free-stream turbulence, Flat plates

Summary for Lay Audience

Various engineering applications involve interactions between a fluid and a solid surface with heat exchange. When a fluid flows over a solid surface, a thin layer of fluid in contact with this surface develops, which is called a boundary layer. The motion between the fluid and the surface involves friction (or resistance) to the movement as well as heat exchange (known as convection). For instance, when wind blows over a photovoltaic solar panel, the former takes heat from the latter which influences the panel's electrical efficiency. The strength of resistance to motion (friction) and heat loss is numerically represented by skin friction and convective heat transfer coefficients (CHTC), respectively. Additionally, the air flow generally is chaotic and irregular with fluctuating velocities. Such complex flow is defined as turbulent and can be characterized by the level of velocity fluctuations (turbulence intensity) and the average size of the turbulent eddies (length scale). The present study applies computational methods known as Computational Fluid Dynamics (CFD) to evaluate the influence of different air flow parameters (velocity, turbulence intensity and length scale) on the skin friction and CHTC of flat plates. Furthermore, this work provides new equations for the estimation of skin friction and CHTC for a given set of air flow parameters, which is useful for the design of many engineering devices, such as photovoltaic panel systems.

Co-Authorship Statement

This thesis was organized in an integrated article format, in which two chapters are co-authored articles by Ivian Magalhaes and Eric Savory. In those articles, Ivian Magalhaes was responsible for designing and executing the numerical simulations, as well as analyzing data, comparing the results with the literature and the writing of the manuscripts. Eric Savory provided guidance and recommendations to all these stages and manuscript reviewing.

Chapter 2 presents the investigation of the effect of free-stream turbulence on flat plate turbulent boundary layers and is intended to be submitted to the Journal of Fluids Engineering.

Chapter 3 discusses the effect of free-stream turbulence on convective heat transfer from flat plates and is aimed to be submitted to the Journal of Heat Transfer.

Acknowledgments

Firstly, I would like to express my sincere gratitude to my supervisor, Dr. Eric Savory, for his support and guidance throughout the duration of my M.E.Sc. program.

I would also like to acknowledge the support and assistance I received from the members of the Advanced Fluid Mechanics (AFM) group at Western University.

I am also grateful for the financial support I received from the department of Mechanical and Materials Engineering at Western University. I would like to acknowledge the Shared Hierarchical Academic Research Computing Network (SHARCNET) and Compute/Calcul Canada for their facilities.

Finally, I would like to thank my husband for his support, love and patience and my family and friends for their continued encouragement.

Table of Contents

List of Tables

List of Figures

List of Abbreviations, Symbols and Nomenclature

Latin Symbols

A	Coefficient used in Simonich and Bradshaw's (1978) correlation
A_1, A_2	Decay coefficients used in Sarkar's (2018) expressions
a_1, c_1	Constants used in the SST-k-ω model to compute the turbulent viscosity
B_1, B_2, B_3, B_4	Coefficient and exponents used in total skin friction correlation
b_1, b_2, b_3, b_4	Coefficient and exponents used in local skin friction correlation
C_1, C_2, C_3, C_4	Coefficient and exponents used in total Nusselt and Stanton correlations
c_1, c_2, c_3, c_4	Coefficient and exponents used in local skin friction correlation
C_f	Total skin friction coefficient
$c_{f,l}$	Local skin friction coefficient for a laminar flow
$c_{f,t}$	Local skin friction coefficient for a turbulent flow
$c_{f,x}$	Local skin friction coefficient
$c_{f,xo}$	Initial local skin friction coefficient (no free-stream turbulence)
C_p	Specific heat capacity of air (J/kgK)
D_ω	Cross-diffusion term
F_1, F_2	Blending functions for the SST-k-ω turbulence model
G_1, G_2, G_3	Three-dimensional grids used in grid independence test
G_b	Generation of turbulent kinetic energy due to buoyancy

G_k	Generation of turbulent kinetic energy due to the mean velocity gradients
G_ω	Generation of ω
H	Shape factor
h	Local convective heat transfer coefficient (W/m^2K)
HB	Hancock-Bradshaw parameter
k	Turbulent kinetic energy (m^2/s^2)
k'	Non-dimensional TKE
k_{eff}	Effective thermal conductivity (W/mK)
k_l	Laminar kinetic energy (m^2/s^2)
k_m	Molecular thermal conductivity (W/mK)
k_P	Turbulent kinetic energy at centre point P of wall-adjacent wall (m^2/s^2)
k_{sgs}	Sub-grid scale kinetic energy (m^2/s^2)
k_t	Turbulent thermal conductivity (W/mK)
L	Plate length (m)
L_e^u	Turbulent dissipation scale (m)
L_u	Integral length scale at the plate leading edge (m)
L_{uo}	Integral length scale at the inlet (m)
L_{uref}	Integral length scale reference value (m)
L_{uTE}	Integral length scale at the plate trailing edge (m)
L_{ux}	Local integral length scale (m)

L_x, L_y, L_z	Dimensions of the computational domain in x, y and z directions
M_1, M_2, M_3	Two-dimensional grids used in grid independence test
n_1, n_2	Decay exponent in Sarkar's (2018) expressions
Nu	Nusselt number
Nu_L	Total Nusselt number
Nu_x	Local Nusselt number
p	Pressure (Pa)
Pr	Prandtl number
Pr_t	Turbulent Prandtl number
q_x	Local heat flux (W/m^2)
Re	Reynolds number
$Re_{\Delta 2}$	Reynolds number based on the enthalpy thickness
Re_θ	Momentum-thickness Reynolds number
Re_L	Reynolds number based on the plate length
Re_x	Local Reynolds number
S_k	User defined source term for turbulent kinetic energy
St	Stanton number
St_x	Local Stanton number
St_{xo}	Initial local Stanton number (no free-stream turbulence)
S_ω	User defined source term for turbulence specific dissipation rate

T	Temperature (K)
t	Time (s)
T_o	Free-stream temperature (K)
T_p	Plate temperature (K)
TI	Free-stream turbulence intensity at the plate leading edge
TI_{av}	Average of the plate leading and trailing edge turbulence intensity values
TI_{dif}	Percentage different between the free-stream turbulence intensity at the leading and trailing edge of the plate
TI_{LE}	Free-stream turbulence intensity at plate leading edge
TI_o	Free-stream turbulence intensity at the inlet
TI_{TE}	Free-stream turbulence intensity at plate trailing edge
TI_x	Local free-stream turbulence intensity
TLR	Correlating parameter in Ames and Moffat's (1990) expression
U	Mean velocity (m/s)
u^*	Boundary-layer friction velocity (m/s)
u', v', w'	Velocity fluctuations in x, y and z directions (m/s)
u_i	Velocity vector component along the i-th base coordinates
U_o	Free-stream velocity (m/s)
x	Distance along the streamwise direction from the plate leading edge (m)
x_j	Cartesian coordinate component along the j-th base vector

x_o	Distance along the streamwise direction from the inlet (m)
x_{vo}	Virtual origin (m)
Y_k	Dissipation of k due to turbulence
Y_ω	Dissipation of ω due to turbulence
y_p	Distance (normal) of centre point P of wall-adjacent cell to the wall (m)
y^+	Dimensional wall normal distance
z	Distance (normal) of a point to the plate (m)

Greek symbols

α^*	Coefficient for Low-Reynolds number correction for the SST-k-ω model
β	Volumetric thermal expansion of air (1/K)
β^*_∞	Turbulence model constant
Δ_2	Enthalpy thickness (m)
ΔT	Temperature difference (K)
Δx, Δy	Grid-cell size (m)
δ	Boundary layer thickness (m)
δ^*	Displacement thickness (m)
δ_l	Laminar boundary layer thickness (m)
δ_T	Thermal boundary layer thickness (m)
δ_t	Turbulent boundary layer thickness (m)
ε	Turbulent kinetic energy dissipation rate (m^2/s^3)

θ	Momentum thickness (m)
μ	Dynamic viscosity (Ns/m^2)
μ_t	Turbulent viscosity (Ns/m^2)
ρ	Density (kg/m^3)
ν	Kinematic viscosity (m^2/s)
σ_k	Turbulent Prandtl number of turbulent kinetic energy
σ_ε	Turbulent Prandtl number of turbulent dissipation rate
σ_ω	Turbulent Prandtl number of turbulent specific dissipation rate
τ_{ij}	Sub-grid scale stresses (N/m^2)
τ_ω	Wall shear stress (N/m^2)
ω	Specific dissipation rate of turbulent kinetic energy (s^{-1})

Abbreviations

BL	Boundary Layer
CFD	Computational Fluid Dynamics
CHTC	Convective heat transfer coefficient
COST	European Cooperation in Science and Technology
DNS	Direct Numerical Simulation
FST	Free-Stream Turbulence
LBL	Laminar Boundary Layer
LE	Leading Edge

LES	Large Eddy Simulation
LRNM	Low Reynolds Number Modelling
NIST	National Institute of Standards and Technology
RANS	Reynolds-Averaged Navier Stokes
SIMPLE	Semi-Implicit Method for Pressure-Linked Equations
SST	Shear Stress Transport
TBL	Turbulent Boundary Layer
TE	Trailing Edge
TKE	Turbulent Kinetic Energy

Chapter 1

1 Introduction

Numerous engineering applications involve incident turbulence on boundary layers, such as photovoltaic panel systems and turbomachines. Studies to analyze the effect of incident turbulence on heat transfer were conducted in different fields, such as blade surfaces of gas turbine combustors (Nix et al., 2007) and external convection coefficients for building surfaces and photovoltaic systems (Palyvos, 2008). The investigation of the effect of free-stream turbulence (FST) on boundary layers (BL) is essential for these systems because their performance highly depends on how they interact with free-stream flows. A schematic of the interaction between a photovoltaic solar panel system installed on a house roof and the free-stream is presented in Figure 1.1.

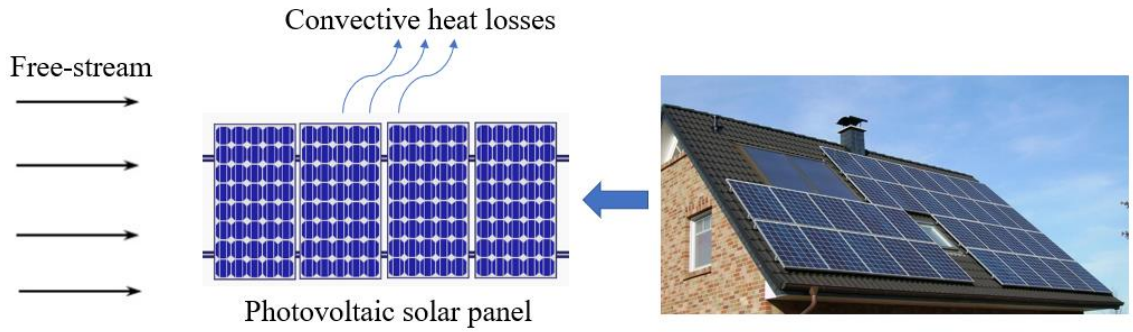

Figure 1.1 – Schematic of a photovoltaic solar panel (Adapted from Public Domain via Pixabay, 2016)

Many studies were conducted to analyze the effects of FST on various aspects such as laminar-turbulent transition, laminar and turbulent boundary layers parameters, convective heat transfer and skin friction (Simonich and Bradshaw, 1978; Blair, 1983; Maciejewski and Moffat, 1992; Péneau et al., 2004).

The geometries involved in many engineering applications can be complex, but studies of simpler cases, such as flat plates, are relevant since they have the advantage of developing thicker boundary layers (Kondjoyan et al., 2002), as well as having correlations already established for laminar and turbulent boundary layer integral parameters and mean velocity

profiles, which are extremely useful for the validation of computational models and comparisons with results obtained when free-stream conditions are modified. For that reason, the current study will focus on flat plate boundary layers.

1.1 Flat plate boundary layers

The flat plate boundary layer is a thin layer adjacent to a flat plate where the velocity is considerably lower than the free-stream (Schlichting, 1999). Due to the "no-slip" condition, the velocity inside the boundary layer grows from zero at the wall to 99% of the free-stream velocity (U_o) over a distance called the boundary layer thickness (δ), which increases with distance from the plate leading edge. Similarly, for a constant plate temperature (T_p), a thermal boundary layer develops on a flat plate when there is a difference between the plate temperature and the free-stream temperature (T_o). The thickness of a thermal boundary layer (δ_T) is given by the height at which $\frac{T-T_o}{T_p-T_o} = 0.99$, where T is the temperature at a given location. A diagram of a developing boundary layer on a plate of length L is shown in Figure 1.2.

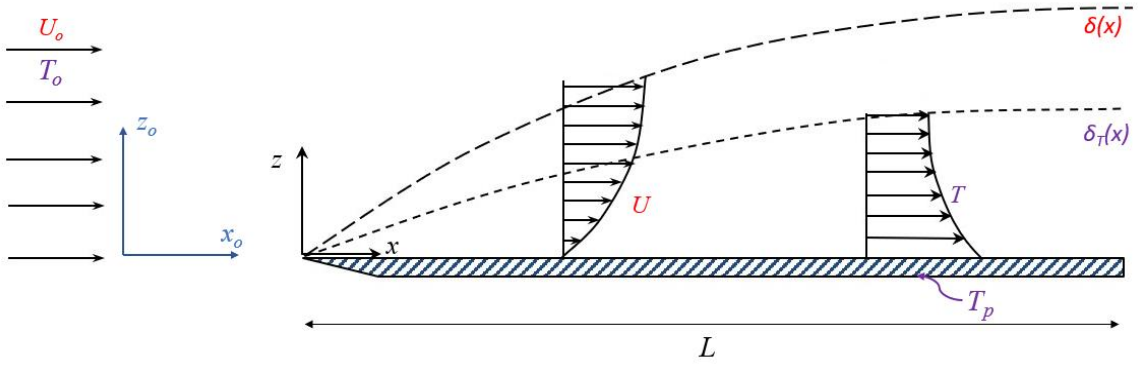

Figure 1.2 – Diagram of a flat plate velocity and thermal boundary layer

Two sets of coordinates are given, one with respect to the origin of the numerical domain or the test section inlet of an experimental study and the other with respect to the plate leading edge. The flow can be either laminar or turbulent and there is also a laminar-turbulent transition region. The flow regime is generally determined by the local Reynolds number (Re_x) expressed as follows:

$$Re_x = \frac{\rho U_o x}{\mu} \tag{1.1}$$

where ρ is the density of air, x is the streamwise distance from the plate leading edge and μ is the dynamic viscosity of air. The critical Reynolds number for a smooth flat plate subjected to a uniform free-stream with no turbulence is determined as the point where the laminar-turbulent transition process begins and is normally defined as 10^5 (White, 2016). This transition process can continue until $Re_x = 3\text{x}10^6$, but an engineering critical Reynolds number is generally defined as $5\text{x}10^5$, above which the flow is most likely to be turbulent (White, 2016). Experimentally, the flat plate transition range has been defined for Re_x from 10^5 to 10^6 (Dryden, 1936). Theoretically, the thicknesses of laminar (δ_l) and turbulent (δ_t) boundary layers are defined as follows:

$$\delta_l \cong \frac{5x}{(Re_x)^{1/2}} \tag{1.2}$$

$$\delta_t \cong \frac{0.16x}{(Re_x)^{1/7}} \tag{1.3}$$

These expressions assume a smooth, thin, infinitely wide and long, horizontal plate subjected to a uniform, incompressible incident flow with no turbulence (Schlichting, 1999). Furthermore, it is assumed that the mean velocity profile of the turbulent boundary layer can be expressed as a one-seventh power law (Nikuradse, 1950), given by: $\frac{U}{U_o} = \left(\frac{z}{\delta}\right)^{1/7}$, where U is the mean velocity in the streamwise direction. Another important parameter is the wall shear stress (τ_w), that can be expressed by:

$$\tau_w = \mu \left.\frac{\partial U}{\partial z}\right|_{z=0} \tag{1.4}$$

Then the local skin friction coefficient can be defined as:

$$c_{f,x} = \frac{\tau_{w,x}}{0.5\rho U_o^2} \tag{1.5}$$

Additionally, the local skin friction coefficients for laminar ($c_{f,l}$) and turbulent ($c_{f,t}$) flows are determined by Eq. (1.6) and Eq. (1.7) respectively (Çengel and Cimbala, 2010).

$$c_{f,l} = \frac{0.664}{Re_x{}^{1/2}} \tag{1.6}$$

$$c_{f,t} = \frac{0.027}{Re_x{}^{1/7}} \tag{1.7}$$

These expressions assume the same conditions mentioned for Eq. (1.2) and Eq. (1.3). Then the average (or total) skin friction over the entire length of the plate for a laminar and turbulent boundary layer can be calculated by the following equations:

$$C_f = \frac{1.328}{Re_L{}^{1/2}} \qquad \text{For laminar flow} \tag{1.8}$$

$$C_f = \frac{0.032}{Re_L{}^{1/7}} \qquad \text{For turbulent flow} \tag{1.9}$$

where Re_L is the Reynolds number based on the plate length in the streamwise direction ($Re_L = \frac{\rho U_o L}{\mu}$). These equations are obtained assuming that the flow is laminar or turbulent from the leading edge of the plate onwards. These expressions are useful for validation of the flow fields simulated using numerical models. The present study also includes heat transfer and, therefore, the useful equations for the analysis of heat transfer coefficients will be analyzed next.

1.2 Convective heat transfer from flat plates

Convection is the mechanism by which heat transfer occurs in the presence of bulk fluid motion. It is a combination of conduction through molecular interactions and energy transport by fluid motion. When this motion is driven by gravity or induced density gradients, the mechanism is called natural convection. When the fluid motion is sustained by external devices, such as pumps or fans, it is called forced convection (Incropera et al, 2007).

One important parameter to analyze the relative significance of natural convection with respect to forced convection is the Richardson number (*Ri*), defined as (Nicholl, 1970):

$$Ri = \frac{Gr}{Re_L{}^2} \tag{1.10}$$

where *Gr* is the Grashof number, given by Eq. (1.11) (Incropera et al., 2007):

$$Gr = \frac{g\beta(T_p - T_o)L^3}{\nu^2} \tag{1.11}$$

where β is the volumetric thermal expansion of air, that can be calculated by $\beta = 1/T_o$, and ν is the kinematic viscosity of air ($\nu = \mu/\rho$). Richardson number expresses the influence of natural convection with respect to forced convection, i.e., the relative influence of buoyancy forces with respect to flow inertia (Nicholl, 1970). When *Ri* is less than 0.1, also known as the 'critical value', natural convection is negligible. When *Ri* is between 0.1 to approximately 10, the heat transfer regime is mixed, because neither natural nor forced convection can be neglected. If *Ri* is greater than 10, natural convection is dominant and forced convection can be neglected. This analysis will then be included when the problem conditions for the heated plate are presented in Chapter 3.

Considering flow over flat plates, the local convective heat transfer coefficient (CHTC) can be determined by Newton's law of cooling:

$$h = \frac{q_x}{T_p - T_o} \tag{1.12}$$

where h is the local CHTC, q_x is the local heat flux from the plate surface, T_p is the plate temperature and T_o is the external flow temperature. The horizontal flat plate is a widely investigated geometry since it is simple and CHTC correlations are already known and, therefore, can be used for the validation of models. The dimensionless correlations for local CHTC of laminar and turbulent boundary layers are expressed by Eq. (1.13) and (1.14) (Incropera et al., 2007).

$$Nu_x = 0.332 {Re_x}^{1/2} Pr^{1/3} \quad \text{For laminar flow} \tag{1.13}$$

$$Nu_x = 0.0296 {Re_x}^{4/5} Pr^{1/3} \quad \text{For turbulent flow} \tag{1.14}$$

where Nu_x is the local Nusselt number and *Pr* is the Prandtl number, given by Eq. (1.15) and Eq. (1.16) respectively.

$$Nu_x = \frac{hx}{k_m} \tag{1.15}$$

$$Pr = \frac{\mu C_p}{k_m} \tag{1.16}$$

where k_m is the molecular thermal conductivity of air and C_p is the specific heat at constant pressure. These correlations are valid if the plate is kept at a constant temperature, there is no free-stream turbulence and fluid properties are constant. For laminar correlations, *Pr* can vary from 0.6 to 50, but for turbulent flows *Pr* must be approximately 1. Besides that, the mean velocity profile of the TBL follows the one-seventh power law. The total CHTC for laminar and turbulent flows can be expressed by Eq. (1.17) and (1.18).

$$Nu_L = 0.664 {Re_L}^{1/2} Pr^{1/3} \quad \text{For laminar flow} \tag{1.17}$$

$$Nu_L = 0.037 {Re_L}^{4/5} Pr^{1/3} \quad \text{For turbulent flow} \tag{1.18}$$

where Nu_L is the Nusselt number based on the plate length in the streamwise direction ($Nu_L = \frac{\bar{h}L}{k_m}$, where $\bar{h} = \frac{1}{L}\int_0^L h\, dx$). The assumptions of these expressions are that the flow is either laminar or turbulent from the leading edge of the plate onwards, as well as the conditions presented for Eq. (1.13) and Eq. (1.14).

In contrast, the external flow in engineering applications, as mentioned before, is usually turbulent. In consequence, various studies investigated the influence of free-stream turbulence on boundary layers, skin friction and heat transfer coefficients of plate plates. An overview of those different studies will be analyzed next.

1.3 Incident turbulence on flat plates

The free-stream turbulence (FST) is generally characterized by an average integral length scale of an eddy (L_u) and a turbulence intensity (*TI*) defined as:

$$TI = \frac{\sqrt{\frac{1}{3}\left(\overline{u'^2} + \overline{v'^2} + \overline{w'^2}\right)}}{U} \times 100 \tag{1.19}$$

where u', v', w' are the velocity fluctuations in the x, y and z directions respectively. They are obtained considering that the instantaneous velocity (u) is equal to an average velocity (U) plus a fluctuating term ($u = U + u'$).

The problem analyzed in the current study can then be represented by Figure 1.3.

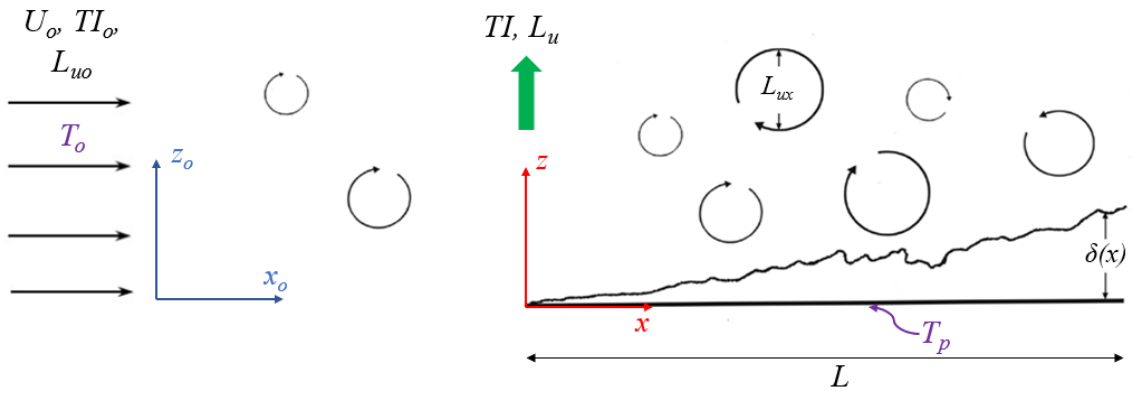

Figure 1.3 – Problem diagram with main variables

A uniform free-stream with constant velocity U_o, initial turbulence intensity TI_o, initial integral length scale L_{uo} and constant temperature T_o reaches a flat plate of length L and constant temperature T_p. The turbulence intensity and integral length scale at the leading edge of the plate are TI and L_u, respectively. Initially, the problem is analyzed without heat transfer in Chapter 2.

Considering the effects of free-stream turbulence on skin friction, experimental studies show an increase in skin friction coefficients with increasing free-stream turbulence intensity (Simonich and Bradshaw, 1978; Blair, 1983; Hoffmann and Mohammadi, 1991; Barret and Hollingsworth, 2003). Simonich and Bradshaw (1978) observed an increase of up to 20% when TI is increased from 0.1% to 7%, which is the same observation made by Blair (1983). Hoffmann and Mohammadi (1991) presented an enhancement of approximately 14% for TI of 5% while Barret and Hollingsworth (2003) reported an increase by up to 16% for TI of 8%. It should be noted that there is a quantitative discrepancy between the results from these studies, which is also observed for studies involving heat transfer.

As for the effects of FST on CHTC, experiments show even more contradictions. While earlier studies concluded that there was no significant effect of free-stream turbulence on CHTC (Kestin et al., 1961 and Junkhan and Sevory, 1967), most later studies agreed that the heat transfer coefficients are higher as the free-stream turbulence intensity increases (Simonich and Bradshaw, 1978; Blair, 1983; Maciejewski and Moffat, 1992; Péneau et al., 2004). Although the overall qualitative conclusion was the same, the quantitative effect of turbulence on CHTC varied greatly: Simonich and Bradshaw (1978) concluded that the CHTC could be up to 30% higher for *TI* of 7%; Blair (1983) experiments showed an increase of 18% for *TI* of 7%; Maciejewski and Moffat (1992) found up to a 300% increase of CHTC for *TI* levels of 55% and Péneau et al. (2004) reported an increase of 200% for *TI* of 10%. These differences could be due to a variety of factors, such as differences in turbulence generators (grid or jet turbulence), experimental conditions such as the distance of the plate from the inlet turbulence generator, integral length scale values and range of Reynolds number, among others.

In an effort to account for different free-stream conditions, various studies tried to develop a correlation between skin friction (or heat transfer) coefficient increase and those conditions (Simonich and Bradshaw, 1978; Hancock and Bradshaw, 1983; Blair, 1983; Ames and Moffat, 1990). Initially, Simonich and Bradshaw (1978) proposed that the $c_{f,x}$ and St_x increase would depend only on the local turbulence intensity (TI_x), then Hancock and Bradshaw (1983) included the ratio between local length scale (L_{ux}) and boundary layer thickness, Blair (1983) incorporated the momentum-thickness Reynolds number and Ames (1990) included the momentum thickness instead of boundary layer thickness. It is possible to affirm that there are still contradictions regarding the inclusion of different parameters in correlations for skin friction and convective heat transfer coefficients. Furthermore, most of the correlations derived from these studies depend on the knowledge of the boundary layer development, such as boundary layer or momentum thickness and, hence, it would be difficult to estimate skin friction or CHTC having only the free-stream conditions.

Another important aspect is that the studies mentioned above did not take into account the decay of free-stream turbulence in the plate region and only considered the turbulent intensity and length scales at the inlet or the local values of these parameters. Such inlet

conditions are not the ones to which the plate is subjected since turbulence intensity decays with distance from the turbulence generator (Pope, 2000), as represented below:

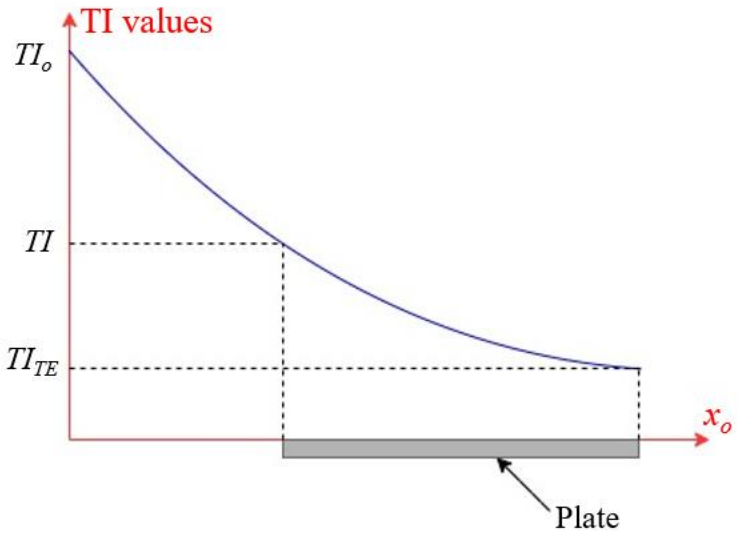

Figure 1.4 – Representation of the turbulence intensity decay in the streamwise distance

where TI_{TE} is the turbulence intensity at the plate trailing edge. Additionally, the integral length scale increases with distance from the turbulence generator, as represented in Figure 1.5.

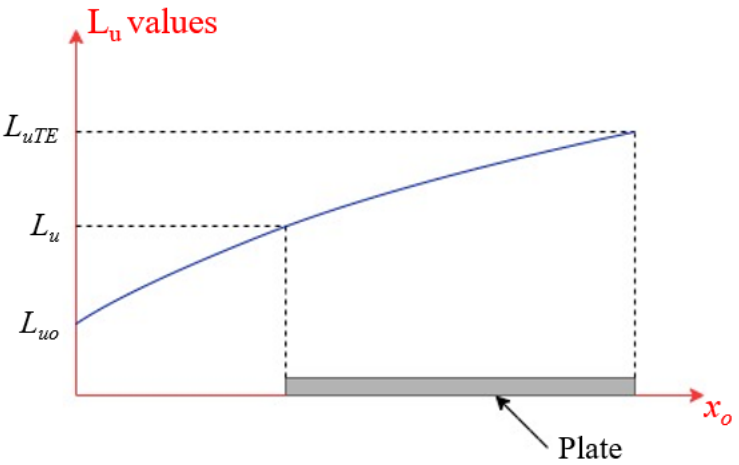

Figure 1.5 - Representation of the integral length scale growth in the streamwise distance

The current study will then consider the investigation made by Sarkar (2018) that quantified the streamwise decay of turbulent kinetic energy and identified a region of almost uniform turbulent conditions inside the domain. The percentage difference between the TI at the leading and trailing edge will then be an important factor, that can be calculated as $TI_{dif}(\%) = \frac{(TI - TI_{TE})}{(TI + TI_{TE})/2} x100$. Considering now this gap in the literature and the inconsistencies mentioned from previous studies, the objectives for the current research can be determined.

1.4 Objectives and scope

The main objective of this study is to evaluate the influence of difference free-stream conditions (*TI*, L_u and *Re*) on flat plate boundary layers, mainly the skin friction and convective heat transfer coefficients (local and total). In addition, the current work aims to develop a generalized dimensionless correlation for local and total skin friction and CHTC taking into account those different free-stream conditions and the free-stream turbulence intensity decay along the plate region.

This investigation will be conducted using a computational fluid dynamics (CFD) method and so another aim will be to identify the appropriate numerical setup and turbulence models that can accurately predict the TI decay, as well as the skin friction and convective heat transfer coefficients.

Finally, this research will help to shed light upon inconsistencies from previous studies that reached different conclusions regarding the quantitative effects of free-stream conditions and, thereby, consolidate the knowledge of the effect of free-stream turbulence on flat plate boundary layers, considering different parameters separately (*TI*, L_u and *Re*).

To attain these objectives, 3-D steady Reynolds-Averaged Navier-Stokes (RANS) simulations with an unheated plate and 2-D steady RANS with a heated plate were conducted to evaluate the influence of different free-stream conditions on boundary layers, skin friction and CHTC. The free-stream velocities were defined as 40m/s, 60m/s or 80m/s and the local Reynolds numbers were up to 1.0×10^7 while the Reynolds number based on the plate length varied from 5.1×10^6 to 1.0×10^7. The plate leading edge turbulence intensity

varied from 0.1% to 12.6% and the length scales were defined as 0.02m, 0.05m, 0.07m and 0.1m. The percentage difference of free-stream TI in the plate region was kept below 25%. The temperature difference between the plate and the free-stream was kept at 20K. The reasons for selecting all these parameter values are provided in Chapters 2 and 3.

Besides these base cases, the skin friction correlations derived from the 3-D RANS simulations were also compared with other 3-D steady RANS cases with the plate at regions of TI decay of up to 56%. For these cases, the free-stream velocity was defined as 40m/s, the range of Re_x was from $1.3\text{x}10^6$ to $7.7\text{x}10^6$ and Re_L varied from $5.1\text{x}10^6$ to $7.7\text{x}10^6$. The TI values were specified from 2.0% to 21.6% and the length scale was kept as 0.1m.

The flow fields were validated with the correlations presented for a horizontal flat plate subjected to a uniform flow with no turbulence. Then, a systematic analysis was presented varying one of the free-stream conditions while keeping the other conditions constant. Finally, dimensionless correlations for skin friction or CHTC were established incorporating the different free-stream conditions, and later validated with experimental data from previous studies.

1.5 Thesis layout

Chapter 1 presented the general background regarding flat plate boundary layers, convective heat transfer and incident turbulence on flat plates, along with an overview of the importance of the current work, main objectives and scope. The effect of incident turbulence on turbulent boundary layers is discussed in Chapter 2, beginning with a detailed review of the literature followed by an analysis of the influence of different free-stream parameters (TI, L_u and U_o) on skin friction and integral boundary layer parameters (boundary layer thickness and momentum thickness). These parameters are incorporated into correlations for local and total skin friction coefficients as well as momentum thickness that are validated with data from previous studies.

In Chapter 3, the literature concerning turbulence effects on convective heat transfer from flat plates is reviewed first and then the influence of free-stream parameters (TI, L_u and U_o)

on CHTC from flat plates is examined separately and then included into dimensionless correlation for local and average CHTC.

Finally, the main conclusions of the present work and recommendations for future work are presented in Chapter 4.

1.6 Summary

This chapter introduced the problem investigated in the current study, including the fundamentals of flat plate boundary layers and convective heat transfer from flat plates. Additionally, the importance of the current work and objectives were presented, along with the contradictions from results of previous studies and the gaps in the literature. The current investigation will help to shed light upon these inconsistencies and deepen the knowledge of the effect of free-stream turbulence on local and average skin friction and convective heat transfer coefficients.

The next chapter presents the investigation of the influence of different free-stream parameters (TI, L_u and U_o) on skin friction and integral boundary layer parameters (boundary layer thickness and momentum thickness).

References

Ames, F. E. and Moffat, R. J. (1990) Heat transfer with high intensity, large scale turbulence: the flat plate turbulent boundary layer and the cylindrical stagnation point, Report No. HMT-44, Department of Mechanical Engineering, Stanford University, CA, USA.

Barrett, M. J. and Hollingsworth, D. K. (2003) Heat transfer in turbulent boundary layers subjected to free-stream turbulence - Part I: Experimental results. Journal of Turbomachinery, 125(2), pp. 232–241.

Barrett, M. J. and Hollingsworth, D. K. (2003) Heat transfer in turbulent boundary layers subjected to free-stream turbulence - Part II: Analysis and correlation. Journal of Turbomachinery, 125(2), pp. 242–251.

Blair, M. F. (1983a) Influence of free-stream turbulence on turbulent boundary layer heat transfer and mean profile development, Part I - Experimental data. Journal of Heat Transfer, 105(1), pp. 33–40.

Blair, M. F. (1983b) Influence of free-stream turbulence on turbulent boundary layer heat transfer and mean profile development, Part II - Analysis of results. Journal of Heat Transfer, 105(1), pp. 41–47.

Çengel, Y. A. and Cimbala, J. M. (2010) Fluid mechanics: Fundamentals and applications. Boston, MA, USA: McGraw-Hill Higher Education, 2nd edition, pp. 35-600.

Dryden, H.L. (1936) Air flow in the boundary layer near a plate. NACA Technical Report No. 562. National Bureau of Standards, Washington, DC, USA.

Hancock, P. E. and Bradshaw, P. (1983) The effect of free-stream turbulence on turbulent boundary layers. Journal of Fluids Engineering, 105(3), pp. 284–289.

Hoffmann, J. A. and Mohammadi, K. (1991) Velocity profiles for turbulent boundary layers under freestream turbulence. Journal of Fluids Engineering, 113(3), pp. 399–404.

Incropera, F. P., Dewitt, D. P., Bergman, T. L. and Lavine, A. S. (2007) Fundamentals of Heat and Mass Transfer. New York, NY, USA: John Wiley & Sons, 6th edition, pp. 377-516.

Junkhan, G. H. and Serovy, G. K. (1967) Effects of free-stream turbulence and pressure gradient on flat-plate boundary-layer velocity profiles and on heat transfer. Journal of Heat Transfer, 89(2), pp. 169–175.

Kestin, J., Maeder, P. F. and Wang, H. E. (1961) Influence of turbulence on the transfer of heat from plates with and without a pressure gradient. International Journal of Heat and Mass Transfer, 3(2), pp. 133–154.

Kondjoyan, A., Péneau, F. and Boisson, H. (2002) Effect of high free stream turbulence on heat transfer between plates and air flows: A review of existing experimental results. International Journal of Thermal Sciences, 41(1), pp. 1–16.

Maciejewski, P. K. and Moffat, R. J. (1992) Heat transfer with very high free-stream turbulence: Part I - Experimental data. Journal of Heat Transfer, 114(4), pp. 827–833.

Maciejewski, P. K. and Moffat, R. J. (1992) Heat transfer with very high freestream turbulence: Part II - Analysis of the results. Journal of Heat Transfer, 114(4), pp. 834–839.

Nicholl, C. I. H. (1970) Some dynamical effects on a turbulent boundary layer. Journal of Fluid Mechanics, 40(2), pp. 361–384.

Nikuradse, J. (1950) Laws of flow in rough pipes. NACA Technical Memorandum 1292. National Advisory Commission for Aeronautics, Washington, DC, USA.

Nix, A. C., Diller, T. E., Ng, W. F. (2007) Experimental measurements and modeling of the effects of large-scale freestream turbulence on heat transfer. Journal of Turbomachinery, 129(3), pp. 542-550.

Palyvos, J. A. (2008) A survey of wind convection coefficient correlations for building envelope energy systems' modeling. Applied Thermal Engineering, 28(8–9), pp. 801–808.

Péneau, F., Boisson, H., Kondjoyan, A. and Djilali, N. (2004) Structure of a flat plate boundary layer subjected to free-stream turbulence. International Journal of Computational Fluid Dynamics, 18(2), pp. 175–188.

Pope, S. B. (2000) Turbulent flows. Cambridge, UK: Cambridge University Press, pp. 1-385.

Sarkar, D. (2018) A numerical tool for predicting the spatial decay of freestream turbulence. MESc Thesis, Electronic Thesis and Dissertation Repository, The University of Western Ontario, London, Canada. 5331.

Schlichting, H. (1999) Boundary layer theory. New York, NY, USA: McGraw-Hill, 8th edition, pp. 1-643.

Simonich, J. C. and Bradshaw, P. (1978) Effect of free-stream turbulence on heat transfer through a turbulent boundary layer. Journal of Heat Transfer, 100(4), pp. 671–677.

White, F. M. (2016) Fluid mechanics. New York, NY, USA: McGraw-Hill, 8th edition, pp. 139-526.

Chapter 2

2 Effect of free-stream turbulence on a flat plate turbulent boundary layer

This chapter presents an overview of what is known about the effect of free-stream turbulence on flat plate turbulent boundary layers in Section 2.1. This includes a discussion on the quantitative inconsistencies of previous studies regarding the increase of skin friction with increasing free-stream turbulence (FST), as well as the importance of considering the streamwise decay of turbulence intensity (TI), which was not mentioned in previous works. These inconsistencies and gaps in the literature are examined in the present study using Computational Fluid Dynamics (CFD) techniques. The numerical method is presented in Section 2.2, where the computational domain, grid, methodology, boundary conditions and validation of the flow field are discussed. In Section 2.3, different free-stream conditions are analyzed, resulting in correlations for the variation of skin friction (both local and total) and momentum thickness with respect to those examined conditions. The different correlations are analyzed in Section 2.4. The results are then validated with previous studies in Section 2.5. Finally, a summary of this study and conclusions are presented in Section 2.6.

2.1 Background

The effect of FST on boundary layers (BL) on flat plates has been the focus of various studies over the last decades (Dyban et al., 1977; Simonich and Bradshaw, 1978; Blair, 1983; Maciejewski and Moffat, 1992; Kondjoyan et al., 2002). It has been shown that FST affects laminar and turbulent boundary layers as well as the laminar-turbulent transition (Kondjoyan et al., 2002).

Considering laminar boundary layers (LBL), the mean velocity profiles ($\frac{U}{U_o}$ vs. $\frac{z}{\delta}$) seem almost unaffected by turbulence intensity (*TI*) levels of up to 6% for local Reynolds numbers (Re_x) up to $2\text{x}10^4$ (Dyban et al., 1977; Dyban and Epik, 1985). The *TI* and Re_x were defined by Eq. (1.19) and Eq. (1.1) respectively in Chapter 1.

In their study, the normalized velocity profiles showed an increased velocity gradient near the wall ($\left.\frac{\partial U}{\partial z}\right|_{z=0}$), but the overall profile shape was the same as the Blasius solution (Blasius, 1908), which corresponds to a LBL with no FST. For *TI* varying from 7 to 9%, the authors mentioned that a region similar to the wake of a turbulent boundary layer (TBL) was apparent, although no logarithmic behaviour was noticed and the BL thickness was still similar to the theoretical Blasius solution for a LBL. This profile was then denominated as pseudo-laminar due to its characteristics (Dyban et al., 1977).

Furthermore, the laminar-turbulent transition is highly affected by the increase in FST. Previous studies show that an earlier transition occurs when FST is increased and this effect is less pronounced for higher TI values, e.g. when FST is increased from 11 to 55%, the difference between the respective transition Reynolds numbers is around 16% (Dyban et al., 1977; Maciejewski and Moffat, 1992), but this difference is around 84% when FST varies from 0 to 4% (Çengel and Cimbala, 2010; Kestin et al., 1961), as shown in Figure 2.1. The laminar-turbulence transition when there is no turbulence at the free-stream starts when the Re_x is around $5x10^5$ (Çengel and Cimbala, 2010), but it can occur at $Re_x = 8x10^4$ when *TI* is around 3-4% (Kestin et al., 1961), at $Re_x = 6x10^4$ when *TI* is 5% (Junkhan and Sevory, 1967), at $Re_x = 3\text{-}4x10^4$ when *TI* is up to 11% (Dyban et al., 1977) or even at $Re_x = 2.5x10^4$ when *TI* is up to 55% (Maciejewski and Moffat, 1992).

Péneau et al. (2004) investigated numerically the flat plate BL for a FST range of 1.5-10% and local Reynolds number (Re_x) up to $7x10^4$ using Large Eddy Simulation (LES). In this study, they also noticed the occurrence of an earlier transition and the authors mentioned an increase in local skin friction ($c_{f,x}$) until it reached 94-99% of the theoretical value for a turbulent BL when *TI* = 10% and $Re_x > 5x10^4$. This finding can be observed in Figure 2.2. The local skin friction coefficient for laminar ($c_{f,l}$) and turbulent flows ($c_{f,t}$) were expressed by Eq. (1.6) and Eq. (1.7) respectively.

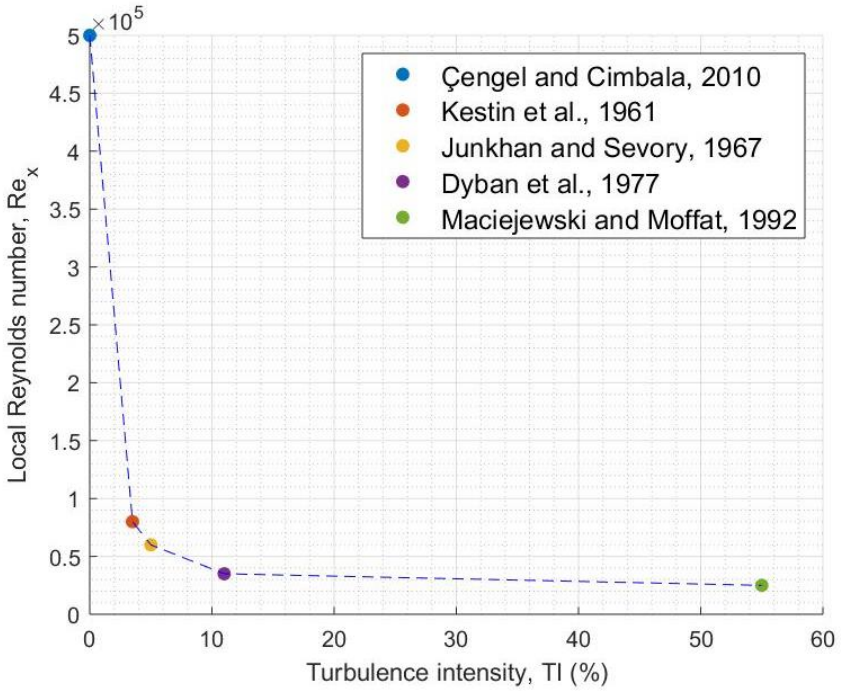

Figure 2.1 – Local Reynolds numbers (Re_x) where the laminar-turbulent transition starts for various turbulence intensity levels (TI)

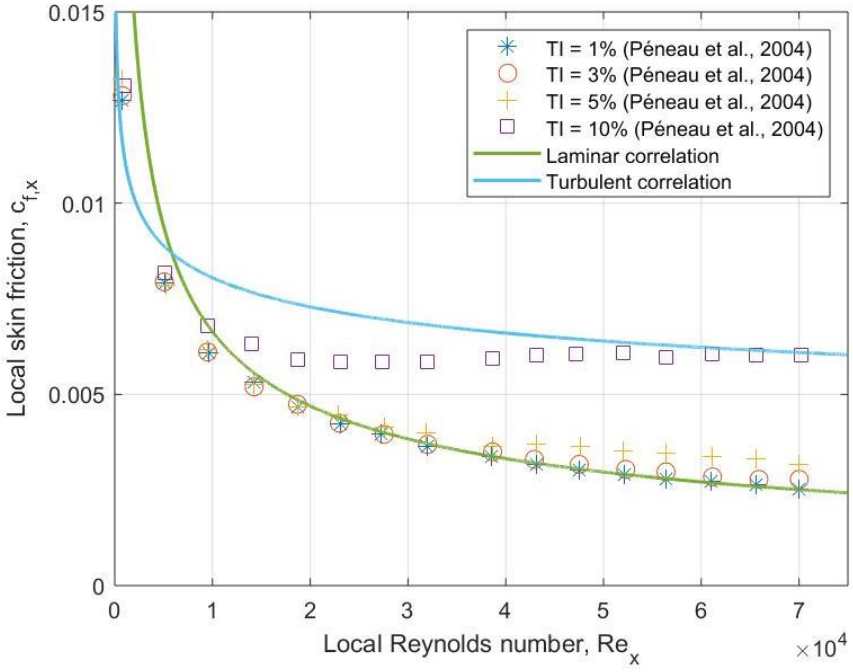

Figure 2.2 - Effect of varying free-stream TI on local skin friction ($c_{f,x}$) and comparison with laminar and turbulent correlations, adapted from Péneau et al. (2004)

Regarding the turbulent boundary layer (TBL), studies showed that the boundary layer becomes thicker and skin friction is higher with increasing FST (Simonich and Bradshaw, 1978; Hancock and Bradshaw, 1983; Blair, 1983; Kondjoyan et al., 2002). Additionally, no significant changes were observed in the mean velocity profiles, especially in the near wall and logarithmic region, for *TI* of up to 55% (Blair, 1983; Maciejewski and Moffat, 1992). These authors also observed an increase momentum thickness (θ), given by Eq. (2.1).

$$\theta = \int_0^\infty \frac{U}{U_o}\left(1 - \frac{U}{U_o}\right) dz \tag{2.1}$$

These observations mentioned by previous studies and the influence of other parameters such as integral length scale (L_u) and Re_x on the TBL, as well as correlations derived from previous investigations, are discussed further in the next section.

2.1.1 Previous experimental studies

Numerous parameters can influence the results and effects on boundary layers observed in experiments, e.g. free-stream *TI*, L_u, Re_x. Different experimental studies tried to establish a correlation between local skin friction and these parameters (Simonich and Bradshaw, 1978; Hancock and Bradshaw, 1983; Blair, 1983; Ames and Moffat, 1990). These investigations agree that there is an enhancement in skin friction with increasing FST, but they show inconsistencies regarding the quantitative effect of different variables and they are not sufficient to describe the effect of FST on the BL (Kondjoyan et al., 2002).

Firstly, Simonich and Bradshaw (1978) investigated the effect of FST in the range of 0.03 to 7% and Re_x of up to 6.3×10^6. They assumed that $c_{f,x}$ would vary linearly with respect to TI_x, therefore:

$$\frac{c_{f,x} - c_{f,xo}}{c_{f,xo}} = A\, TI_x \tag{2.2}$$

where $c_{f,xo}$ is the local skin friction value when there is no FST, A is a constant and TI_x is the local value of free-stream turbulence. The best fit of their data was achieved for A=2, but there was a large scatter in their results. Hancock and Bradshaw (1983) proposed that

such scatter was related to the fact that Eq. (2.2) did not take into account the effect of the local integral length scale (L_{ux}), which according to Hancock and Bradshaw (1983) is more significant when L_{ux} is of the same order of magnitude as the boundary layer thickness (δ). The range of *TI* and Re_x was similar to those of Simonich and Bradshaw (1978) and the L_{ux}/δ ratio varied from approximately 0.5 to 5. Thus, they proposed the following expression:

$$\frac{c_{f,x}-c_{f,xo}}{c_{f,xo}} \propto \left(\frac{TI_x}{2+{}^{L_u^e}/_{\delta}}\right) \tag{2.3}$$

Where L_u^e is the dissipative length scale, calculated by two-thirds of the rate of turbulent energy dissipation. For isotropic homogeneous turbulence, $L_u^e = 1.5\, L_{ux}$ (Blair, 1983). The parameter used in Eq. (2.3) $\left(\frac{TI_x}{2+{}^{L_u^e}/_{\delta}}\right)$, generally called Hancock-Bradshaw parameter (*HB*), is purely empirical and was chosen by trial and error to describe the data from Hancock and Bradshaw (1978). However, Baskaran et al. (1989) evaluated the skin friction enhancement with FST for conditions similar to Simonich and Bradshaw's (1978) study and observed a large scatter between their experimental results and the predicted values from Eq. (2.3). Blair (1983) noted that the effects of FST on skin friction were less intense for higher Reynolds number and almost insignificant for a momentum-thickness Reynolds number (Re_θ) in the range of 2000 to 5000. Then, the author proposed a modification to Eq. (2.3) that included Re_θ, as expressed by Eq. (2.4). It is important to note that Blair conducted experiments over a similar range of *TI* (0.25-7%), with zero pressure gradient, higher Re_x (up to $6\text{x}10^6$) and focused on fully turbulent boundary layers.

$$\frac{c_{f,x}-c_{f,xo}}{c_{f,xo}} \propto \left(\frac{TI_x}{\left(2+{}^{L_u^e}/_{\delta}\right)\left(1+3e^{-Re_\theta/400}\right)}\right) \tag{2.4}$$

The expression would be the same as Eq. (2.3) but divided by an exponential relationship ($1+3exp(-Re_\theta/400)$). This relationship tends to 1 for values of Re_θ above 2000 and so this term takes into account the effect of low values of Re_θ. However, Blair's modified correlation underpredicts the increase in skin friction for cases with higher FST, especially above 20% (MacMullin et al., 1989; Young et al., 1992; Kondjoyan et al., 2002). The

discrepancies may be related to the fact that, in order to generate higher TI experimentally it is necessary to use jets or ventilators, which leads to greater turbulence anisotropy (Young et al., 1992). Ames and Moffat (1990) also proposed a correlation including similar parameters, but using θ instead of δ as shown in Eq. (2.5). The right-hand side of Eq. (2.5) was defined by Ames and Moffat (1990) as the *TLR* parameter. Their study included experiments with *TI* of up to 19%. They highlighted that there was not enough evidence to define a list of parameters that could represent the effects of free-stream turbulence on flat plate boundary layers.

$$\frac{c_{f,x}-c_{f,xo}}{c_{f,xo}} \propto TI_x \left(\frac{\theta}{L_u^e}\right)^{1/3} \left(\frac{Re_\theta}{1000}\right)^{1/4} \tag{2.5}$$

Other experimental studies presented an enhancement of skin friction with increasing *TI*: Hoffmann and Mohammadi (1991) presented a percentage increase of $c_{f,x}$ of approximately 14% for *TI* of 5% while Barret and Hollingsworth (2003) reported an increase by up to 16% for *TI* of 8%, but there was still a large scatter when their results were compared to previous experimental studies from Hancock and Bradshaw (1983) or Ames and Moffat (1990).

One important factor that needs to be considered is the streamwise decay of turbulent kinetic energy (TKE), which may explain the discrepancies between the results from previous studies. Blair (1983) noted that free-stream TKE decayed with distance downstream of the grid but did not investigate how this decay affects the results observed. From Figure 2.3 it is possible to see that, depending on the plate position in the domain or test section and the initial TI, the FST conditions at the plate leading edge and the turbulence intensity in the plate region can vary to a great extent. In Ames and Moffat's (1990) study, for example, the percentage difference of TI between the leading and trailing edge of the plate ($TI_{dif}(\%) = \frac{(TI-TI_{TE})}{(TI+TI_{TE})/2} x100$) can be as high as 96%.

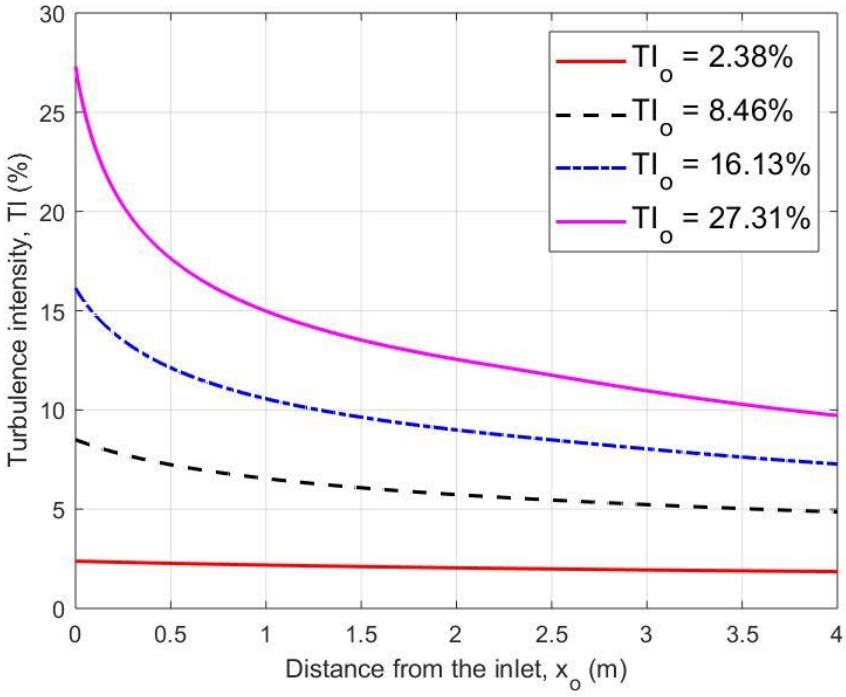

Figure 2.3 – Free-stream TI decay with distance from the inlet for varying initial turbulence intensity (TI_o) for L_{uo} = 0.1m, based on TKE decay correlations presented by Sarkar (2018)

The above-mentioned studies did not indicate that the effect of non-uniform TI in the x-direction could be neglected. Besides, the turbulence intensity of the flow approaching the plate might be one of the reasons for the discrepancies and contradictions between these studies (Kondjoyan et al., 2002). The current study investigates the influence of the incoming flow turbulence intensity and length scale on local and total skin friction while keeping the turbulence conditions fairly uniform in the plate region. Therefore, it is important to correctly model and quantity the free-stream turbulent properties and a discussion regarding TI decay and the choice of appropriate numerical models will de discussed in the next section.

2.1.2 Previous numerical studies

It is known that Reynolds-Averaged Navier Stokes (RANS) modelling is suitable for many engineering applications and less expensive computationally than Large Eddy Simulation

(LES) or Direct Numerical Simulation (DNS). Considering RANS simulations, the laminar-turbulent transition on flat plates predicted by different turbulence models for a free-stream with no turbulence was investigated by Abdollazadeh et al. (2017) and the comparison between those models is presented in Figure 2.4. From this graph, it is possible to conclude that the k-k_l-ω model would be the most suitable for predicting transition, but it is possible to see that most models can predict correctly the fully turbulent region, with the exception of the Low Re k-ε model.

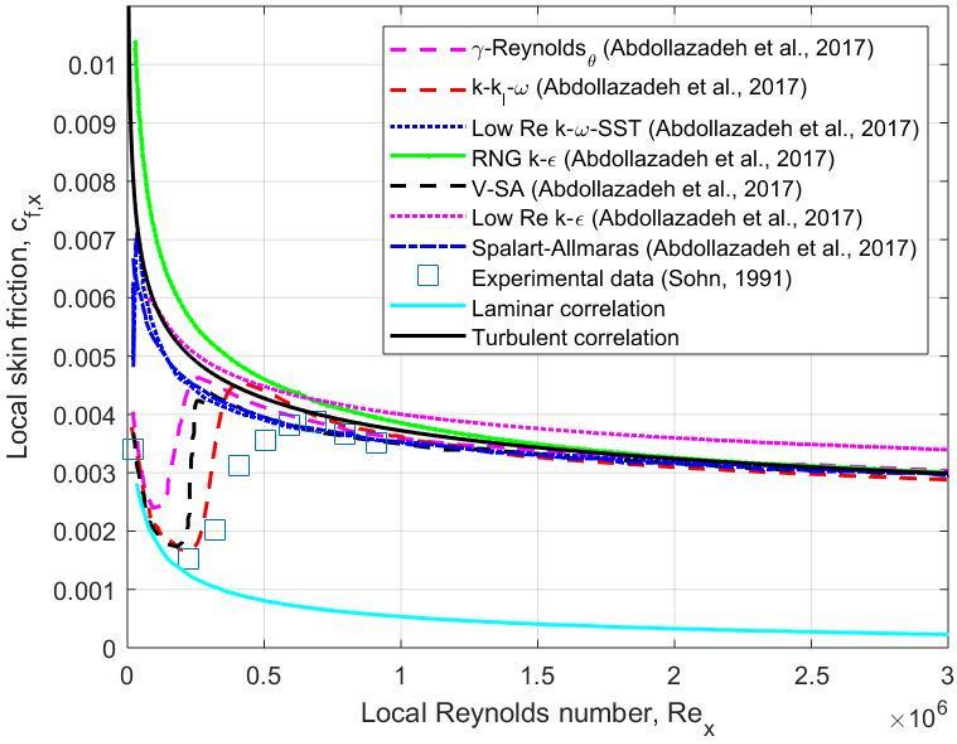

Figure 2.4 – Comparison between $c_{f,x}$ results from different RANS models and experimental data, laminar and turbulent correlations (Eq. (1.6) and Eq. (1.7), respectively), adapted from Abdollazadeh et al. (2017)

Although the k-k_l-ω model predicts laminar-turbulent transition correctly, it is relevant to mention that this model is not suitable for predicting the free-stream turbulence intensity decay and the recommended corrections were not able to solve the erroneous, rapid TKE decay that occurs in the flow away from the wall (Lopez and Walters, 2016).

Since the correct TI decay and local skin friction prediction are fundamental in this study, the Low Re k-ω SST model is the appropriate choice. Firstly, although its prediction of laminar-turbulent transition is delayed, the $c_{f,x}$ results are predicted correctly in the turbulent region (Abdollazadeh et al., 2017). Secondly, it is capable of estimating the correct decay of TKE (Sarkar, 2018).

Furthermore, Sarkar (2018) demonstrated a numerical tool that can accurately predict the turbulent intensity and integral length scales at the leading edge of the plate if the parameters at the inlet are known and *vice-versa*. Consequently, it was possible to investigate not only the TKE decay but also the region in the domain where the TI levels would be almost uniform. Considering initial TI levels of up to 30%, the author observed that starting from x_o = 2m there is a 2m region where the percentage variation of TI was only up to 14%. This variation is fairly small when compared to the difference in the initial region (from x_o = 0m to x_o = 2m) that could be up to 41% (Sarkar, 2018). The previous experimental studies on the effect of free-stream turbulence on flat plate boundary layers, discussed in Section 2.1.1, did not mention how this percentage variation of TI within plate region could affect the measured boundary layer data and did not focus on discussing correlations between skin friction enhancement and leading edge turbulence conditions. Despite these considerations, previous numerical studies reached the same overall conclusions found from those experimental studies, i.e., an increase in FST leads to skin friction enhancement and a thicker boundary layer (Ivyer and Yavuzkurt, 1999; Péneau et al., 2004; Lioznov et al., 2012). Ivyer and Yavuzkurt (1999) investigated TI levels of up to 25.7% but affirmed that the k-ε model implemented in computer code TEXTAN resulted in over-prediction of more than 50% for local skin friction when compared to Ames and Moffat's (1990) data. Lioznov et al. (2012) observed a percentage increase of only 11% for a TI of 9% but the authors did not compare their results with previous studies. A comparison between the key parameters from the main numerical and experimental studies presented so far and the effect observed on local skin friction is presented in Table 2.1. Note that the percentage increase of $c_{f,x}$ is given by $\frac{c_{f,x}-c_{f,xo}}{c_{f,xo}} x100\%$. The range of L_u examined in some studies was not mentioned and this is indicated by 'N/A'. The experimental and numerical studies are indicated by 'Exp' and 'Num', respectively.

Table 2.1 - Main experimental and numerical studies on the effect of FST on skin friction

Authors	**Type of study**	**Re_x up to**	**Range of *TI***	**Range of L_u**	**$c_{f,x}$ percentage increase**
Dyban et al. (1977)	Exp	$2.0x10^4$	0.1-9%	N/A	Up to 56%
Simonich and Bradshaw (1978)	Exp	$6.3x10^6$	0.03-7%	N/A	Up to 20%
Hancock and Bradshaw (1983)	Exp	$6.3x10^6$	0.1-7%	2-7 cm	Up to 24%
Blair (1983)	Exp	$6.0x10^6$	0.25-7%	1-3 cm	Up to 20%
Ames and Moffat (1990)	Exp	$3.2x10^6$	0.1-17%	9-13 cm	Up to 22%
Hoffmann and Mohammadi (1991)	Exp	$1.6x10^6$	0.1-5%	3-5 cm	Up to 14%
Ivyer and Yavuzkurt (1999)	Num	$6.0x10^6$	0.1-25.7%	N/A	Up to 50%
Barrett and Hollingsworth (2003)	Exp	$1.0x10^6$	0.1-8%	1-3 cm	Up to 16%
Péneau et al. (2004)	Num	$7.0x10^4$	1-10%	2-14 cm	Up to 140%
Lioznov et al. (2012)	Num	$3.0x10^6$	1.5-9%	N/A	Up to 11%

Therefore, there were contradictions and discrepancies regarding the quantitative effect of different parameters, such as *TI* and *Lu*, on local skin friction and the different correlations proposed by previous experimental investigations, as presented in Section 2.1.1, were not able to predict correctly those effects (Kondjoyan et al., 2002). The discrepancies are

related to the wide range of Re_x, different incoming flow conditions and differences in the streamwise decay of turbulence intensity. Thus, the present numerical study will focus on determining a correlation that describes this overall conclusion while incorporating the influence of all the key parameters (TI, L_u, Re) and the streamwise free-stream TKE decay. Only fully turbulent boundary layers are considered, to avoid inconsistencies due to transition effects, as well as a lack of turbulence closure models that can accurately predict laminar-turbulent transition and TKE decay. The numerical method used in the current study is presented next.

2.2 Numerical Method

The problem is represented by the diagram below (Figure 2.5), where a free-stream with uniform velocity U_o, initial turbulence intensity TI_o and initial integral length scale L_{uo} approaches a flat plate of length L on which a boundary layer of thickness $\delta(x)$ develops.

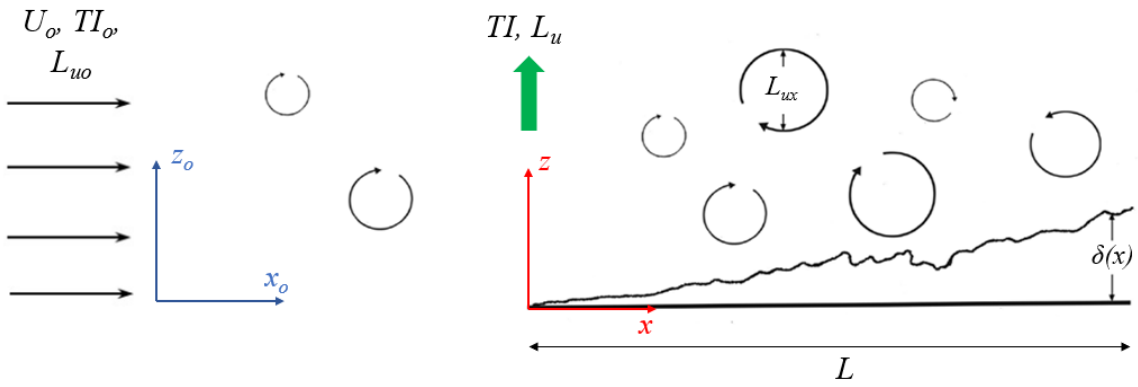

Figure 2.5 – Problem diagram with main variables and coordinate system

2.2.1 Computational domain

The 3-D computational domain for this problem is presented in Figure 2.6. The domain dimensions are L_x = 4.0m, L_y = 0.5m and L_z = 0.5m. L_x was set as 4.0m because between x_o = 2.0m to x_o = 4.0m there is a nearly uniform turbulence region as mentioned before (Sarkar, 2018), so for most cases the plate leading edge is positioned at x_o = 2.0m. Furthermore, some cases were also analyzed with the leading edge of the plate located at

x_o = 1.5m and x_o = 1.0m to investigate the effect of higher TKE decay rates on the turbulent boundary layer.

The other domain dimensions (L_y and L_z) were defined in such a way that the boundary conditions imposed at the walls, which will be presented later, would not affect the flat plate boundary layer. These dimensions are then analyzed with respect to the turbulent boundary layer thickness (δ_t), defined by the Eq. (1.3).

The turbulent boundary layer developed at the plate trailing edge is 35.2mm, so $L_y/\delta = L_z/2\delta$ = 14.2. These dimensions are large enough to avoid erroneous boundary layer profiles due to imposed wall boundary conditions (Kawai and Larsson, 2012; Mukha et al., 2018). Additionally, the plate has zero thickness, i.e., a thickness of a node unit, to avoid flow separation at the leading edge.

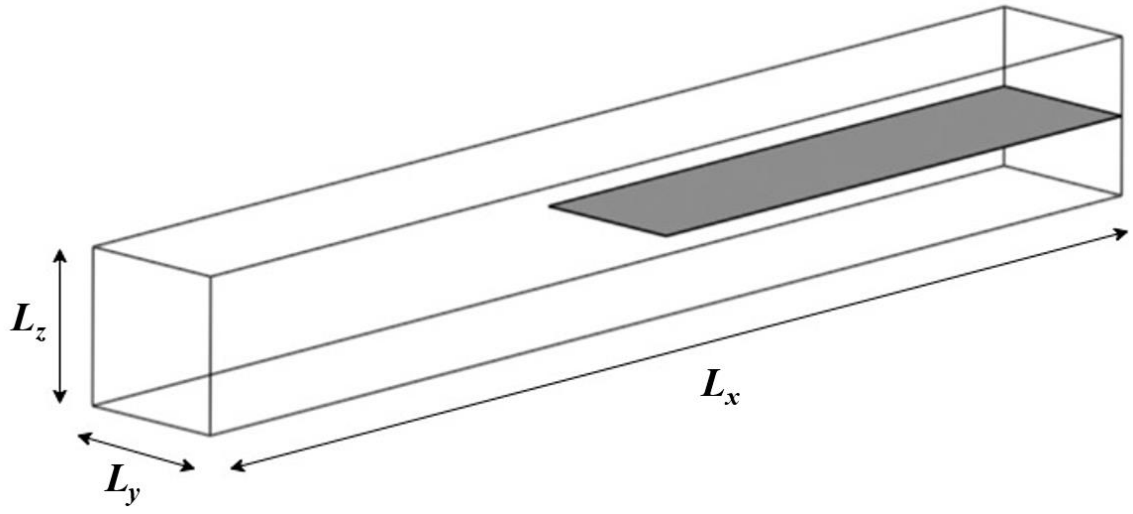

Figure 2.6 – 3D Computational domain

2.2.2 Grid generation

The meshes were created using ICEM CFD 19.1 and all of them are orthogonal hexahedral meshes since they are more suitable for unidirectional flow over a plane surface, because the grid lines should be perpendicular to the wall (Frank et al., 2007) and it produces a more precise numerical solution (Baker et al., 2019). The mesh topology is presented in Figure 2.7.

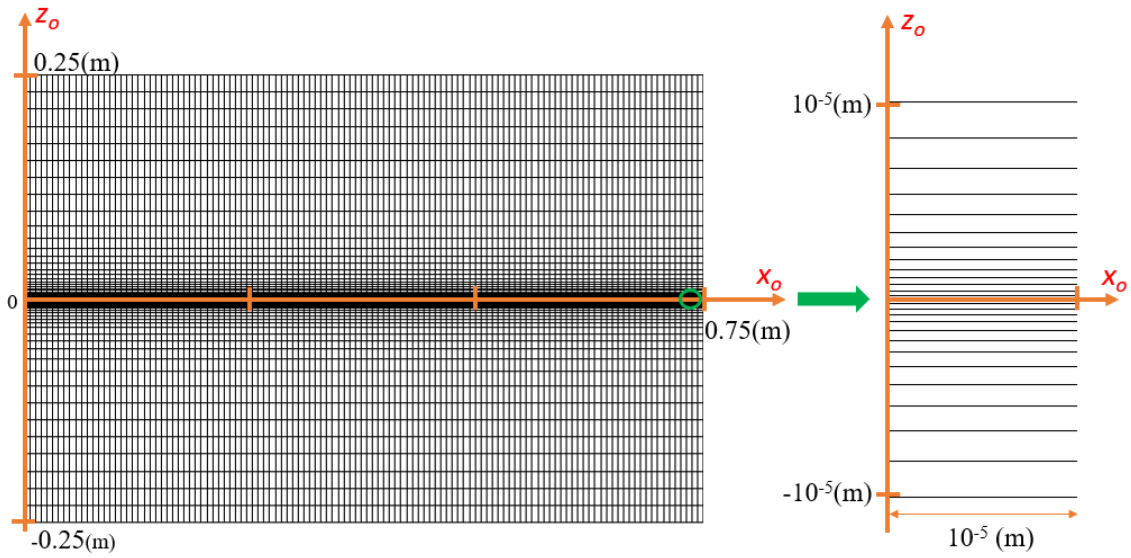

Figure 2.7 – Mesh topology in x-z plane

In the y-direction the mesh is equally spaced. Note that there is a better refinement near the plate, since the viscous region is resolved using the Low Reynolds Number Modelling (LRNM) approach as recommended by Blocken et al. (2009). This model resolves the viscosity-affected region including the viscous sub-layer but requires high grid resolution near the plate. This resolution is defined by the dimensionless wall distance $y+$ values, given by Eq. (2.6), and growth ratio.

$$y^+ = \frac{\rho u^* y_p}{\mu} \tag{2.6}$$

where u^* is the friction velocity and y_p is the distance from the first grid point to the wall. This value should be less than 1 to solve the near wall region and generate an appropriate LRNM grid (Blocken et al., 2009), so in this study $y^+ \approx 0.8$. This generates at least 20 points inside the whole boundary layer, which is desirable to compute the boundary layer region, including the viscous region (Versteeg and Malalasekera, 1995; Defraeye et al, 2010). Besides that, the growth ratio was defined as 1.2, which is the highest recommended value according to COST Guidelines (Franke et al, 2007). The grid in the other directions is equally spaced with Δx=0.0066m and Δy=0.0067m, which was sufficient to provide grid independent results, as will be presented later.

2.2.3 Methodology

2.2.3.1 Solver

All cases were studied using the commercial software FLUENT 19.1. The software was set for a 3-D domain and the option “double precision” was enabled for better accuracy (ANSYS, 2013). The general setup for the solver was pressure-based, since it is appropriate for incompressible flows (Chorin, 1968). This solver is based on the projection method, where the continuity (mass conservation) of the velocity field is resolved by pressure or pressure correction equations (Chorin, 1968). The pressure equation is obtained from the continuity and momentum equations so that the velocity field satisfies continuity when corrected by the pressure. Then the set of governing equations is solved for as many iterations as needed to achieve a converged solution.

2.2.3.2 Governing equations and turbulence model

The instantaneous conservation equations of mass and momentum can be expressed by Eq. (2.7) and Eq. (2.8) respectively.

$$\frac{\partial \rho}{\partial t} + \frac{\partial}{\partial x_i}(\rho u_i) = 0 \tag{2.7}$$

$$\frac{\partial}{\partial t}(\rho u_i) + \frac{\partial}{\partial x_j}(\rho u_i u_j) = -\frac{\partial p}{\partial x_i} + \frac{\partial}{\partial x_j}\left[\mu\left(\frac{\partial u_i}{\partial x_j} + \frac{\partial u_j}{\partial x_i}\right)\right] \tag{2.8}$$

where t is time, u_i is the instantaneous velocity, x_i is the axial coordinate and p is the pressure. These equations are computationally expensive to calculate directly because turbulence is characterized by fluctuating velocity fields. In order to consume less computational resources, the instantaneous governing equations can be time-averaged, and a modified set of equations obtained.

Thus, substituting a parameter ϕ by its mean value and a fluctuating component ($\phi = \bar{\phi} + \phi'$), we obtain the following equations for an incompressible, steady flow:

$$\frac{\partial U_i}{\partial x_i} = 0 \tag{2.9}$$

$$\frac{\partial}{\partial x_j}\left(\rho U_i U_j\right) = -\frac{\partial p}{\partial x_i} + \frac{\partial}{\partial x_j}\left[\mu\left(\frac{\partial U_i}{\partial x_j} + \frac{\partial U_j}{\partial x_i}\right)\right] + \frac{\partial}{\partial x_j}\left(-\rho\overline{u_i' u_j'}\right) \tag{2.10}$$

where U denote the mean velocity. These equations are commonly referred to as the Reynolds-Averaged Navier-Stokes (RANS) equations. They are almost equivalent to the instantaneous equations when the instantaneous velocity is substituted by its mean value. The only additional terms are the Reynolds stresses, $\tau_{ij} = -\rho\overline{u_i' u_j'}$, that represent the effects of turbulence on the flow. These unknown terms are then solved by additional equations, which are defined depending on the selected turbulence model.

This numerical work was conducted using the SST k-w model with Low-Re corrections since it can predict the correct decay of TKE (Sarkar, 2018) and the skin friction, as well as the integral parameters of turbulent boundary layers (Abdollazadeh et al., 2017).

2.2.3.2.1 Shear Stress Transport (SST) k-ω model

The Shear Stress Transport k-ω model was developed by Menter (1994) with the objective of combining the standard k-ω model near the wall, due to its accuracy and robustness in computing the viscous sub-layer, and the k-ε model at the free-stream (Launder and Spalding, 1974).

This is a two-equation model, one for the turbulent kinetic energy (k) and one for the dissipation rate (ω) expressed by Eq. (2.11) and Eq. (2.12) (Menter, 1994).

$$\frac{\partial}{\partial x_i}(\rho k u_i) = \frac{\partial}{\partial x_j}\left(\Gamma_k \frac{\partial k}{\partial x_j}\right) + G_k - Y_k \tag{2.11}$$

$$\frac{\partial}{\partial x_j}\left(\rho\omega u_j\right) = \frac{\partial}{\partial x_j}\left(\Gamma_\omega \frac{\partial \omega}{\partial x_j}\right) + G_\omega - Y_\omega + D_\omega \tag{2.12}$$

where G_k represents the production of turbulence kinetic energy, G_ω represents the generation of ω, and Γ_k and Γ_ω represent the effective diffusivity of k and ω, respectively, which are calculated by Eq. (2.13) and Eq. (2.14). Y_k and Y_ω represent the dissipation of k and ω due to turbulence, and D_w represents the cross-diffusion term.

$$\Gamma_\omega = \mu + \frac{\mu_t}{\sigma_\omega} \tag{2.13}$$

$$\Gamma_k = \mu + \frac{\mu_t}{\sigma_k} \tag{2.14}$$

where σ_k and σ_ω are the turbulent Prandtl numbers for k and ω, respectively.

The constants for this model are defined as (Menter, 1994):

$$\sigma_{k,1} = 1.176, \qquad \sigma_{\omega,1} = 2.0, \qquad \sigma_{k,2} = 1.0, \qquad \sigma_{\omega,2} = 1.168,$$

$$a_1 = 0.31, \qquad \beta_{i,1} = 0.075, \qquad \beta_{i,2} = 0.0828$$

2.2.3.3 Solution parameters

The solutions method was set as SIMPLE pressure-velocity coupling since it is suitable for steady cases (Patankar et al, 1972). The second order spatial discretization scheme was selected for pressure, momentum and turbulence parameters (specific dissipation rate and turbulent kinetic energy), because it provides better accuracy (Barth and Jespersen, 1989). The gradients were computed using the least squares cell-based gradient evaluation since it is less expensive computationally and accurate for structured meshes. The convergence criteria were defined as 10^{-4} for all equations and the solution residuals observed were less than 10^{-8}.

2.2.4 Boundary conditions

The proper choice of boundary conditions is essential for correct development of the flow field, as well as for accurate representation of the influence of the surroundings. In this case, it is extremely important to define properly the inlet conditions. The incoming flow is uniform, and the inlet condition is defined by the velocity, turbulent kinetic energy and specific dissipation rate.

The turbulent parameters at the inlet were calculated using desired predetermined values at the leading edge and the established decay of TKE expressed by Eq. (2.15) and Eq. (2.16) (Sarkar, 2018).

$$log(k') = \log(k'_o) - n_1 log\left(\frac{A_1 (k'_o)^{0.5} (x_o - x_{vo})}{L_u} + 1\right) \tag{2.15}$$

$$log(k') = \log(k'_o) - n_2 log\left(\frac{A_2(k'_o)^{0.5}(x_o - x_{vo})}{L_{uo}} + 1\right) \quad (2.16)$$

where x_{vo} denotes the virtual origin, which is the streamwise distance from the grid origin where the turbulence is well-developed and nearly isotropic and homogeneous. In the current study, it is coincident with the origin of the numerical domain, i.e., x_{vo} = 0m. The value of x_o would be the position of the plate leading edge inside the domain where the turbulent parameters are defined beforehand. Note that k_o and L_{uo} indicate the values at the inlet, and the values of k and L_u at the leading edge are known. The constants in these equations are:

$$A_1 = 0.27;\ A_2 = 0.44;\ n_1 = 2.38;\ n_2 = 1.16$$

They were defined in a way that the expressions presented quantify the streamwise decay of homogeneous and isotropic turbulence. The values of ω are then obtained from the correlation involving k and L_u: $\omega = \frac{k^{0.5}}{\beta^*_\infty L_u}$

Sarkar (2018) also showed that for the correct free-stream TKE decay, the parameter β^*_∞ used in the turbulence model must be changed from the default value of 0.09 to 0.046.

Furthermore, the plate surface was set as no-slip, the outlet as a pressure-outlet and the other walls as symmetric, as represented in the diagram below. The symmetry condition is more appropriate since the pure-slip condition does not guarantee that the gradients of all parameters (especially turbulent kinetic energy and specific dissipation rate) are zero at the boundaries (Versteeg and Malalasekera, 1995).

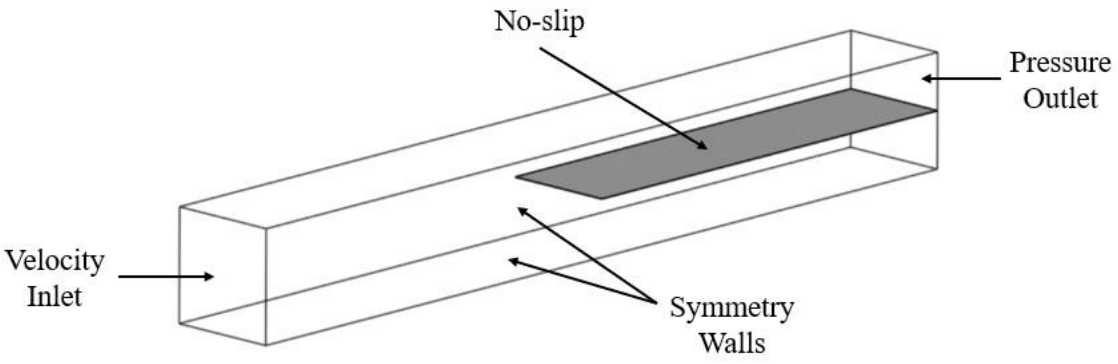

Figure 2.8 – Numerical domain with boundary conditions

2.2.5 Grid independence study

In order to ensure that the results are not affected by the grid chosen and that discretization errors are minimized, a study was conducted using three different grids with 2,436,228 (G1), 3,653,786 (G2) and 5,897,654 (G3) nodes. Note that the refinement ratio between the grids is at least 1.5, as recommended by the COST guidelines (Frank et al., 2007). The results were validated by comparing the local skin friction coefficient, as well as the mean velocity profile.

In this case, the free-stream velocity was set as 40 m/s and the turbulence intensity was kept at a low value (TI_o = 0.1%, L_{uo} = 0.1m), which corresponds to TKE and specific dissipation rate values of 2.4×10^{-3} J/kg and 5.44 s^{-1} respectively, so that the boundary layer flow field could be validated with respect to theoretical correlations. The comparison between the skin friction coefficient values is presented in Figure 2.9 and the mean velocity profiles in Figure 2.10.

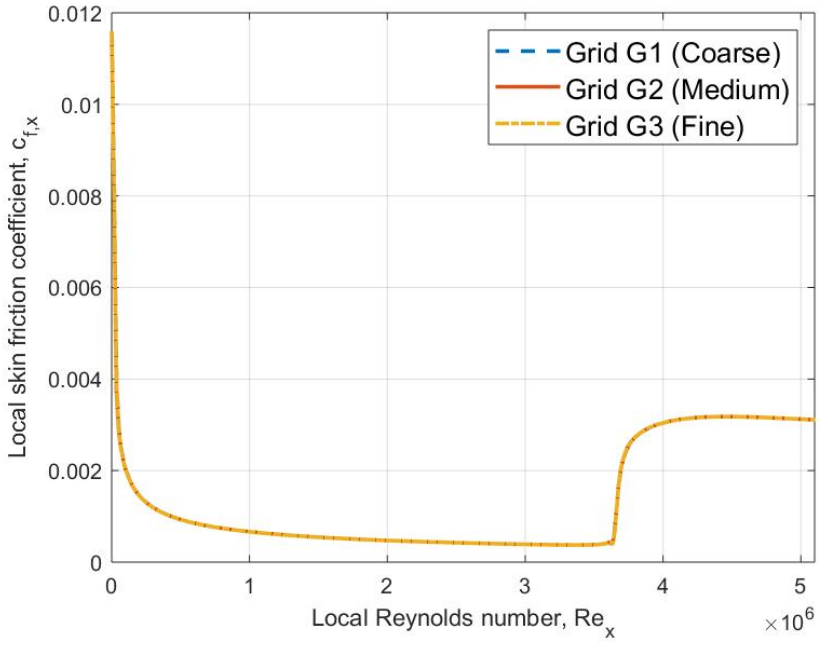

Figure 2.9 - Grid independence study – comparison between local skin friction coefficient results from grids G1, G2 and G3

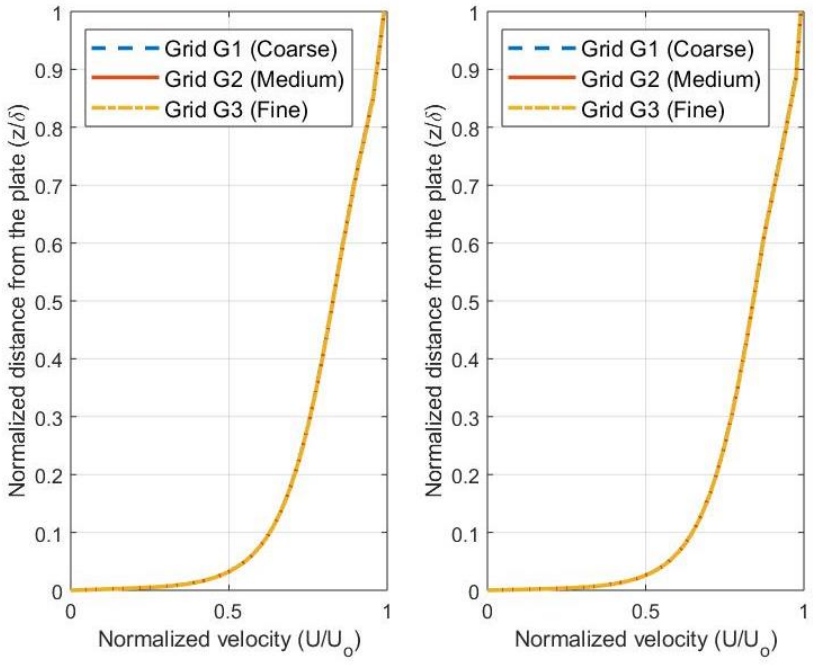

Figure 2.10 – Grid independence study – comparison between velocity profiles at the locations *x/L* = 0.75 (a) and *x/L* = 1.0 (b) from grids G1, G2 and G3

The difference between both results are less than 1% comparing G1 with G2 as well as G2 with G3, therefore the simulations are grid independent. Hence, the main study was conducted using grid G2.

2.2.6 Validation of the flow field with theoretical correlations

The theoretical local skin friction coefficient for laminar ($c_{f,l}$) and turbulent flows ($c_{f,t}$) are known and were presented as Eq. (1.6) and Eq. (1.7) respectively. The comparison between these correlations and the results for the low-turbulence case (TI_o = 0.1%) is then shown in Figure 2.11.

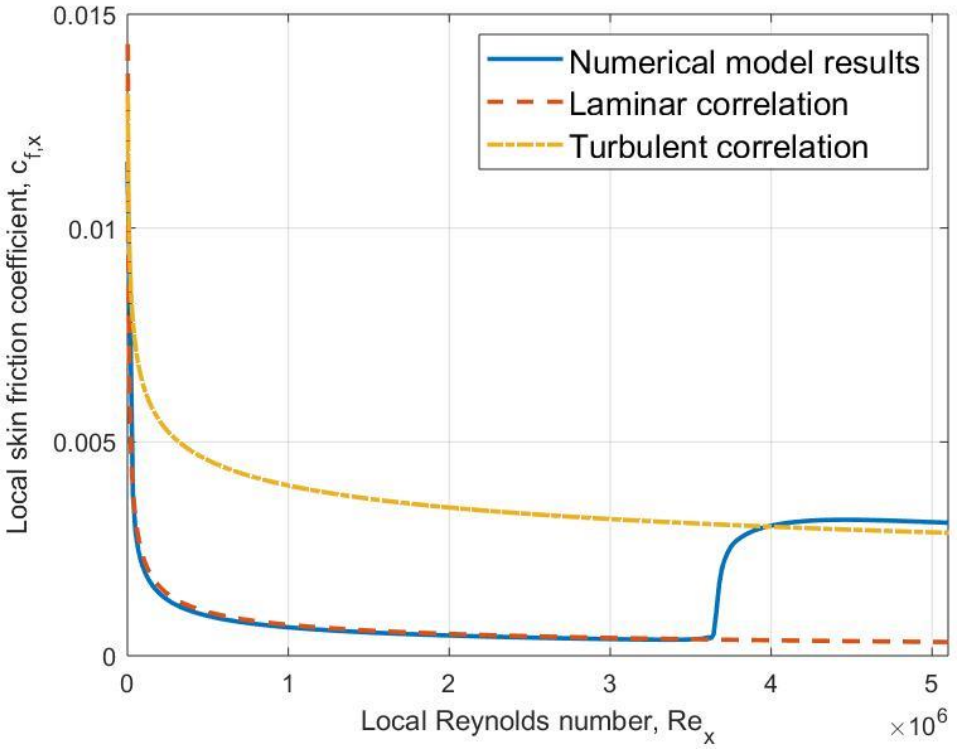

Figure 2.11 – Variation of local skin friction ($c_{f,x}$) with local Reynolds number (Re_x) and comparison with laminar and turbulent correlations

The difference between the numerical results and the laminar and turbulent correlations is less than 1% and 5%, respectively. It is possible to affirm that the model has a good agreement with the expected values, although the transition is delayed, and the flow is not yet fully turbulent at the end of the domain. The delayed transition is one of the

characteristics of the chosen turbulent model, but this will not affect this study since the interest here is not in transition and only in fully turbulent flows. As mentioned in Section 2.1, the increase in FST leads to an earlier laminar-turbulent transition. In the current study, the transition occurs close to the leading edge for *TI* = 2% and the fully turbulent region will be analyzed further in Section 2.3.

Furthermore, the mean velocity profiles were compared to the Nikuradse power law profile (Nikuradse, 1950), given by Eq. (2.17).

$$\frac{U}{U_o} = \left(\frac{z}{\delta}\right)^{1/n}, for\ z \leq \delta \tag{2.17}$$

The comparison between the velocity profile at *x/L* (normalized distance from the leading edge) = 1 and the power law profiles is presented in Figure 2.12.

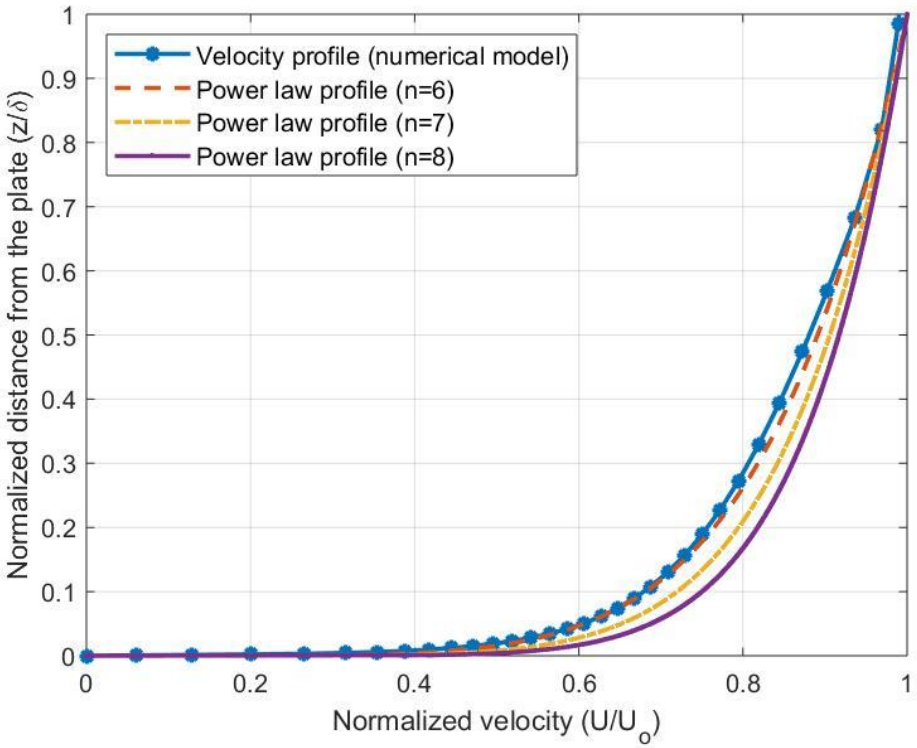

Figure 2.12 – Validation of the velocity profile at *x/L* = 1 with respect to turbulent power law profiles with different exponents

Although the flow is not fully turbulent, the velocity profile is similar to the power law one. The best fit is given when n = 6 and the numerical result lies within 2% of this curve. Therefore, the model is a good representation of the flow when compared to empirical correlations. It should be noted that in this case (for TI_o = 0.1%) the flow regime is still mixed rather than fully turbulent, but when the FST is increased the laminar-turbulent transition moves upstream. Fully turbulent regimes can be expressed by the one-seventh power law for Re_x from $5x10^5$ to 10^7 (Nikuradse, 1950), which is the expression used for all correlations, i.e., local and total skin friction coefficients and momentum thickness.

2.3 Analysis of different free-stream conditions

2.3.1 Effect of turbulence intensity

Various cases with different values of free-stream turbulence (FST) were analyzed. The free-stream velocity was defined as 40 m/s (Re_x up to $5.11x10^6$) because most of the boundary layer developed on the plate would be turbulent and laminar-turbulent transition effects on the observed results would not be significant. Four different values of turbulence intensity at the leading edge (2.0%, 5.7%, 9.0% and 12.6%) were examined while keeping the length scale as L_u = 0.1m. These values were selected based on the TKE decay correlations presented before as Eq. (2.15) and Eq. (2.16) in such a way that the initial turbulence conditions at the inlet were still within the validity of these expressions (TI≤30%). The inlet turbulence conditions are presented below, where the TKE and ω are normalized by U_o^2 and L_{uo}/U_o, respectively.

Table 2.2 – Inlet normalized turbulence conditions with varying leading edge TI value for U_o = 40m/s and L_u = 0.1m

TI at the leading edge (u'/U_o)	**TKE at the inlet (k_o/U_o^2)**	**ω at the inlet ($\omega_o L_{uo}/U_o$)**
2.0%	$0.1x10^{-2}$	0.44
5.7%	$1.1x10^{-2}$	1.89

9.0%	3.9×10^{-2}	4.34
12.6%	11.2×10^{-2}	9.23

The comparison of local skin friction between these cases and the turbulent correlation given by Eq. (1.7) is presented in Figure 2.13.

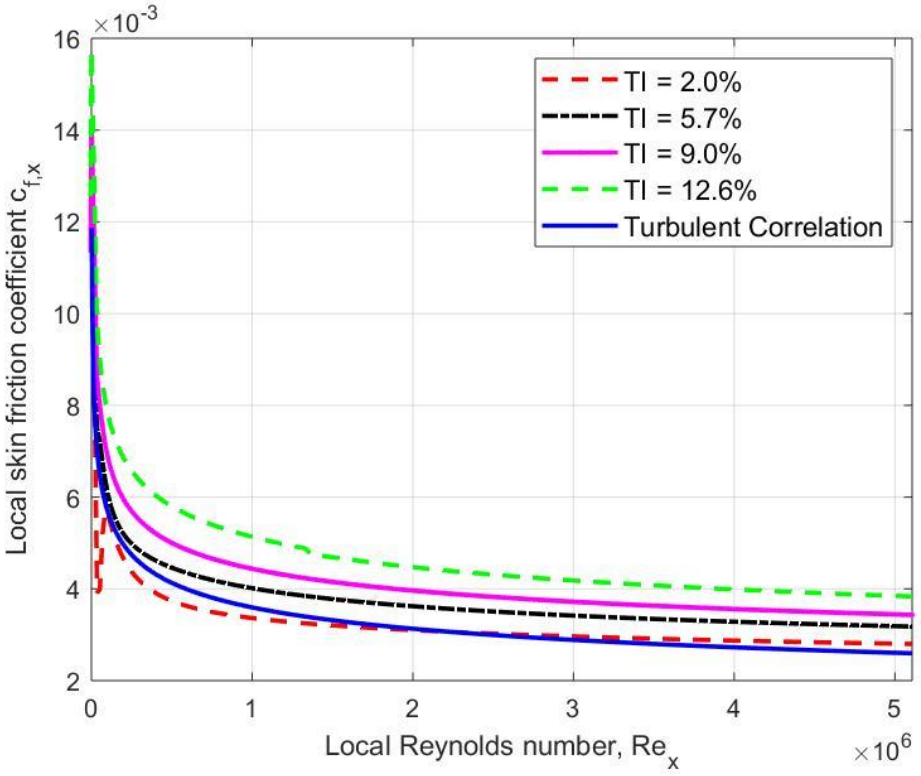

Figure 2.13 – Local skin friction comparison – effect of varying free-stream TI at the plate leading edge and comparison with turbulent correlation for *TI* = 0%

It may be seen that the local skin friction values increase with higher turbulence intensity, as expected from the literature (Kondjoyan et al, 2002). Considering the results for *TI* = 2.0%, the $c_{f,x}$ value is within 5% of the turbulent correlation when $Re_x = 1.28 \times 10^6$ (x/L = 0.25) and then surpasses it for $Re_x > 2.5 \times 10^6$ ($x/L \approx 0.5$) by up to 5% at $Re_x = 5.1 \times 10^6$ ($x/L \approx 1.0$). The local skin friction coefficient for *TI* = 12.6% is 33% higher than the value for *TI* = 2.0% at $Re_x = 5.1 \times 10^6$. The percentage increase for a given parameter Q is calculated by the difference with respect to a reference value divided by the reference value

(Q_0), i.e., $\%increase = \frac{Q-Q_0}{Q_0} x100$. Moreover, the flow is already turbulent from *x/L* = 0.25, so the analysis for local skin friction will consider the region from *x/L* = 0.25 to *x/L* = 1. The influence of other parameters, such as L_u, on the local skin friction coefficient will be presented in the next sections.

Now considering the total (or average) skin friction of the plate using Eq. (2.18).

$$C_f = \frac{1}{0.75L} \int_{0.25L}^{L} c_{f,x} dx \tag{2.18}$$

The results obtained for the total skin friction are then presented in Figure 2.14.

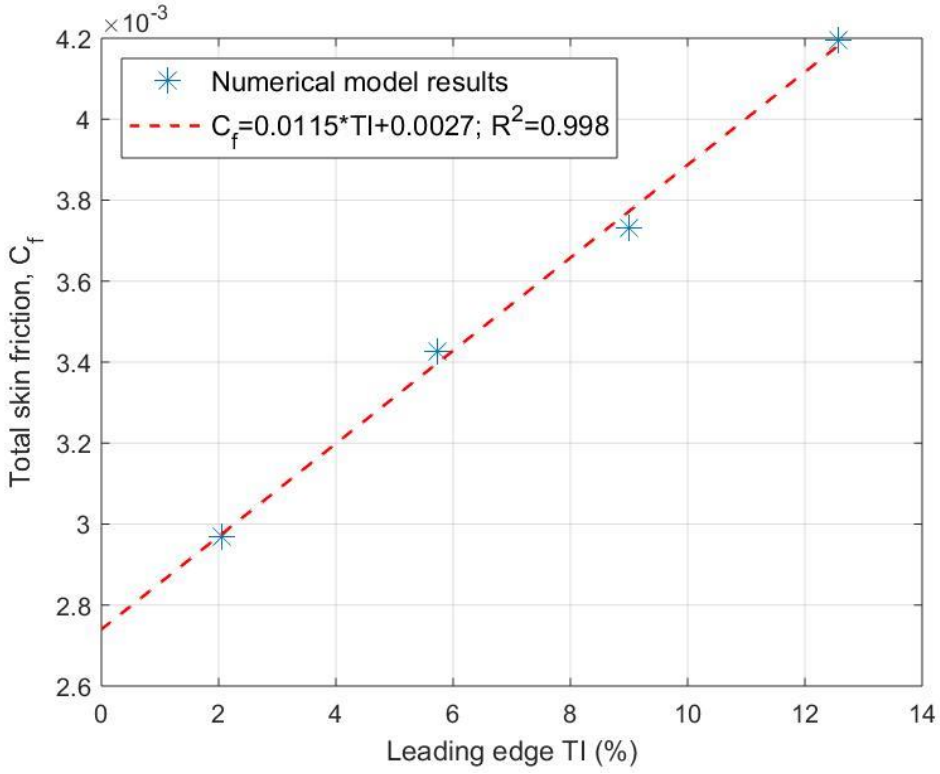

Figure 2.14 – Variation of total skin friction (C_f) with plate leading edge turbulence intensity (*TI*) for Re_L = 5.1x10^6 and L_u = 0.1m

The percentage increase in total skin friction is up to 41% when *TI* = 12.6% with respect to C_f for *TI* = 2.0%. The enhancement so far can be expressed by a linear equation, as presented above, with a good correlation since R^2 = 0.998. Furthermore, the local skin

friction for a fully turbulent boundary layer with zero free-stream turbulence intensity was expressed by Eq. (1.9). Although the turbulence model used in the current study (SST k-ω model) does not predict transition with accuracy and, therefore, the case with very low free-stream turbulence is not yet fully turbulent, the percentage difference between the skin friction value calculated from the linear expression for TI = 0% and the theoretical expression given by Eq. (1.9) is 14%. The predicted linear equation also does not include the variation of other parameters, such as L_u. This linear expression will be further improved when other parameters are added to the analysis, as will be presented next.

Examining next the BL thickness, from Figure 2.15 it is possible to observe that it increases with higher levels of TI, as mentioned in other studies (Hancock and Bradshaw, 1978; Blair, 1983).

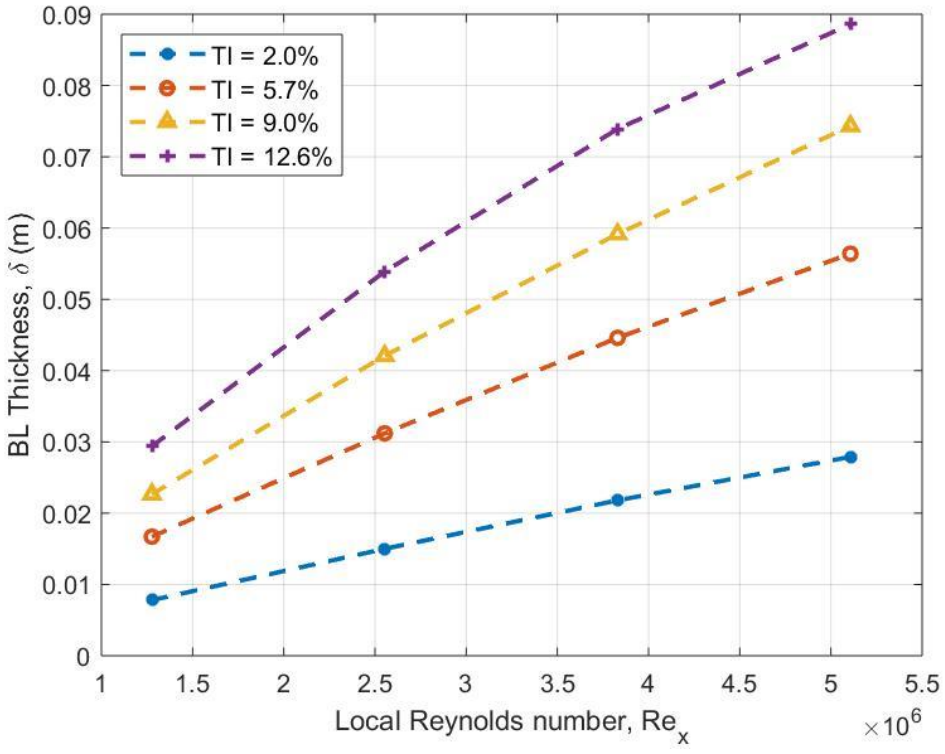

Figure 2.15 – Boundary layer thickness (δ) values with increasing leading edge turbulence intensity (TI) for $Re_L = 5.1\text{x}10^6$ and $L_u = 0.1\text{m}$

The percentage increase in BL thickness is up to 218% for *TI* = 12.6% compared to *TI* = 2.0% at the trailing edge of the plate ($Re_x = 5.1x10^6$). Another important parameter to be considered is the momentum thickness (θ), given by Eq. (2.1). It is generally used by authors to express the increase in skin friction or to present data in terms of momentum-thickness Reynolds number (Re_θ) instead of local Reynolds number (Blair, 1983; Ames and Moffat, 1992; Kondjoyan et al., 2002). The increase in momentum thickness with leading edge *TI* is shown in Figure 2.16.

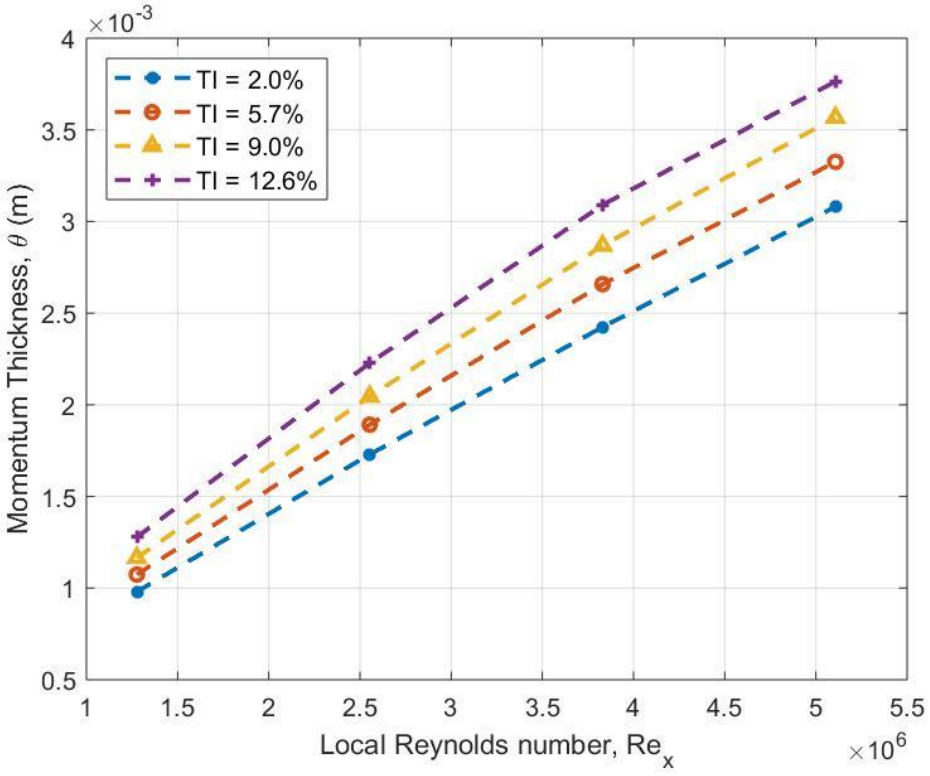

Figure 2.16 - Momentum thickness (θ) values with increasing leading edge turbulence intensity (*TI*) for $Re_L = 5.1x10^6$ and $L_u = 0.1$m

This percentage increase of θ is by up to 22% for *TI* = 12.6% with respect to *TI* = 2.0% at the plate trailing edge ($Re_x = 5.1x10^6$), which is lower than the percentage increase of BL thickness in the same conditions. The momentum thickness varies with *TI* and it would be necessary to know how the boundary layer develops under different conditions to be able to predict the skin friction using expressions than include θ. Additionally, there are more

parameters to be included in this analysis, such as the turbulence integral length scale which will be considered next.

2.3.2 Effect of length scale

In order to analyze the effect of length scale on turbulent boundary layers, four different values of L_u were examined besides L_u = 0.10m, specifically L_u = 0.02m; 0.05m and 0.07m. These values were defined knowing that the effect of free-stream turbulence was reported as being most significant when the length scale was of the same order of magnitude as the boundary layer (Hancock and Bradshaw, 1983). The length scale should also be large enough to perturb the boundary layer. In this study, the boundary layer thickness at $x = L$ with no free-stream turbulence intensity is δ = 35.2mm. Thus, most of the length scales analyzed here were greater than the BL thickness, except for L_u = 0.02m.

It is also important to observe that with a decreasing initial L_u, the TKE decays faster (see Eq. (2.15) and (2.16)) and, therefore, higher values of TI need to be specified at the inlet until it is not feasible to attain the same leading edge TI as used in the cases with L_u = 0.1m. For instance, in order to achieve TI = 9.0% at the leading edge with L_u = 0.05m, TI_o must be around 26% and it would not be feasible to achieve leading edge TI of 12.6%, because not even specifying TI_o of 80% would result in leading edge TI of 12.6%. Note also that the decay expressions (Eq. (2.15) and (2.16)) are valid for TI_o of up to 30%. The viable cases and conditions are then presented below.

Table 2.3 -Inlet normalized turbulence conditions with varying leading edge TI values for U_o = 40m/s and L_u = 0.02m

TI at the leading edge (u'/U_o)	**TKE at the inlet (k_o/U_o^2)**	**ω at the inlet ($\omega_o L_{uo}/U_o$)**
2.0%	$0.2\text{x}10^{-2}$	3.9
5.8%	$13.2\text{x}10^{-2}$	116.5

Table 2.4 -Inlet normalized turbulence conditions with varying leading edge TI values for U_o = 40m/s and L_u = 0.05m

TI at the leading edge (u'/U_o)	**TKE at the inlet (k_o/U_o^2)**	**ω at the inlet ($\omega_o L_{uo}/U_o$)**
2.1%	0.1×10^{-2}	0.8
5.7%	2.1×10^{-2}	5.2
9.1%	10.2×10^{-2}	18.1

Table 2.5 – Inlet normalized turbulence conditions with varying leading edge TI values for U_o = 40m/s and L_u = 0.07m

TI at the leading edge (u'/U_o)	**TKE at the inlet (k_o/U_o^2)**	**ω at the inlet ($\omega_o L_{uo}/U_o$)**
2.1%	0.1×10^{-2}	0.5
5.8%	1.5×10^{-2}	2.5
9.0%	5.9×10^{-2}	6.9
12.7%	20.1×10^{-2}	18.1

The comparison between local skin friction for varying L_u while keeping $TI \approx 2.0\%$ is presented in Figure 2.17. The difference between $c_{f,x}$ values when comparing any of those cases is less than 0.1%. This is also true when TI ≈ 5.7%, as shown in Figure 2.18.

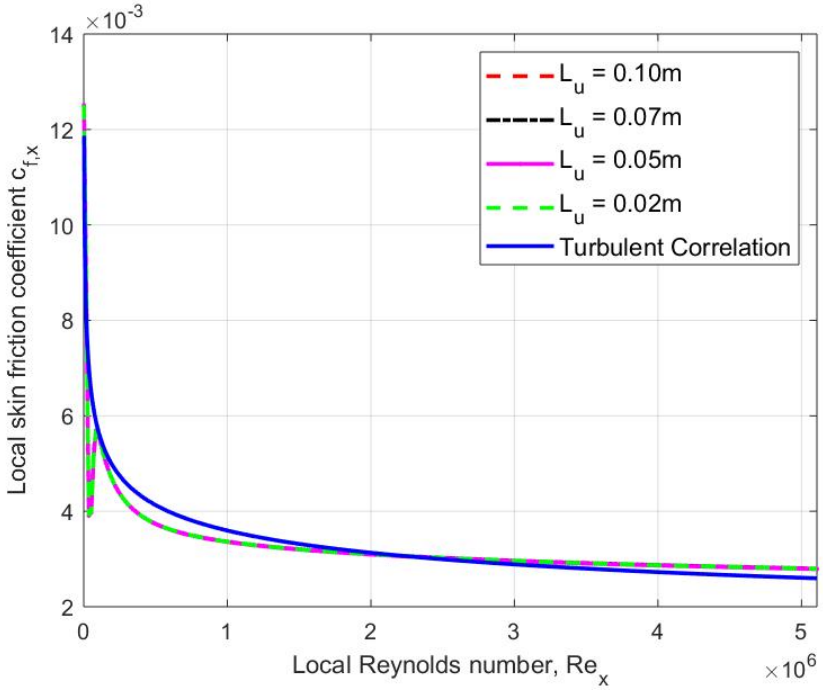

Figure 2.17 – Comparison of local skin friction ($c_{f,x}$) values with respect to local Reynolds number (Re_x) for different length scales (L_u) and TI = 2.0%

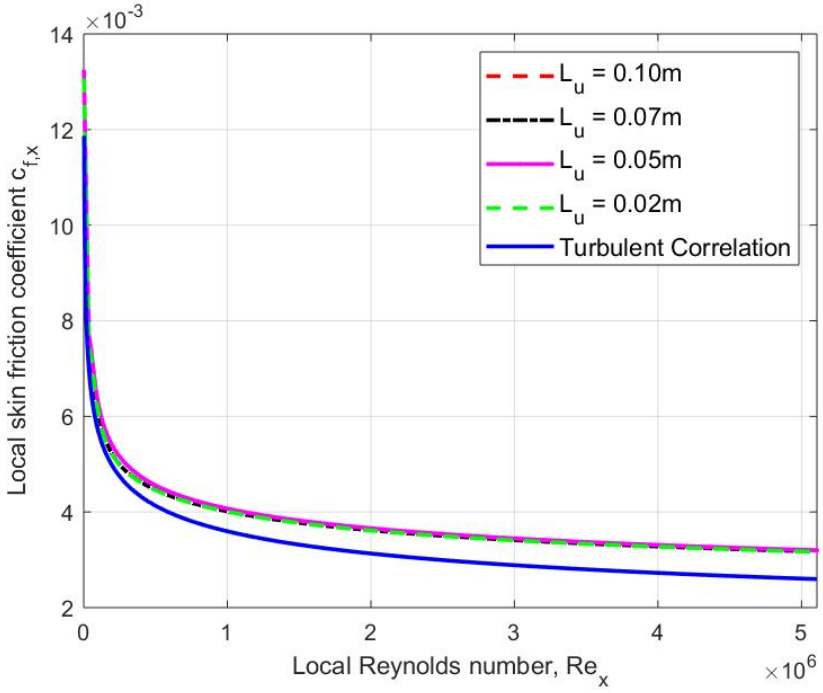

Figure 2.18 - Comparison of local skin friction ($c_{f,x}$) values with respect to local Reynolds number (Re_x) for different length scales (L_u) and TI = 5.7%

Comparing the cases with $TI \approx 9.0\%$ and 12.6%, the difference in $c_{f,x}$ values is less than 1% and 2%, respectively, which is a fairly small effect when compared to the skin friction enhancement produced by the increase in TI presented in the previous section. The total skin friction does not change significantly, with the difference of C_f when varying L_u while keeping TI the same being only up to 2% compared to the value for L_u = 0.1m for any given TI, as shown in Figure 2.19.

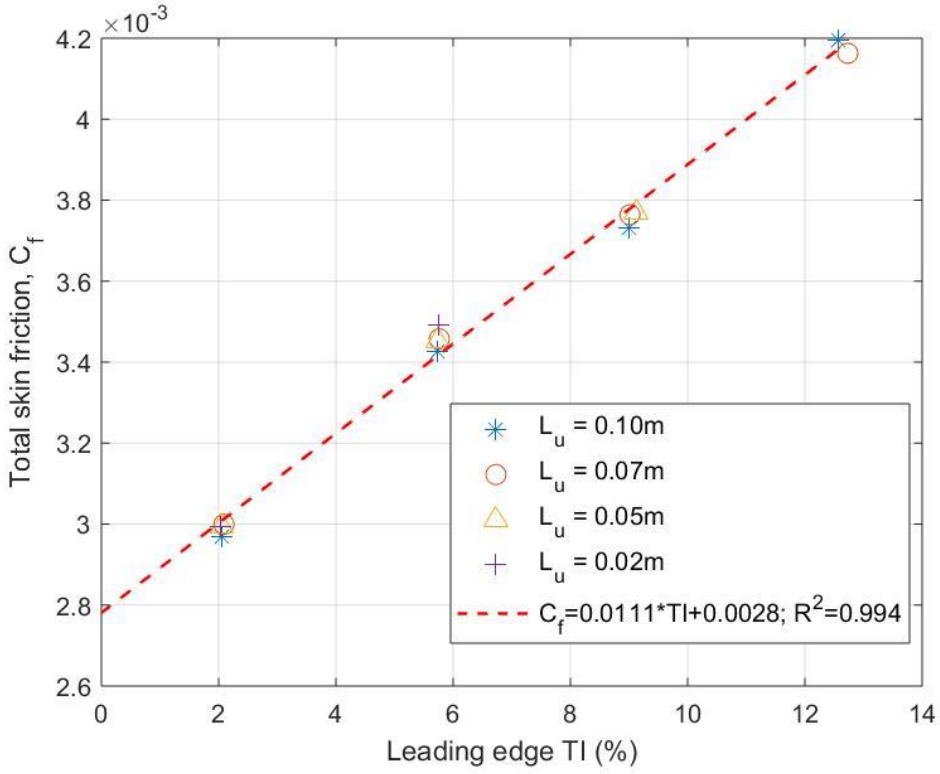

Figure 2.19 - Variation of total skin friction (C_f) with plate leading edge turbulence intensity (TI) while also varying L_u for Re_L=5.1x10^6

The linear expression derived including the variation in L_u now predicts the total skin friction in the case of a free-stream with no turbulence, as presented in Eq. (1.9), within 3%. Therefore, the effect of L_u on local and total skin friction, considering the range of L_u examined in the current study, was not significant. Previous studies by Hancock and Bradshaw (1983) and Blair (1983) stated that when the length scale is smaller than the BL thickness, the effect of FST on skin friction is smaller when compared to cases where both dimensions are of the same order. However, both studies varied L_u while also varying TI

and so it is not possible to isolate the effect of only one parameter. Besides that, they stated that lower values of L_u (smaller than the BL thickness) were only possible with lower *TI* levels (around 2%) or positioning the plate closer to the turbulence generator, which leads to higher TKE decay rates. In contrast, in the present study it was possible to achieve different values of L_u while keeping *TI* along the plate fairly uniform, as shown in Figure 2.20.

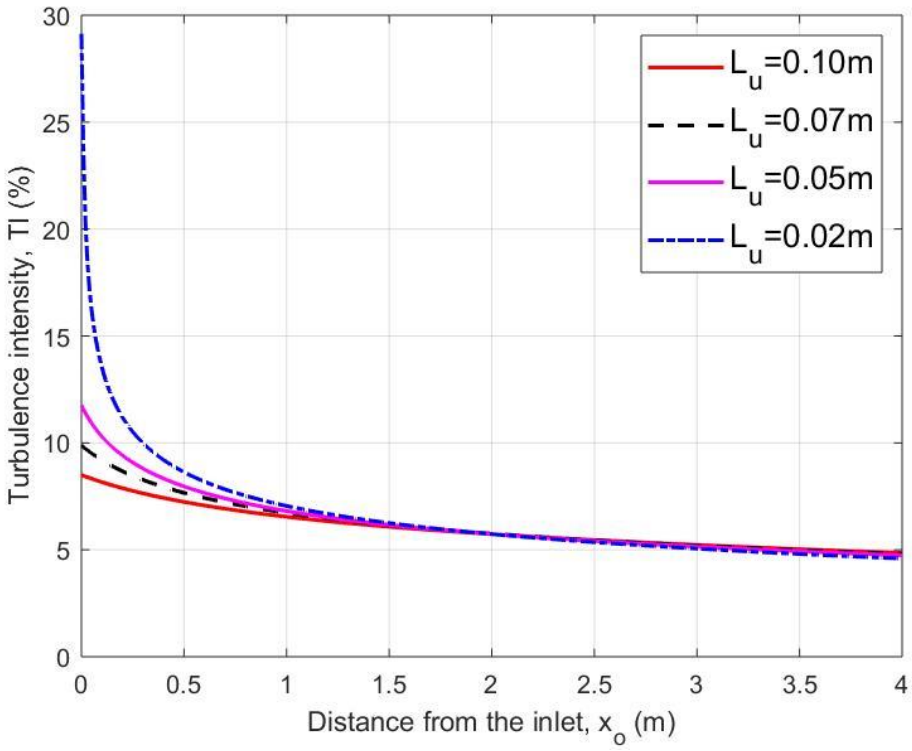

Figure 2.20 – Turbulence intensity decay with varying length scales (L_u) and leading edge *TI* = 5.7%

The percentage difference of TI between the plate leading and trailing edge is below 22% for any of these cases with varying L_u and keeping *TI* = 5.7%. For instance, the case that Hancock and Bradshaw (1983) examined with L_u being around 70% of the BL thickness at the trailing edge, the percentage difference of TI along the plate was up to 60%. The effect of L_u on skin friction observed by Hancock and Bradshaw (1983) may be due to the TI decay in the plate region.

As for the BL thickness, it does not vary by more than 1% for *TI* = 5.7%, as shown in Figure 2.21.

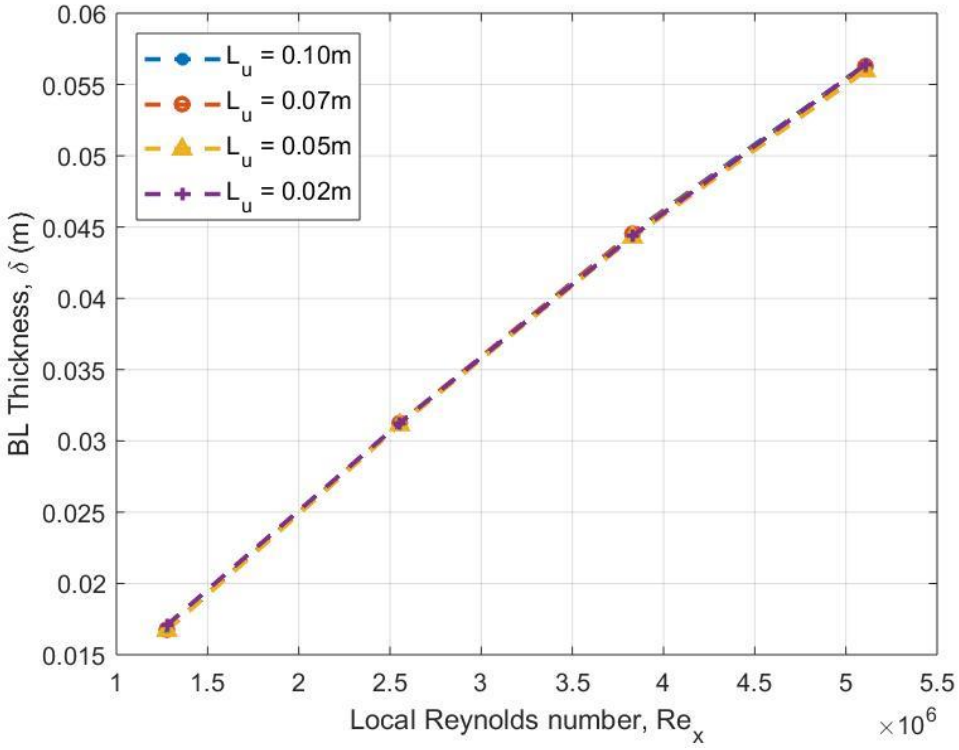

Figure 2.21 - Variation of BL thickness (δ) with varying length scale (L_u) for *TI* = 5.7%

This is the highest value of TI attained for all length scales, but the maximum variation of 1% in BL thickness, when comparing cases with different L_u at the same Re_x, is also true for the other *TI* values. It is also the highest difference in momentum thickness for *TI* = 5.7% when varying L_u as shown in Figure 2.22.

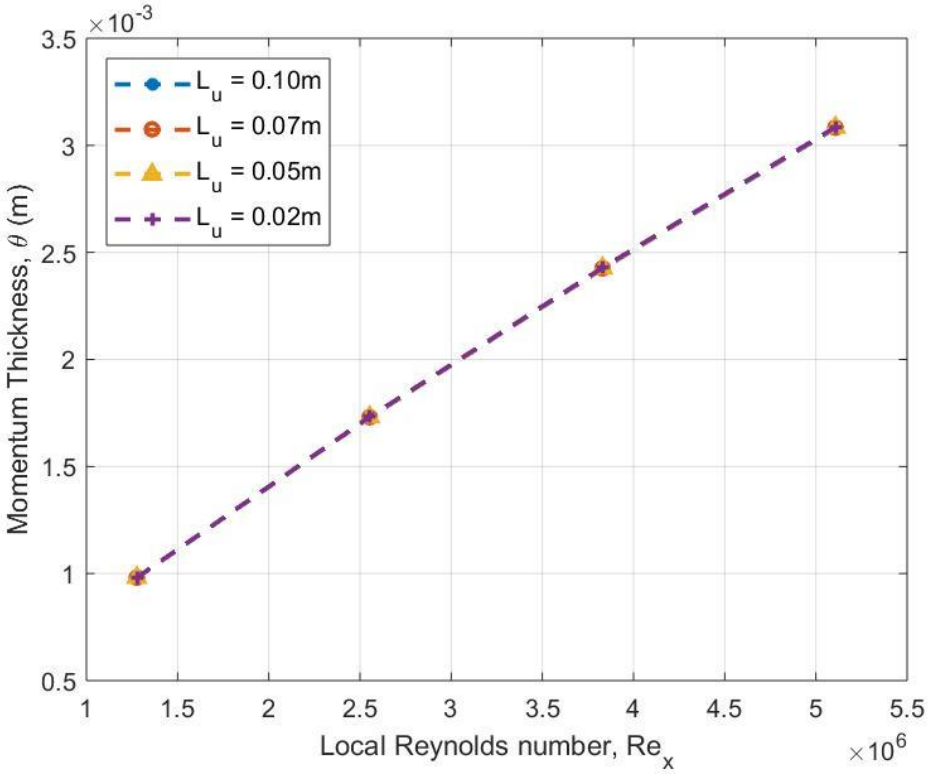

Figure 2.22 - Variation of momentum thickness (θ) with varying length scale (L_u) for TI = 5%

The maximum variation of momentum thickness, when comparing cases with different L_u at the same Re_x, is 1.5% when TI = 12.6%. Therefore, it is possible to conclude that the length scale range analyzed in the current study did not result in a significant effect on the skin friction values, BL thickness or momentum thickness. Next the effect of varying the free-stream velocity on local and total skin friction is examined.

2.3.3 Effect of Reynolds number

With the aim of analyzing the effect of Reynolds number, two more values of free-stream velocity were examined: U_o = 60m/s and 80m/s (Re_x and Re_L up to 1.02×10^7). These values ensured that the boundary layer would be fully turbulent while keeping the flow incompressible. The length scale was kept at 0.1m since it allows for a good range of TI. The conditions at the inlet were the same normalized conditions used for U_o = 40m/s and

presented in Table 2.2. The local skin friction when *TI* = 2% for these different free-stream velocities is presented in Figure 2.23.

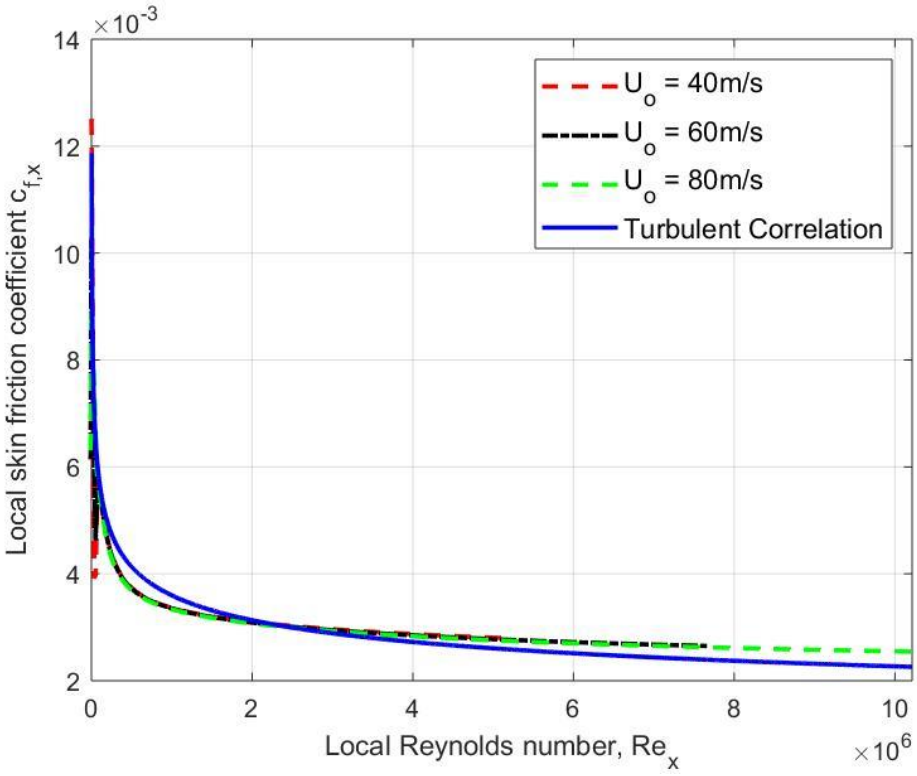

Figure 2.23 – Variation of local skin friction ($c_{f,x}$) with local Reynolds number (Re_x) for various free-stream velocities (U_o) for *TI* = 2% and L_u = 0.1m and comparison with turbulent correlation (Eq. 1.7)

The variation of local skin friction, when considering the same Re_x and *TI*, is at the most 1% when free-stream velocity is changed from 40m/s to 60m/s or 80m/s. Now there is a wider range of Re_x to be included in correlations. The total skin friction for these different free-stream velocities with varying *TI* is presented below.

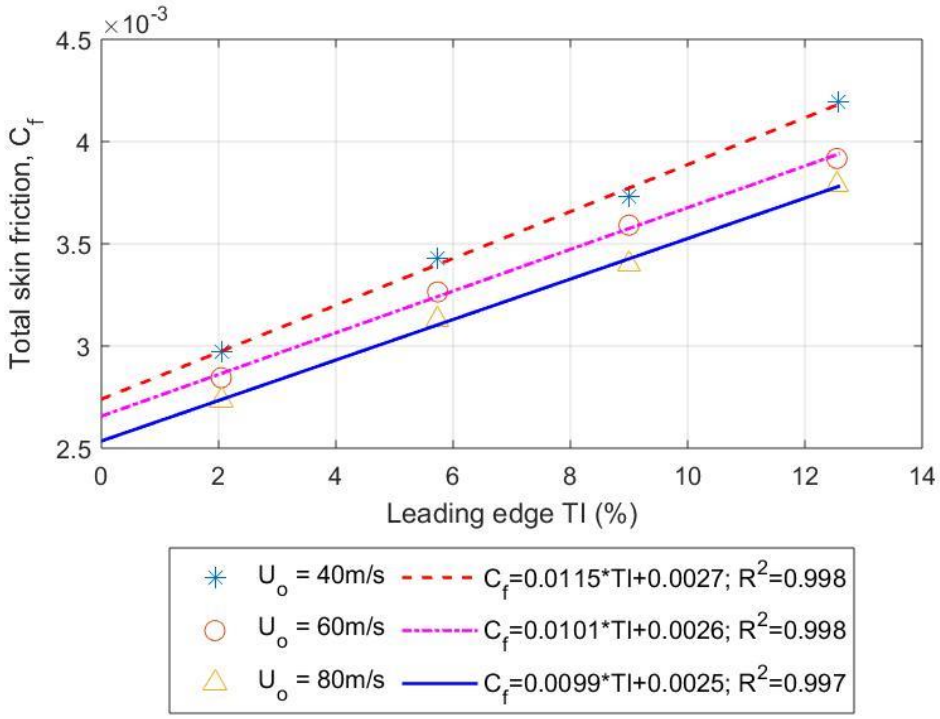

Figure 2.24 - Variation of total skin friction (C_f) with plate leading edge turbulence intensity (TI) while also varying U_o

The percentage increase in total skin friction is up to 41% for any of these free-stream velocities for TI = 12.6% with respect to TI = 2.0%. The prediction of C_f for a free-stream with no turbulence, using the linear correlations presented in Figure 2.24, is more accurate for higher free-stream velocities. While the prediction when U_o = 40m/s is within 14% of the empirical correlation for a turbulent flow (Eq. (1.9)), the value predicted for U_o = 80m/s is within 7% of the empirical C_f. Now it is possible to consider all the different parameters presented (TI, L_u and Re_x or Re_L) to develop a correlation for skin friction (both local and total), as well as for momentum thickness.

2.4 Development of correlations for skin friction and momentum thickness

Considering the parameters analyzed in the current study and the results from the different cases examined, it is possible to propose expressions for the local and total skin friction. Assuming the following equations:

$$c_{f,x} = b_1 {Re_x}^{-1/7}(1 + b_2 TI)\left(1 + {L_u}/{L_{uref}}\right)^{b_3} \tag{2.19}$$

$$C_f = B_1 {Re_L}^{-1/7}(1 + B_2 TI)\left(1 + {L_u}/{L_{uref}}\right)^{B_3} \tag{2.20}$$

The exponent of Re_x and Re_L were kept constant at -1/7 (or -0.143) so that the correlations are consistent with expressions for fully turbulent boundary layers with no free-stream turbulence (refer to Eq. (1.7) and Eq. (1.9)). The correlations were also defined with a linear dependence with respect to TI, as shown in Sections 2.3.1, 2.3.2 and 2.3.3. The dimension L_{uref} was defined as 0.1m since it is the largest integral length scale examined in the current study and it is also of the same order of magnitude of the largest eddy within a turbulent boundary layer in previous studies (Hancock and Bradshaw, 1983; Ames and Moffat, 1990). This reference value was also chosen to nondimensionalize the L_u value in a way that it would not be necessary to know the TBL characteristics, such as BL thickness.

Considering the local skin friction coefficient, the results from x/L = 0.25 to x/L = 1 may be taken as discussed before. There are more than 200 points in this region for each case and so an analysis was conducted to investigate the effect of considering a smaller number of points on the coefficient and exponents of Eq. (2.19).

Two points (x/L = 0.25 and x/L = 1) were initially considered and then equally spaced points between those two were added for a resulting number of 4, 8, 16, 32, 64 and 128 points. The case with four different locations is shown in Figure 2.25.

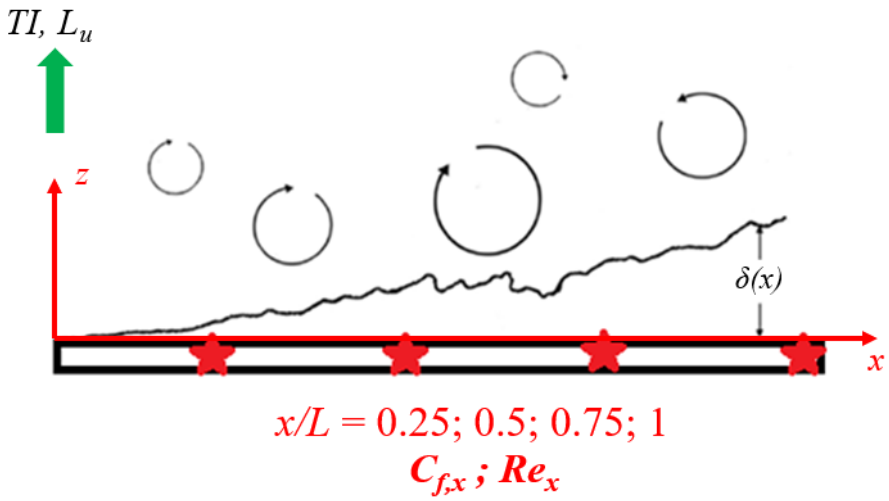

Figure 2.25 – Plate diagram with data locations used for local skin friction plots

The variation observed in the coefficient and exponents of Eq. (2.19) is presented in Figure 2.26.

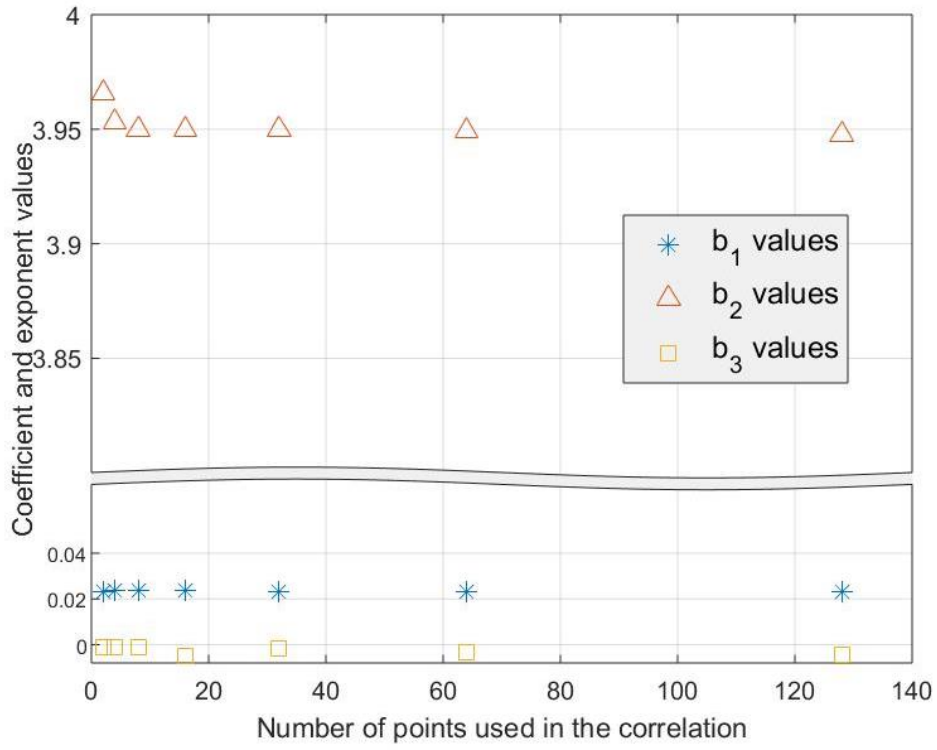

Figure 2.26 – Variation of coefficient and exponents values of local skin friction correlation (Eq. 2.20) with number of points being considered

The variation in coefficient or exponents is up to 4% when the number of points is increased from 2 to 4, but this variation is kept below 0.5% when the number of points is increased from 4 to any given value. Therefore, the correlations will be given considering the four locations presented in Figure 2.25.

The local skin friction expression factors are b_1 = 0.024, b_2 = 3.951 and b_3 = -0.001 (R^2 = 0.988). The comparison between the results derived from this expression and the numerical model results is presented in Figure 2.27.

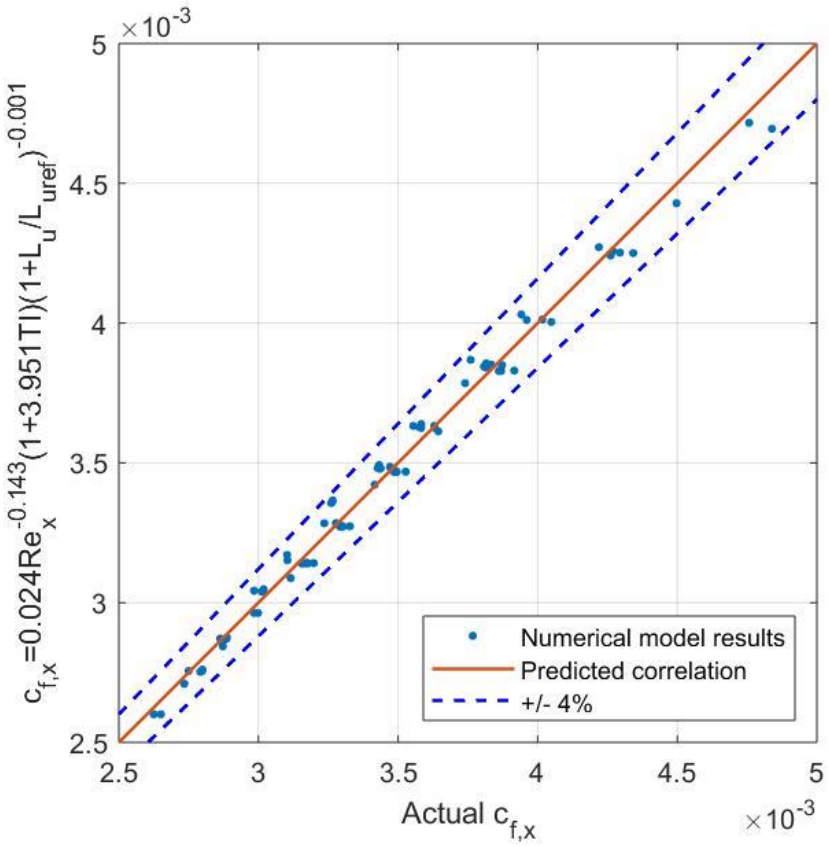

Figure 2.27 - Comparison of the local skin friction values obtained from the predicted correlation with the numerical results from cases with varying U_o and leading edge *TI* and L_u

The numerical results lie within ±4% of the derived expression. It is possible to observe that the length scale influence on skin friction is fairly small when compared to the other parameters, which agrees with the analysis presented before.

As for the total skin friction (Eq. 2.20), B_1 = 0.026, B_2 = 3.863 and B_3 = -0.019 (R^2 = 0.992). The numerical model results lie within ±3% of this correlation as shown in Figure 2.28.

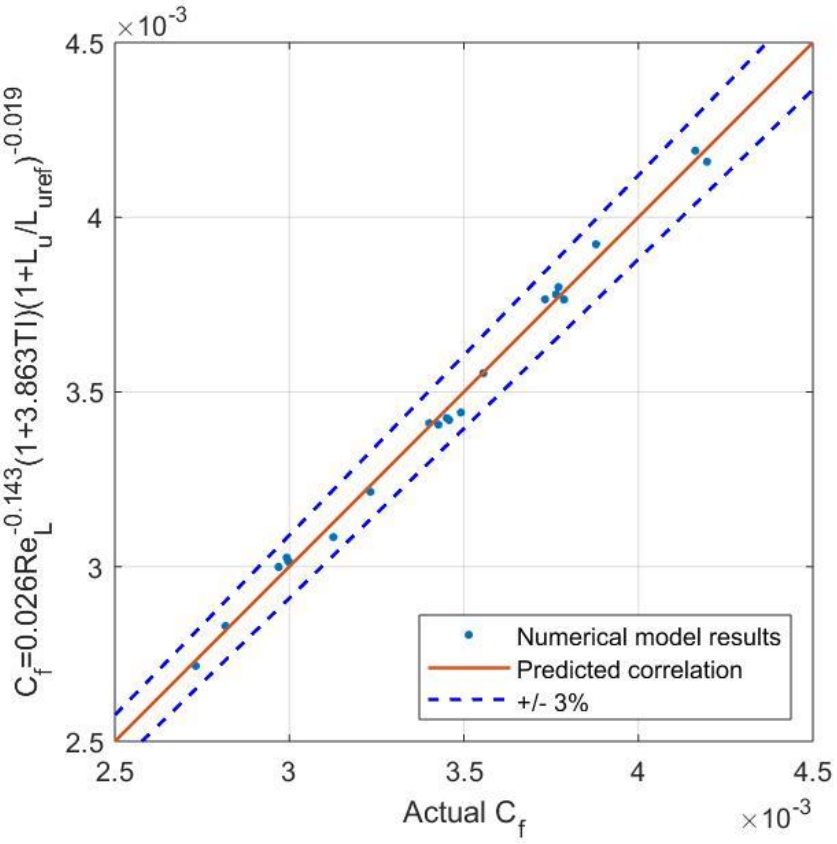

Figure 2.28 - Comparison of the total skin friction values obtained from the predicted correlation with the numerical results from cases with varying U_o and leading edge *TI* and L_u

The qualitative behaviour of skin friction with varying free-stream velocity, turbulence intensity and length scale agree with previous studies (Kondjoyan et al., 2002). One important aspect regarding the present work is that the correlations shown here were derived for cases where the plate was positioned in regions of almost uniform turbulence conditions. Taking the values of TI outside the boundary layer (z = 0.15m), the maximum percentage difference observed of the free-stream turbulence from the plate leading to the trailing edge was 25% (for the case when *TI* = 12.55%).

Other cases were then examined by positioning the plate leading edge (LE) closer to the inlet (x_o = 1.5m and x_o = 1.0m). These simulations were used to check the validity of the derived expressions for higher TKE decays. For these cases, U_o = 40m/s and L_u = 0.1m. The inlet turbulence conditions are presented below.

Table 2.6 – Inlet turbulence conditions for cases with the plate leading edge at x_o = 1.5m

TI at the leading edge (u'/U_o)	**TKE at the inlet (k_o/U_o^2)**	**ω at the inlet ($\omega_o L_{uo}/U_o$)**
2.0%	0.1×10^{-2}	0.4
5.4%	0.8×10^{-2}	1.5
9.8%	3.9×10^{-2}	3.9
14.4%	12.3×10^{-2}	86.3

Table 2.7 - Inlet turbulence conditions for cases with the plate leading edge at x_o = 1.0m

TI at the leading edge (u'/U_o)	**TKE at the inlet (k_o/U_o^2)**	**ω at the inlet ($\omega_o L_{uo}/U_o$)**
2.0%	0.1×10^{-2}	0.4
5.2%	0.6×10^{-2}	1.2
8.7%	2.1×10^{-2}	2.5
11.5%	4.3×10^{-2}	3.8
21.6%	27.6×10^{-2}	12.9

The comparison of the results of local and total skin friction with the correlations presented are shown in Figure 2.29 and Figure 2.30 respectively.

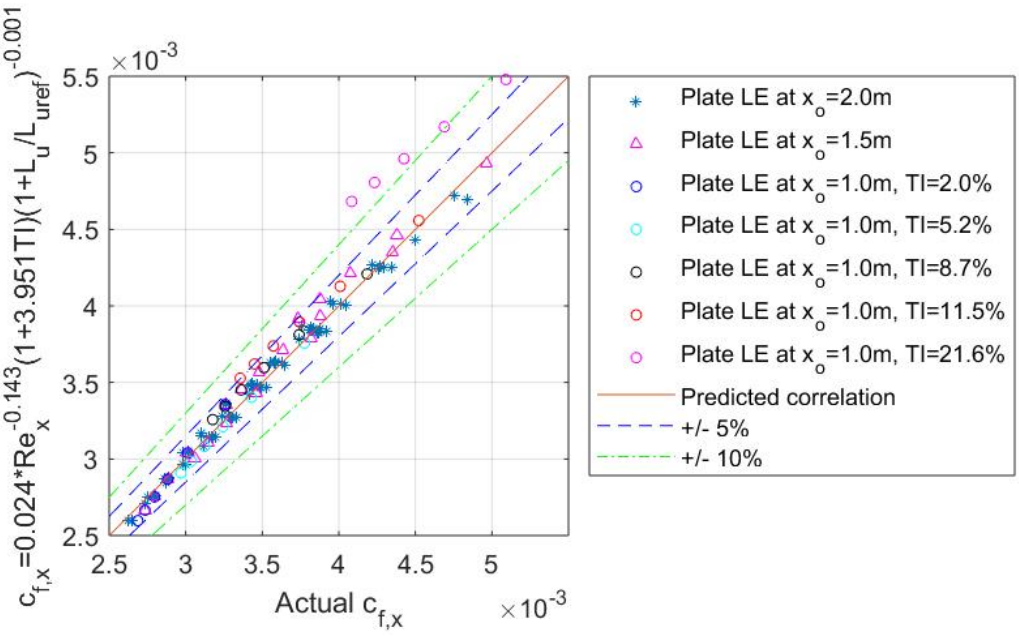

Figure 2.29 - Comparison of the local skin friction values obtained from the predicted correlation with the numerical results from cases with varying leading edge positions

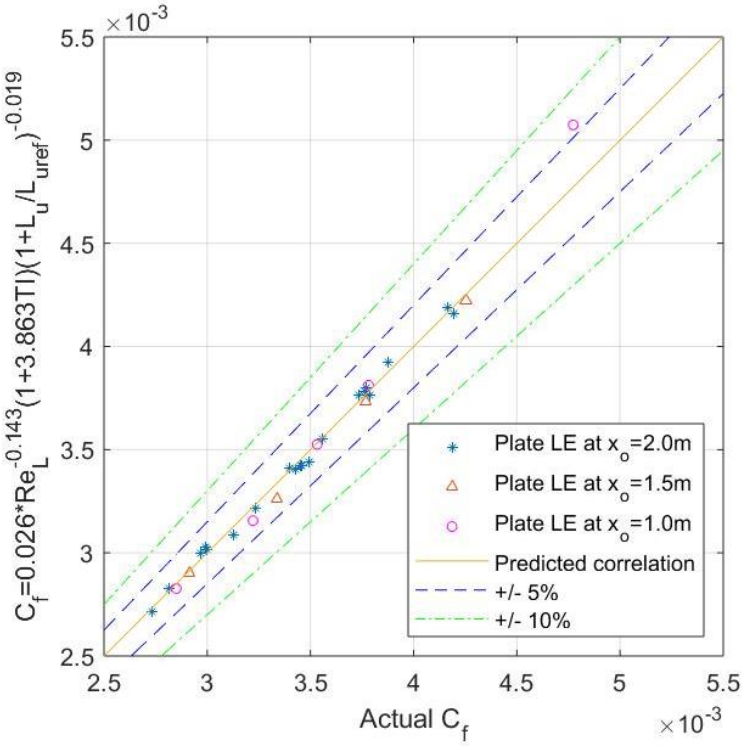

Figure 2.30 - Comparison of the total skin friction values obtained from the predicted correlation with the numerical results from cases with varying leading edge positions

When the plate LE is positioned at x_o = 1.5m, the percentage difference of TI from the LE to the trailing edge is up to 35.6% (for the case when *TI* = 14.4%). The local skin friction in this case lies within ±6% of the predicted correlation, but the total skin friction is still within ±4% of the predicted values. However, for the cases with the plate leading edge at x_o = 1.0m, the percentage difference of TI could be up to 53.8% (for the case when *TI* = 21.6%), resulting in local skin friction values lying within more than 10% of the predicted correlation, but the total skin friction is still within 7% of the predicted values.

For higher TKE decays, the skin friction resulting from the correlations is higher than the actual numerical result. The reason for this is that the equation assumes an almost uniform region of turbulence conditions, but the plate, on average, is submitted to a lower level of TI since the turbulence intensity decays faster. The free-stream conditions at the plate region are then an important factor for the correlation validity. The present equation for local skin friction coefficient is valid to within ±10% when the percentage difference of free-stream TI between the plate LE and TE is within 25%. The correlation for total skin friction coefficient seems less sensitive than the equation for $c_{f,x}$ to higher TKE decays and it is valid to within ±7% for free-stream TI percentage difference between the LE and TE of up to 54%.

It is also useful to determine a correlation for momentum thickness as mentioned before. Assuming then the following expression:

$$\frac{\theta}{x} = b_1 Re_x^{-0.143}(1 + b_2 TI)\left(1 + {L_u}/{L_{uref}}\right)^{b_3} \tag{2.21}$$

when b_1 = 0.014, b_2 = 2.592, b_3 = -0.026 (R^2 = 0.977), the numerical model results lie within ±8% of the correlation, as shown in Figure 2.31.

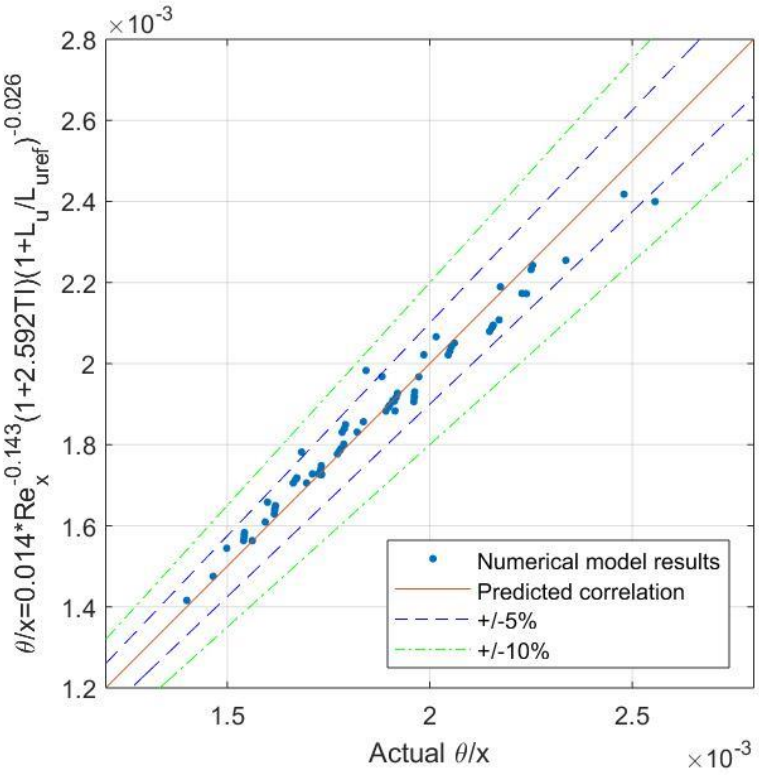

Figure 2.31 - Comparison of the momentum thickness values obtained from the predicted correlation with the numerical results from cases with varying *TI*, L_u and Re_x

Next, an investigation of whether the deduced expressions for $c_{f,x}$, C_f and θ/x in terms of Re_x (or Re_L), *TI* and L_u are a good representation of the data from previous work is presented.

2.5 Comparison with previous studies

Analyzing the correlations for local and total skin friction derived from the numerical model cases expressed by Eq. (2.19) and (2.20), it is possible to observe that the enhancement in skin friction is greatly influenced by the increase in TI. Furthermore, although the length scale affects the variation in skin friction, with lower values of length scale causing less perturbation in the results, this difference was only up to 2% in the L_u range examined in this study.

Another important aspect of the derived correlations is that parameters dependent on the developed boundary layer such as BL thickness or momentum thickness were not included,

unlike the equations presented by Hancock and Bradshaw (1983), Blair (1983), Ames and Moffat (1990). Therefore, to estimate skin friction it is not necessary to have knowledge of boundary layer characteristics *a priori*.

The comparison between the local skin friction results from various studies and the predicted values using Eq. (2.19) is presented in Figure 2.32.

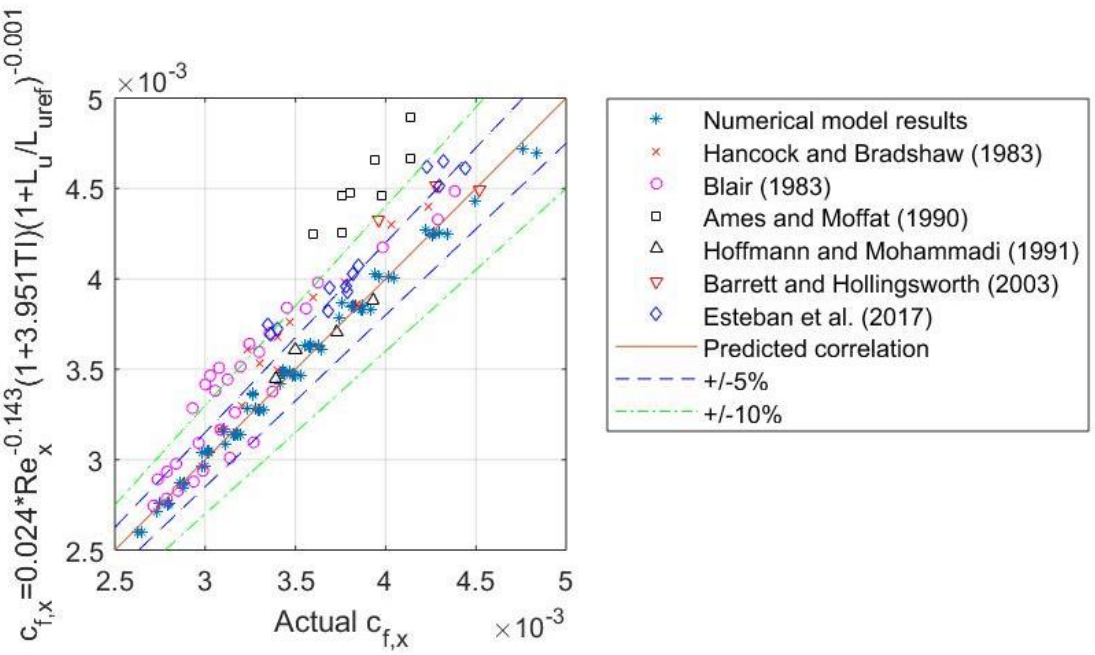

Figure 2.32 – Comparison between the local skin friction values from previous studies and those predicted using the proposed correlation

The correlation predicts most values of local skin friction within ±10%. The data included were collected in points where the boundary layer was fully turbulent, with the range of Re_x from $5x10^5$ to $6x10^6$. Since laminar-turbulent transition occurs earlier in flows subjected to FST, the BL is fully turbulent within this range.

In addition, the *TI* varies from 1.3% to 17%. These values were taken at the leading edge of the plate and were estimated from equations or plots of TKE decay presented by the authors. The local skin friction values that were not predicted by the correlation to within 10% are mostly due to higher TKE decays between the plate LE and TE. For instance, Blair's experimental data that are further away from the proposed equation (within 14%)

were obtained for TI = 7.7%, but with a TI percentage difference from the leading to the trailing edge of the plate (TI_{dif}) of approximately 60%. As for the results from Ames and Moffat (1990), TI = 17% and the difference (TI_{dif}) is even higher (from 57% to 96%), and the predicted values are even less accurate (within up to 21%). This may be due to the fact that the estimated TI is higher, resulting in an overpredicted value of $c_{f,x}$, since the correlation was derived for regions where the free-stream turbulence is almost uniform in the plate region. Overall, it is possible to conclude that the correlation provides a good prediction of local skin friction when the plate is submitted to free-stream turbulence intensity levels that vary by less than 25% over the plate region.

Additionally, considering Eq. (2.19) and substituting the leading edge TI by the local free-stream TI (TI_x), there is still a large scatter between the predicted correlation and the published experimental data, as shown in Figure 2.33.

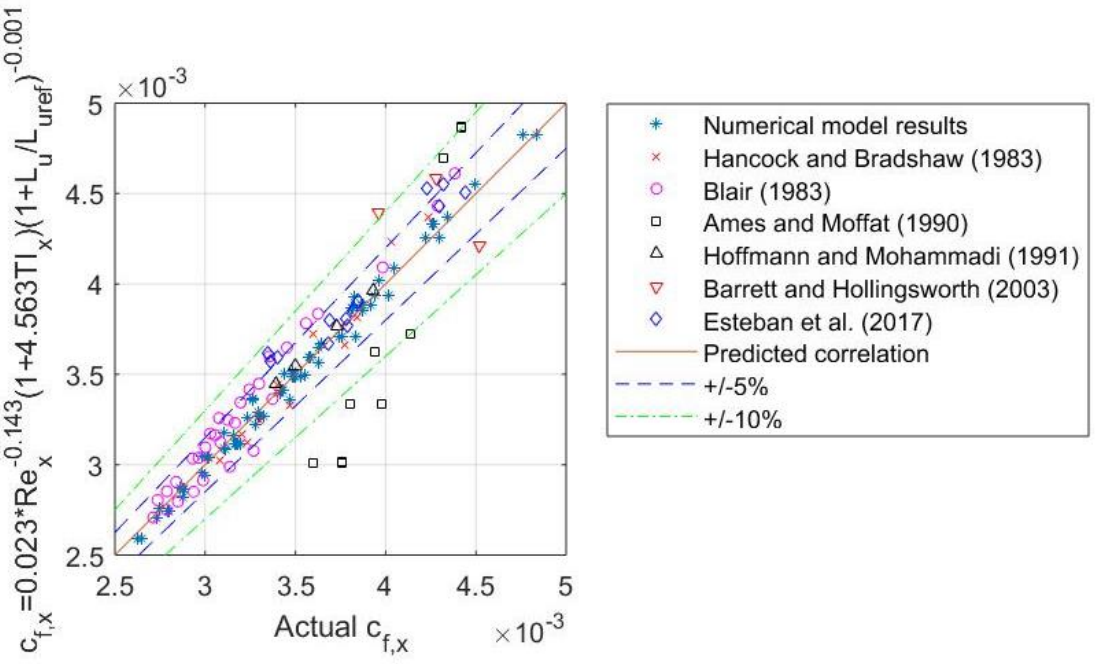

Figure 2.33 - Comparison between the local skin friction values from previous studies and those predicted using the proposed correlation with local TI (TI_x)

These results indicate that the local skin friction coefficient is influenced not only by the TI decay over the plate region but also by the turbulence conditions at which the boundary

layer starts to develop. For instance, the $c_{f,x}$ values from Ames and Moffat (1990) were underpredicted by up to 20%, since the local TI values in these cases (from 3 to 5%) were much lower than the leading edge TI (TI = 17%). In the current study, similar local conditions of TI (TI_x = 5%) were attained, for the same range of Re_x (from 1.5x10^6 to 3.0x10^6), for TI = 5.7%. Furthermore, substituting the leading edge TI in Eq. (2.19) by the average of the turbulence intensity values at the plate LE and TE ($TI_{av} = {(TI_{LE} + TI_{TE})}/{2}$) results in most $c_{f,x}$ values from previous studies being predicted within ±5%, as shown in Figure 2.34.

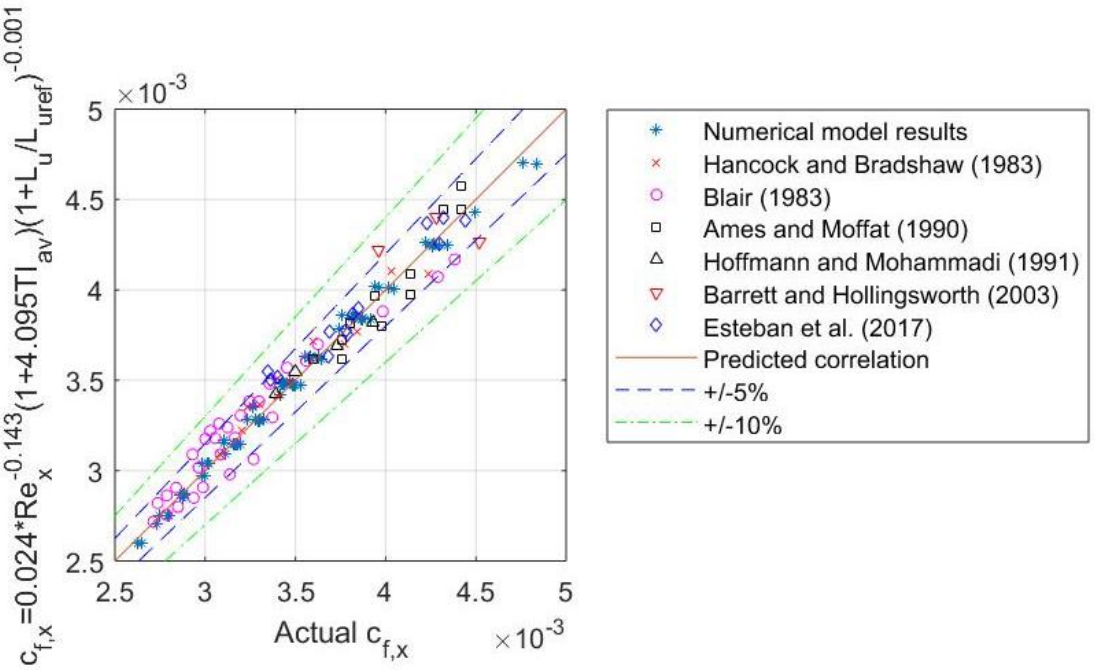

Figure 2.34 - Comparison between the local skin friction values from previous studies and predicted using the proposed correlation with average TI (TI_{av})

Therefore, the use of the mid-value of TI between the LE and TE of the plate improves the collapse of data from previous studies and TI_{av} was used in the correlations for C_f and θ. As for the total skin friction values, experimental results are generally presented in one location at the plate and so only results from three studies, as shown below, were included in the validation, since they present four or more different locations downstream. Additionally, it was necessary to find the best curve that fitted the $c_{f,x}$ data. Considering a

case with a given set of turbulence conditions (TI_{av} and L_u), the curve $c_{f,x} = A_1 x^{-0.143}$ (refer to Eq. (2.19)) was a good approximation ($R^2 > 0.95$ for all cases). Then, an integration of this curve was performed from x = 0.5m to x = 2.0m because it was a common range when comparing the studies and it would be difficult to assume $c_{f,x}$ before x = 0.5m since it is the region where $c_{f,x}$ varies the most.

The comparison of the C_f computed from the resulting correlation (Eq. 2.20) and the values from previous studies estimated using the method presented is shown in Figure 2.35.

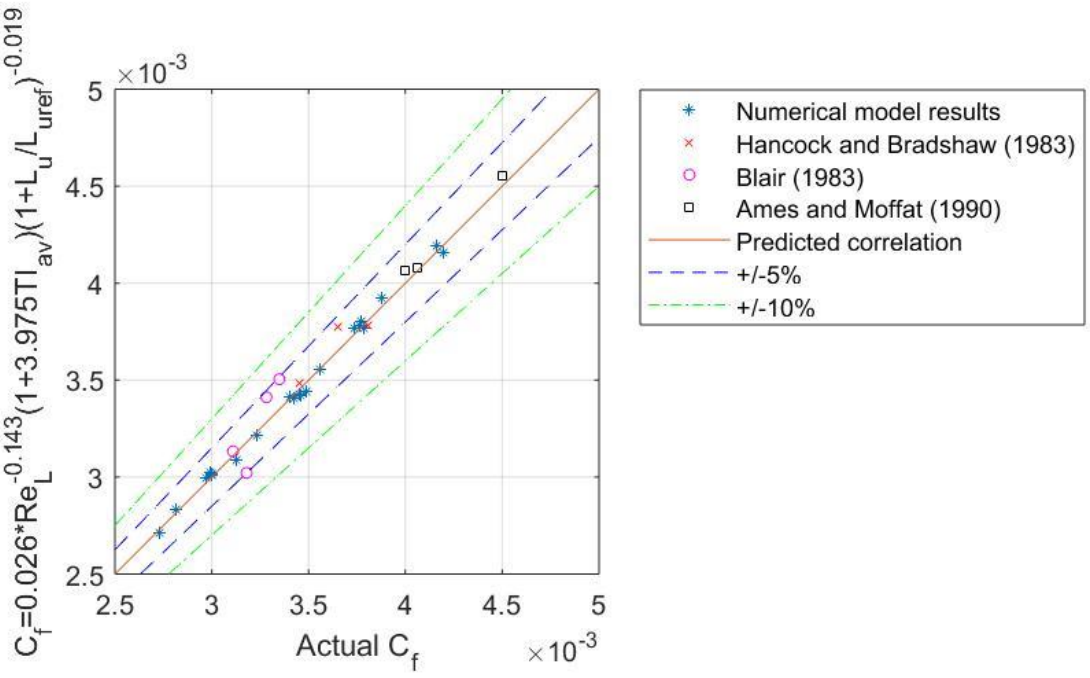

Figure 2.35 - Comparison between the estimated total skin friction values from previous studies and predicted using the proposed correlation with average TI (TI_{av})

The estimated C_f values lie within ±5% of the correlation, even for TI_{dif} of up to 96%. The equation would then be a good estimate of total skin friction for TI of up to 16% and fully turbulent boundary layers.

Regarding momentum thickness, the proposed correlation estimates values within approximately ±10% of those presented by the studies, as shown in Figure 2.36.

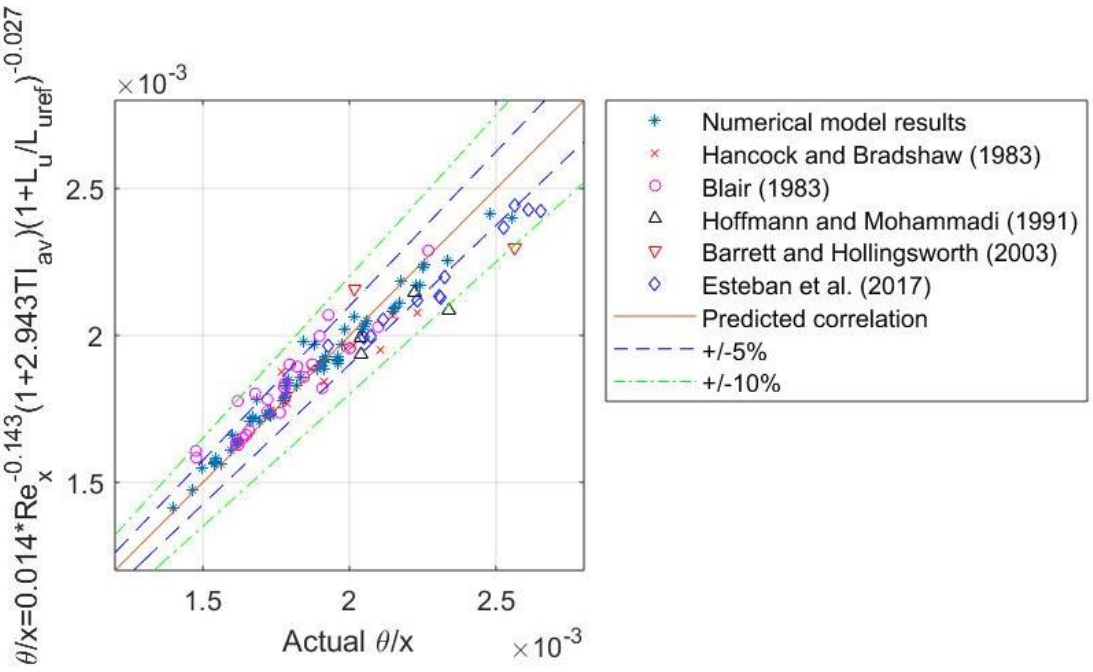

Figure 2.36 - Comparison between the estimated momentum thickness values from previous studies and those predicted using the proposed correlation with average TI (TI_{av})

The momentum thickness correlation provides a good estimate (within ±10%) for cases where TI is up to 13% and TI_{dif} is up to 60%. The effect of L_u on $c_{f,x}$, C_f or θ as presented in the proposed correlations is not significant. Although Hancock and Bradshaw (1983) proposed an expression showing a more significant effect of L_u on $c_{f,x}$ when compared to the current study, other authors (Baskaran et al., 1989; MacMullin et al., 1989; Ames and Moffat, 1990) showed that the correlation from Hancock and Bradshaw (1983) was not capable of predicting the increase in $c_{f,x}$ they observed and there was a large scatter between their data and the predicted values from the expression proposed by Hancock and Bradshaw (1983). Furthermore, the results from Hancock and Bradshaw (1983) lie within ±5% of the correlation proposed in the current work (refer to Eq. (2.19)), but the current numerical model results correlate linearly with the parameter presented by Hancock and Bradshaw (1983) only up to $HB \approx 0.25$ and the local skin friction enhancement is greatly underpredicted by their correlation (refer to Eq. (2.3)) by up to 150%, as shown in Figure 2.37. Note that there is a large scatter between the results from the current study and the values obtained from a linear fit with respect to the HB factor.

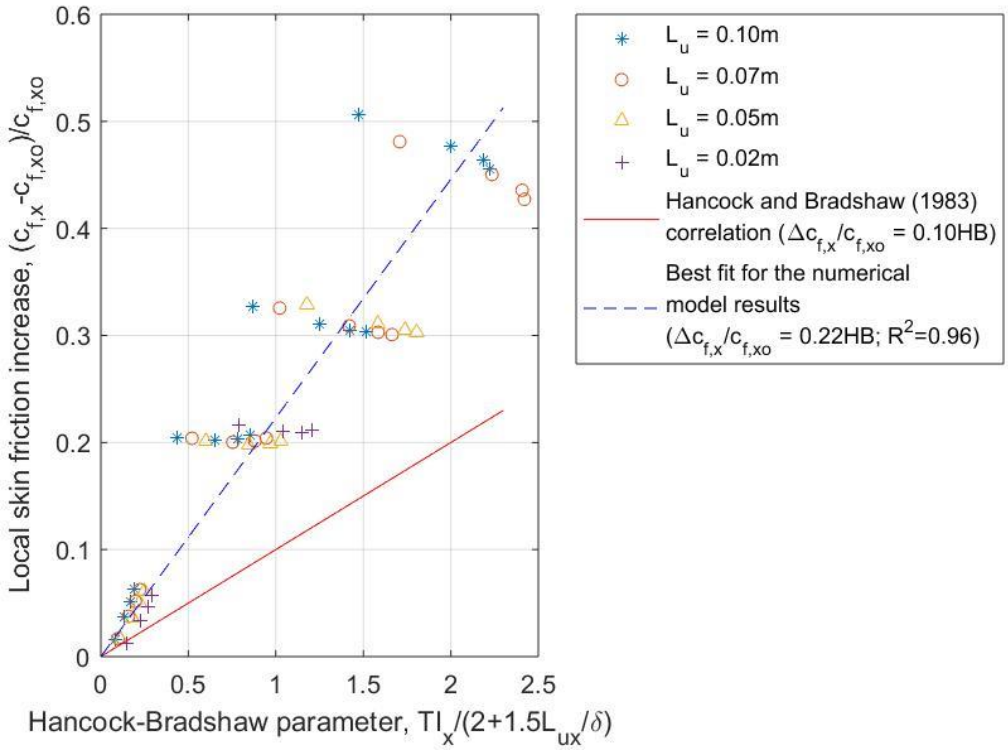

Figure 2.37 – Comparison between the local skin friction increase and the correlating parameter proposed by Hancock and Bradshaw (1983)

Additionally, Blair's (1983) correlation (refer to Eq. (2.4)) reduces to the Hancock and Bradshaw's (1983) expression for the cases examined in the current study, since the momentum-thickness Reynolds number (Re_θ) is always greater than 2000. Considering the expression proposed by Ames and Moffat (1990) (refer to Eq. (2.5)), there is still a large scatter between the results from the current investigation and the values obtained from their correlation, as shown in Figure 2.38. Note that the expression from Ames and Moffat (1990) predicts a negative increase in local skin friction for TI = 0% and the equation was only examined by the authors for TI_x > 2%.

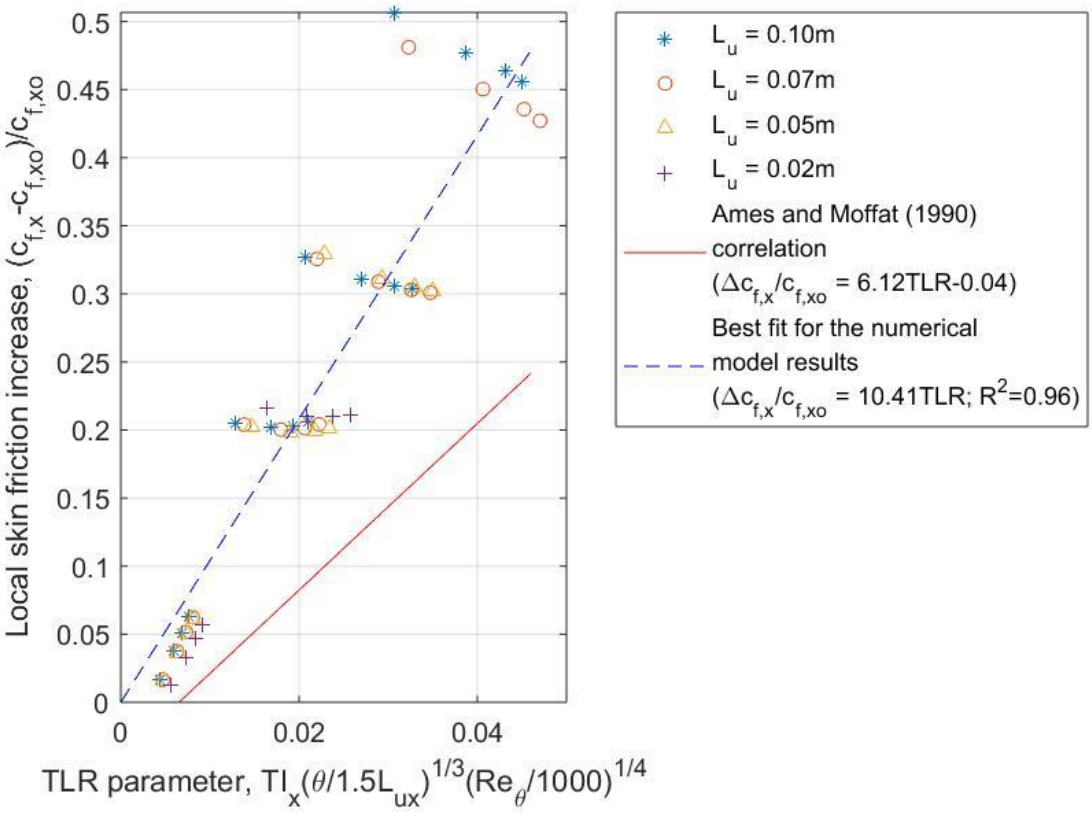

Figure 2.38 - Comparison between the local skin friction increase and the expression proposed by Ames and Moffat (1990)

The $c_{f,x}$ increase is underpredicted by Ames and Moffat's expression by up to 140%. The local skin friction increase also does not correlate linearly with the parameter proposed by Ames and Moffat (*TLR*) and the results lie within up to 45% from the best fit for the numerical model results using the *TLR* parameter. The differences observed between the local skin friction increase and the values predicted by previous correlations may be due to various factors. For instance, the local skin friction coefficient for the current numerical model is underpredicted in the case with low free-stream turbulence since the flow is not fully turbulent. Furthermore, in some cases from previous studies the local value of turbulence intensity, especially for cases where TI_x>5%, was much lower than the leading edge TI, e.g., TI_x values of 5% in studies from Hancock and Bradhsaw (1983), Blair (1983) and Ames and Moffat (1990) were attained in cases where TI_{dif} was 57%, 60% and 96%, respectively.

Additionally, the results from the current study correlate better with the simple expression proposed by Simonich and Bradshaw (1978) if the constant *A* is increased from 2.0 to 4.1 (refer to Eq. (2.2)), particularly for TI_x between 5.0% and 9.5%, as shown in Figure 2.39.

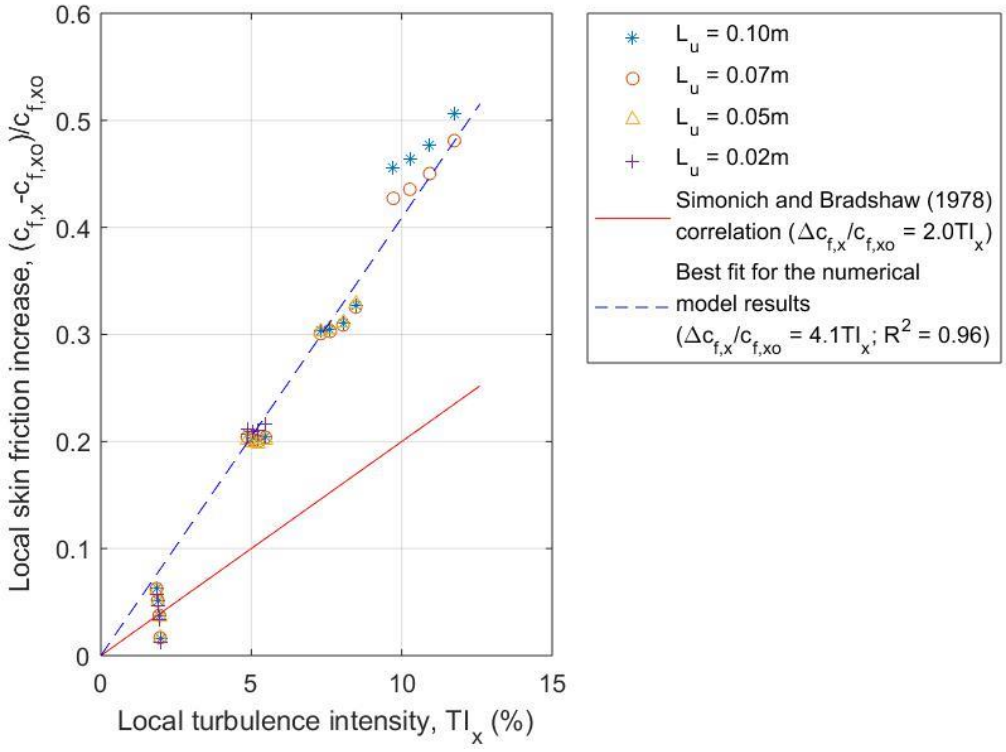

Figure 2.39 - Comparison between the local skin friction increase and the expression proposed by Simonich and Bradshaw (1978)

However, the local skin friction increase is not linearly related to TI_x for $TI_x \approx 2.0\%$ and is within 15% of the best linear fit for the numerical model results for $TI_x > 9.5\%$. The total skin friction increase observed in the current study can be expressed by a linear relation with respect to the leading edge TI, as shown in Figure 2.40, but the constant *A* must be increased from 2.0 to 3.7. Additionally, the total skin friction increase for $TI = 2.0\%$ is overpredicted by 25%.

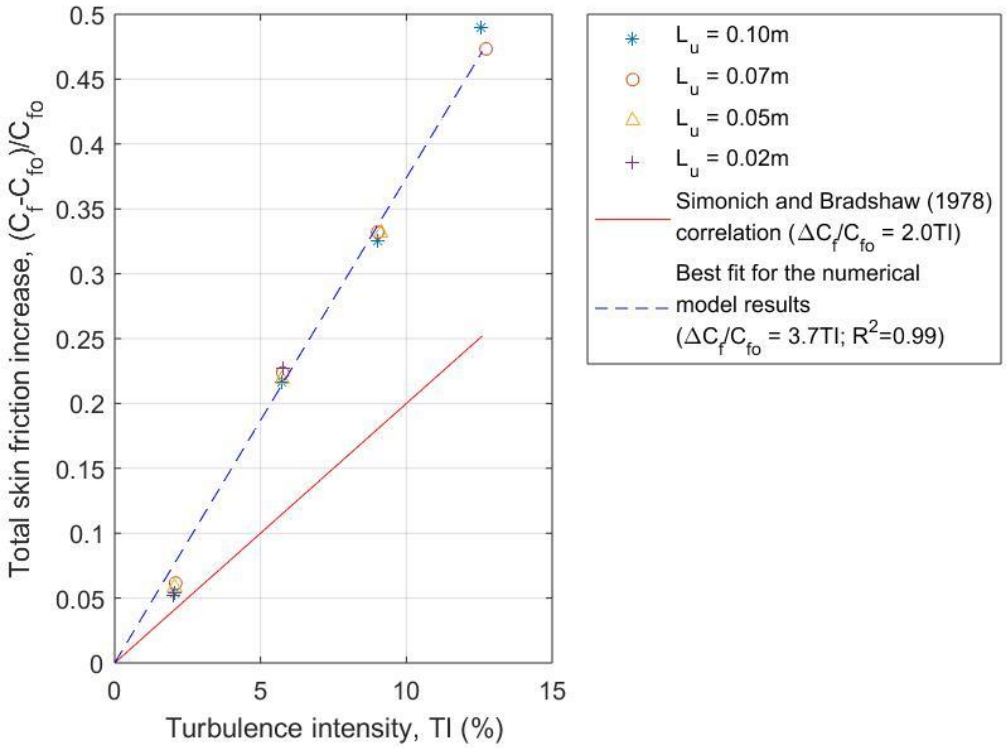

Figure 2.40 - Comparison between the total skin friction increase and the expression proposed by Simonich and Bradshaw (1978)

Note that the linear fit presented in Figure 2.40 is only valid if the leading edge TI is used in the expression and if the percentage difference of turbulence intensity from the plate leading edge and trailing edge is below 25%. Furthermore, Simonich and Bradshaw's (1978) expression was deducted for the local skin friction increase and considered the local value of turbulence intensity, as presented in Figure 2.39. It would be necessary to consider cases with higher TKE decay in the plate region to determine if the total skin friction increase would still be expressed by a linear relation with respect to TI (or TI_{av}). Additionally, the leading edge turbulence intensity in the current study was up to 12.6% and it would be useful to analyze the total skin friction increase for higher values of TI.

Having examined the effect of different parameters (TI, L_u and Re_x or Re_L) on local and total skin friction coefficients and momentum thickness, as well as the correlations for $c_{f,x}$, C_f and θ derived from the current study and validated with data from previous experiments, the next section summarizes the main findings and conclusions from the present work.

2.6 Summary and conclusions

2.6.1 Summary

The overall results from this numerical study can be summarized as follows:

- The SST k-ω model with Low-Re correction provided a good prediction of local skin friction and velocity profiles for turbulent BL regions, although it does not predict accurately the laminar-turbulent transition. This model also provided correct TKE decay when modified as recommended by Sarkar (2018). This is then the most suitable model for this problem once it is focused on turbulent boundary layers and on regions of almost uniform turbulence conditions at the free-stream.

- The local skin friction and mean velocity profiles for a free-stream with low turbulence agree well with the theoretical correlations (refer to Eq. (1.7) and Eq. (2.17)) and, therefore, the numerical model is a good representation of a flow over a flat plate.

- Local and total skin friction are influenced by flow conditions, e.g., Re_x or Re_L, TI and L_u. These parameters were chosen for the development of correlations that could predict the value of skin friction coefficient for different free-stream conditions.

- Skin friction enhancement is observed with increasing TI, as reported in previous studies (Kondjoyan et al., 2002). The effect of L_u on skin friction is less significant when compared to the other parameters. Some of the previous studies (Hancock and Bradshaw, 1983; Blair, 1983) reported that the effect of L_u on skin friction was more significant when L_u was of the same order of magnitude as the BL thickness. However, the turbulence conditions at the leading edge or the TI decay along the plate were not examined by those studies. Furthermore, the correlations for local and total skin friction coefficient derived in the current study predicted the results from Hancock and Bradshaw (1983) and Blair (1983) within 5%.

- The following correlations were derived:

$$c_{f,x} = 0.024{Re_x}^{-0.143}(1 + 4.095TI_{av})\left(1 + {L_u}/{L_{uref}}\right)^{-0.001}$$

$$C_f = 0.026{Re_L}^{-0.143}(1 + 3.975TI_{av})\left(1 + {L_u}/{L_{uref}}\right)^{-0.019}$$

$$\frac{\theta}{x} = 0.014{Re_x}^{-0.143}(1 + 2.943TI_{av})\left(1 + {L_u}/{L_{uref}}\right)^{-0.027}$$

These expressions were examined for Re_x and Re_L of up to 1.0x10^7, length scales varying from 0.02m to 0.13m and *TI* from 0.1% to 21.6%. Considering the values of TI_{av} provided a better collapse of the data when compared to *TI* or TI_x.

- The values of $c_{f,x}$ and C_f were predicted within ±5% for the conditions mentioned above. The derived expressions for local and total skin friction may be applied when the percentage difference of free-stream turbulence intensity between the LE and TE of the plate vary by up to 96%. The momentum thickness correlation was examined only for TI_{dif} of up to 60% and the values of θ were predicted within ±10%.

2.6.2 Conclusions

A numerical model was implemented to evaluate the influence of free-stream turbulence on turbulent boundary layers. The simulations were performed using the SST k-ω model with Low-Re correction, because it provided a good prediction of turbulent boundary layers and TKE decay. The turbulent boundary layer was then validated with theoretical correlations for BL when there is no free-stream turbulence.

Various numerical studies were examined with different FST conditions. It was possible to investigate cases with a *TI* range of 0.1 – 21.6%, L_u from 0.02m to 0.10m, Re_x of up to 1.0x10^7 and Re_L from 5.1x10^6 to 1.0x10^7. These parameters were then included in correlations for $c_{f,x}$ and C_f that were validated with previous studies. This provided new insights into the effect of different free-stream conditions on turbulent boundary layers, especially the TKE decay from the leading to the trailing edge of the plate.

It was demonstrated that the TKE decay over the plate region is an important factor to be considered in the validity of correlations. The current study was focused on positioning the plate in regions where free-stream turbulence intensity varied only by 25% at most. Despite its limitations, the derived correlations are a good tool for skin friction coefficient prediction, since they do not depend on knowledge of boundary layer characteristics such as displacement or momentum thickness.

The next chapter will present a similar investigation of the influence of FST conditions, but on forced convective heat transfer from flat plates.

References

Abdollahzadeh, M., Esmaeilpour, M., Vizinho, R., Younesi, A. and Pàscoa, J. (2017) Assessment of RANS turbulence models for numerical study of laminar-turbulent transition in convection heat transfer. International Journal of Heat and Mass Transfer, 115(PB), pp. 1288–1308.

Ames, F. E. and Moffat, R. J. (1990) Heat transfer with high intensity, large scale turbulence: the flat plate turbulent boundary layer and the cylindrical stagnation point, Report No. HMT-44, Department of Mechanical Engineering, Stanford University, CA, USA.

ANSYS, Inc. (2013) ANSYS Fluent Theory Guide. Canonsburg, PA, USA, pp. 1-814.

Baker, N., Kelly, G. and O'Sullivan, P. D. (2019) A grid convergence index study of mesh style effect on the accuracy of the numerical results for an indoor airflow profile. International Journal of Ventilation, 19(4), pp. 300-314.

Barrett, M. J. and Hollingsworth, D. K. (2003) Heat transfer in turbulent boundary layers subjected to free-stream turbulence - Part I: Experimental results. Journal of Turbomachinery, 125(2), pp. 232–241.

Barrett, M. J. and Hollingsworth, D. K. (2003) Heat transfer in turbulent boundary layers subjected to free-stream turbulence - Part II: Analysis and correlation. Journal of Turbomachinery, 125(2), pp. 242–251.

Barth, T. J. and Jespersen, D. C. (1989) The design and application of upwind schemes on unstructured meshes. Proceedings of the 27th Aerospace Sciences Meeting, Reno, NV, USA, AAIA paper 89-0366, pp. 1-12.

Baskaran, V., Abdellatif, O. E. and Bradshaw, P. (1989) Effects of free-stream turbulence on turbulent boundary layers with convective heat transfer. Proceedings of the 7th Symposium on Turbulent Shear Flows, Stanford, CA, USA, pp. 20.1.1-20.1.6.

Blair, M. F. (1983a) Influence of free-stream turbulence on turbulent boundary layer heat transfer and mean profile development, Part I - Experimental data. Journal of Heat Transfer, 105(1), pp. 33–40.

Blair, M. F. (1983b) Influence of free-stream turbulence on turbulent boundary layer heat transfer and mean profile development, Part II - Analysis of results. Journal of Heat Transfer, 105(1), pp. 41–47.

Blasius, H. (1908) Grenzschichten in Flüssigkeiten mit kleiner Reibung. Journal of Applied Mathematics and Physics, 56(1), pp. 1-37.

Blocken, B., Defraeye, T., Derome, D. and Carmeliet, J. (2009) High-resolution CFD simulations for forced convective heat transfer coefficients at the facade of a low-rise building. Building and Environment, 44(12), pp. 2396–2412.

Çengel, Y. A. and Cimbala, J. M. (2010) Fluid mechanics: Fundamentals and applications. Boston, MA, USA: McGraw-Hill Higher Education, 2nd edition, pp. 35-600.

Chorin, A. J. (1968) Numerical solution of Navier-Stokes Equations. Mathematics of Computation, 22(104), pp. 745–762.

Defraeye, T., Blocken, B. and Carmeliet, J. (2010) CFD analysis of convective heat transfer at the surfaces of a cube immersed in a turbulent boundary layer. International Journal of Heat and Mass Transfer, 53(1-3), pp. 297-308.

Dyban, E. P. and Epik, E. Y. (1985) Heat and mass transfer and hydrodynamics of turbulent flows. Naukova Dumka, Kiev.

Dyban, E. P., Epik, E. Y. and Surpun, T. T. (1977) Characteristics of the laminar layer with increased turbulence of the outer stream. International Journal of Chemical Engineering, 17(3), pp. 501–504.

Esteban, L., Dogan, E., Rodríguez-López, E. and Ganapathisubramani, B. (2017) Skin-friction measurements in a turbulent boundary layer under the influence of free-stream turbulence. Experiments in Fluids, 58(9), pp. 1–7.

Franke, J., Hellsten, A., Schlünzen, H. and Carissimo, B. (2007) Best practice guideline for the CFD simulation of flows in the urban environment, COST action 732. Quality Assurance and Improvement of Microscale Meteorological Models. Hamburg, Germany.

Hancock, P. E. and Bradshaw, P. (1983) The effect of free-stream turbulence on turbulent boundary layers. Journal of Fluids Engineering, 105(3), pp. 284–289.

Hoffmann, J. A. and Mohammadi, K. (1991) Velocity profiles for turbulent boundary layers under freestream turbulence. Journal of Fluids Engineering, 113(3), pp. 399–404.

Ivyer, G. R. and Yavuzkurt, S. (1999) Comparison of low Reynolds number k–ε models in simulation of momentum and heat transport under high free stream turbulence. International Journal of Heat and Mass Transfer, 42(4), pp. 723-737.

Junkhan, G. H. and Serovy, G. K. (1967) Effects of free-stream turbulence and pressure gradient on flat-plate boundary-layer velocity profiles and on heat transfer. Journal of Heat Transfer, 89(2), pp. 169–175.

Kawai, S. and Larsson, J. (2012) Wall-modeling in large eddy simulation: Length scales, grid resolution, and accuracy. Physics of Fluids, 24(1), 015105.

Kestin, J., Maeder, P. F. and Wang, H. E. (1961) Influence of turbulence on the transfer of heat from plates with and without a pressure gradient. International Journal of Heat and Mass Transfer, 3(2), pp. 133–154.

Kondjoyan, A., Péneau, F. and Boisson, H. (2002) Effect of high free stream turbulence on heat transfer between plates and air flows: A review of existing experimental results. International Journal of Thermal Sciences, 41(1), pp. 1–16.

Launder, B. E. and Spalding, D. B. (1974) The numerical computation of turbulent flows. Computer Methods in Applied Mechanics and Engineering, 3(2), pp. 269-289.

Lioznov, G. L., Lushchik, V. G., Makarova, M. S. and Yakubenko, A. E. (2012) Freestream turbulence effect on flow and heat transfer in the flat-plate boundary layer. Fluid Dynamics, 47(5), pp. 590–592.

Lopez, M. and Keith Walters, D. (2016) A recommended correction to the kT−kL−ω transition-sensitive Eddy-Viscosity model. Journal of Fluids Engineering, 139(2), 024501.

Maciejewski, P. K. and Moffat, R. J. (1992) Heat transfer with very high free-stream turbulence: Part I - Experimental data. Journal of Heat Transfer, 114(4), pp. 827–833.

Maciejewski, P. K. and Moffat, R. J. (1992) Heat transfer with very high freestream turbulence: Part II - Analysis of the results. Journal of Heat Transfer, 114(4), pp. 834–839.

MacMullin, R., Elrod, W., and Rivir, R. (1989) Free-stream turbulence from a circular wall jet on a flat plate heat transfer and boundary layer flow. Journal of Turbomachinery, 111(1), pp. 78–86.

Menter, F. R. (1994) Two-equation eddy-viscosity turbulence models for engineering applications. AIAA Journal, 32(8), pp. 1598–1605.

Mukha, T., Johansson, M.E. and Liefvendahl, M. (2018) Effect of wall-stress model and mesh-cell topology on the predictive accuracy of LES for wall-bounded flows. Proceedings of the 7th European Conference on Computational Fluid Dynamics (ECFD 7), Glasgow, UK.

Nikuradse, J. (1950) Laws of flow in rough pipes. NACA Technical Memorandum 1292. National Advisory Commission for Aeronautics, Washington, DC, USA.

Patankar, S. V, Spalding, D. B. and Road, E. (1972) A calculation procedure for heat, mass and momentum transfer in three-dimensional parabolic flows. International Journal of Heat and Mass Transfer, 15(10), pp. 1787–1806.

Péneau, F., Boisson, H., Kondjoyan, A. and Djilali, N. (2004) Structure of a flat plate boundary layer subjected to free-stream turbulence. International Journal of Computational Fluid Dynamics, 18(2), pp. 175–188.

Sarkar, D. (2018) A numerical tool for predicting the spatial decay of freestream turbulence. M.E.Sc. Thesis, Electronic Thesis and Dissertation Repository, The University of Western Ontario, London, Canada. 5331.

Simonich, J. C. and Bradshaw, P. (1978) Effect of free-stream turbulence on heat transfer through a turbulent boundary layer. Journal of Heat Transfer, 100(4), pp. 671–677.

Versteeg, H. K. and Malalasekera, W. (1995) An introduction to computational fluid dynamics - The finite volume method. Harlow, England: Pearson Education Ltd, 1st edition, pp. 1-205.

Young, C. D., Han, J. C., Huang, Y., and Rivir, R. B. (1992) Influence of jet-grid turbulence on flat plate turbulent boundary layer flow and heat transfer. Journal of Heat Transfer, 114(1), pp. 65–72.

Chapter 3

3 Effect of free-stream turbulence on convective heat transfer from flat plates

This chapter presents an overview of what is known from previous experimental and computational model studies about the effect of free-stream turbulence on convective heat transfer from flat plates in Section 3.1. The inconsistencies regarding the quantitative effects of free-stream turbulence (FST) on convective heat transfer coefficients (CHTC) from previous studies are discussed along with the importance of evaluating the streamwise decay of turbulence intensity (TI), which was not examined in previous works. These aspects and gaps in the literature are investigated in the present study by using Computational Fluid Dynamics (CFD) techniques. The numerical method is presented in Section 3.2, where the computational domain, grid, methodology, boundary conditions and validation of the flow field are discussed. In Section 3.3, different free-stream conditions are analyzed and their influence on CHTC examined. The resulting correlations for Nusselt number (local and total) and Stanton number (local and total) with respect to the examined free-stream conditions are analyzed in Section 3.4. The results are then validated with previous studies in Section 3.5. Finally, a summary of this study and the conclusions are presented in Section 3.6.

3.1 Background

The effect of incident turbulence on convective heat transfer from flat plates has been the topic of various studies over the last decades. Some of the earlier studies reached contradictory conclusions: some authors did not observe a significant effect of free-stream turbulence on the CHTC (Kestin et al., 1961; Junkhan and Sevory, 1967) while other authors affirmed that CHTC increases with increasing free-stream turbulence (e.g. Simonich and Bradshaw, 1978; Blair, 1983). Subsequently, an extensive review concluded that heat transfer is enhanced by increasing external flow turbulence intensity (Kodojoyan et al., 2002) and that the contradictory conclusions from earlier studies are probably a result of the small range of turbulence intensity levels that they investigated.

Additionally, many other factors could contribute to the lack of a significant effect observed in some studies, such as: low Reynolds number, a lack of low-turbulence experiments to serve as a base of comparison for the results, or the influence of boundary layer transition effects (Simonich and Bradshaw, 1978), since free-stream turbulence can move the transition point upstream. In order to avoid inconsistencies due to an earlier transition, the present focus is on turbulent boundary layers.

The qualitative increase in CHTC with free-stream turbulence has been observed in many investigations for different ranges of turbulence intensity, but the quantitative data can be contradictory. Comparing the CHTC with respect to a case with low free-stream turbulence (*TI* = 0.1%), Simonich and Bradshaw (1978) concluded that the CHTC could be up to 30% higher for *TI* of 7%; Blair's (1983) experiments showed an increase of 18% for a *TI* of 6% while Maciejewski and Moffat (1992) reached to a 300% increase for *TI* levels of 55%. These differences could be due to a variety of factors, such as differences in free-stream TKE decay rate and the range of local Reynolds numbers or length scales. Moreover, some of these studies were conducted using grid-generated turbulence (e.g. Simonich and Bradshaw, 1978; Blair, 1983), that is, generally homogeneous and isotropic (Pope, 2000). However, in order to achieve higher values of *TI* experimentally, turbulence is generated by jets (Ames and Moffat, 1990; Maciejewski and Moffat, 1992). The observations from different experimental studies and the correlations proposed are discussed in the next section.

3.1.1 Previous experimental studies

Many investigations tried to analyze the parameters necessary to quantify the effect of free-stream turbulence on CHTC from flat plates (Simonich and Bradshaw, 1978; Blair, 1983; Karava et al., 2011). Simonich and Bradshaw (1978) first mentioned that earlier studies (Kestin et al., 1961; Junkhan and Sevory, 1967) concluded that no significant effect of FST was observed on heat transfer due to the small range of *TI* (only up to 3%) and low Re_x (up to $6x10^5$), not much higher than transitional Re. Then, Simonich and Bradshaw (1978) conducted experiments for higher Re flows (Re_x up to $6.3x10^6$) and turbulence intensity of up to 7%. It was proposed by the authors that the increase in CHTC could be expressed as follows:

$$\frac{St_x - St_{xo}}{St_{xo}} = A\, TI_x \tag{3.1}$$

where St_x is the local Stanton number ($St_x = \frac{Nu_x}{Re_x Pr}$), St_{xo} is the Stanton number when there is no FST, A is a constant and TI_x is the local value of free-stream turbulence. The best fit of Eq. (3.1) for their data was given for A = 5, but there was still a large scatter in their results. Hancock and Bradshaw (1983) suggested that the scatter was related to the effect of local integral length scale (L_{ux}), which was neglected by Simonich and Bradshaw (1983). However, Hancock and Bradshaw (1983) only investigated skin friction coefficients. Furthermore, the Stanton number increase observed by Simonich and Bradshaw (1978) was higher than the skin friction enhancement. They observed that when *TI* was increased by 1%, skin friction increased by 2% and Stanton number by 5%. Although Hancock and Bradshaw (1983) only investigated the effect of varying L_{ux} on skin friction coefficients and proposed a correlation for the increase of $c_{f,x}$ with FST, Baskaran et al. (1989) examined Hancock and Bradshaw's (1983) expression when applied to Stanton number increase, as presented by Eq. (3.2):

$$\frac{St_x - St_{xo}}{St_{xo}} \propto \left(\frac{TI_x}{2 + {L_u^e}/{\delta}} \right) \tag{3.2}$$

where L_u^e is the dissipative length scale. For isotropic turbulence, $L_u^e = 1.5 L_{ux}$ (Blair, 1983). Baskaran et al. (1989) evaluated this expression for conditions similar to Simonich and Bradshaw's (1978) study and observed a large disparity between the experimental results and the predicted values from Eq. (3.2). Blair (1983) proposed that the effect of momentum-thickness Reynolds number (Re_θ) should be included in the expression, but this effect was only significant for Re_θ < 2000. Therefore, an exponential relationship ($1 + 3e^{-Re_\theta/400}$) was included in a correlation expressed as follows:

$$\frac{St_x - St_{xo}}{St_{xo}} \propto \left(\frac{TI_x}{\left(2 + {L_u^e}/{\delta}\right)\left(1 + 3e^{-Re_\theta/400}\right)} \right) \tag{3.3}$$

Blair's (1983) study included $Re_x \leq 6x10^6$ and $TI \leq 7\%$. The author also observed that the increase in Stanton number was higher than the increase in skin friction for a given TI_x. It was proposed that this observation could be expressed by Eq. (3.4).

$$\frac{2St_x}{C_{f,x}} = 1.18 + 1.3TI_x \tag{3.4}$$

The ratio $2St_x/C_{f,x}$ is commonly referred to as Reynolds analogy factor. These studies investigated *TI* of only up to 7%, but later MacMullin et al. (1989), Ames and Moffat (1990) and Maciejewski and Moffat (1992) analyzed free-stream flows with *TI* of up to 16%, 17% and 55%, respectively.

MacMullin et al. (1989) showed that there was a large scatter between the experimental results from their study and the values predicted by the correlations proposed by Hancock and Bradshaw (1983) and Blair (1983). MacMullin et al. (1989) highlighted that the effect of L_u on St_x could not be concluded from their results and it would be necessary to examine an independent variation of L_u at the same turbulence intensity conditions to further analyze the effects of L_u on St_x. Ames and Moffat (1990) proposed adapted parameters for the Stanton number correlation, substituting the momentum thickness by the enthalpy thickness (Δ_2) and the momentum-thickness Reynolds number by the enthalpy-thickness Reynolds number ($Re_{\Delta 2}=\rho U\Delta_2/\mu$). They proposed the following expression:

$$\frac{St_x - St_{xo}}{St_{xo}} \propto \left(TI_x \left(\frac{\Delta_2}{L_u^e}\right)^{1/3} \left(\frac{Re_{\Delta 2}}{1000}\right)^{1/4} \right) \tag{3.5}$$

where Δ_2 is defined as:

$$\Delta_2 = \int_0^\infty \frac{U}{U_o}\left(\frac{T-T_o}{T_p-T_o}\right) dz \tag{3.6}$$

The right-hand side of Eq. (3.5) was defined as the *TLR* parameter by Ames and Moffat (1990). However, the authors mentioned that there was not enough evidence to affirm that the parameters used in their expression were sufficient. Other experimental studies presented an increase of St_x with increasing *TI*: Maciejewski and Moffat (1992) reported a percentage increase of local Stanton number ($\frac{St_x - St_{xo}}{St_{xo}} x100\%$) of up to 300% when *TI* is

increased from 0.1% to 55%, while Barret and Hollingsworth (2003) presented an increase of St_x of up to 46% when varying *TI* from 0.1% to 8%.

Another important aspect is that TKE decays with distance from the turbulence generator and Blair (1983) even highlighted the free-stream TI streamwise decay, but the author did not investigate if this factor would influence the correlations proposed. Considering the external flow in a region outside the boundary layer, the free-stream TKE decays along the plate test section (from the leading to the trailing edge of the plate) and this decay was higher for the experiments with jet-generated turbulence when compared to grid-generated turbulence. For instance, in Blair's (1983) experiment with *TI* = 7% the percentage difference of TI ($TI_{dif}(\%) = \frac{(TI - TI_{TE})}{(TI + TI_{TE})/2} x100$) was 60% and for the study of Ames and Moffat (1990) with *TI* = 17%, TI_{dif} was 96%. The differences in TI decay rates may have led to some of the inconsistencies observed in previous studies.

The correlations presented, with the exception of that derived by Simonich and Bradshaw (1978), relate the increase in St_x with BL parameters such as BL or momentum thickness and so it is necessary to know the BL development in order to estimate the increase in heat transfer using this type of expression. Therefore, the present numerical study focuses on regions of almost uniform TI and the analysis of the influence of different parameters (*TI*, L_u and *Re*) to achieve a dimensionless correlation for heat transfer enhancement that does not depend on BL characteristics such as momentum thickness or enthalpy thickness. It is essential to investigate the appropriate numerical modelling to quantity the free-stream turbulent properties and CHTC, thus, a discussion about previous numerical studies and appropriate numerical modelling is presented next.

3.1.2 Previous numerical studies

One important aspect to consider when performing numerical studies is the correct selection of models for the problem. In this case, the appropriate choice of turbulent model for RANS simulation is fundamental, since it is necessary to compute surface coefficients for heat transfer. Wall functions model the near-wall region based on analytical solution and experimental data (Versteeg and Malalasekera, 1995) and, therefore, do not require a refined mesh near the wall, reducing the computational cost. However, it has been shown

that the wall functions available in different models cannot accurately predict the CHTC, providing overestimations of up to 60% (Blocken et al., 2009; Neale et al., 2006). In consequence, it is necessary to build grids with high resolution near the wall in order to accurately compute CHTC. This method is applied using Low-Re number models which can predict heat transfer coefficients within 5% for a case with no turbulence and Re_x of up to $5x10^6$ (Blocken et al., 2009; Ivyer and Yavuzkurt, 1999).

Abdollazadeh et al. (2017) investigated the laminar-turbulent transition and local Stanton number predicted by various turbulent models for flows over flat plates with no FST. The authors concluded that the Spalart-Allmaras and RNG k-ε did not predict transition and the V-SA and γ-Re_θ models predicted it incorrectly. Moreover, the k-k_l-ω model would be the most suitable for predicting transition, but it is possible to see from Figure 3.1 that most models can predict the values for the fully turbulent region, with the exception of the Low Re k-ε model for all the domain and the RNG k-ε for Re_x of up to $2.5x10^6$.

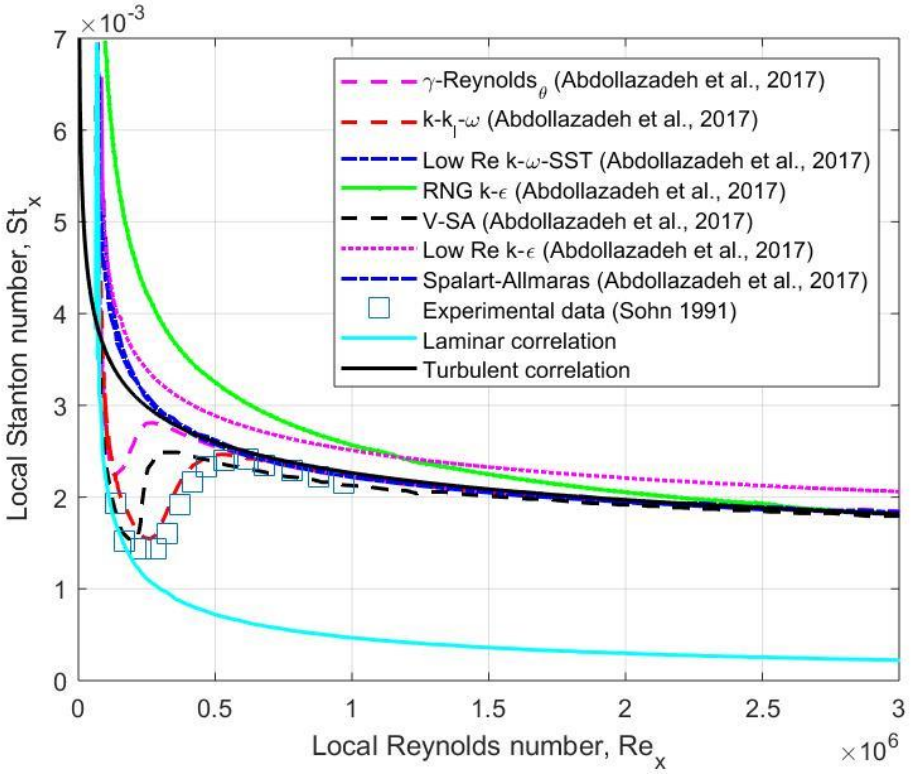

Figure 3.1 – Local Stanton number (St_x) with respect to local Reynolds number (Re_x) for various turbulent models, adapted from Abdollazadeh et al. (2017)

Nevertheless, the k-k_l-ω model predicts an erroneous, rapid TKE decay in the flow away from the wall even with the recommended corrections (Lopez and Walters, 2016). Thus, the SST k-ω model with Low-Re corrections is the most suitable model, since it predicts the correct free-stream TKE decay (Sarkar, 2018) and CHTC (Blocken et al., 2009; Karava et al., 2012),

Furthermore, Karava et al. (2012) investigated the effect of varying free-stream TI from 0.1% to 30% on CHTC for a Re_x range of $6.6\text{x}10^6$ to $8.2\text{x}10^6$. The authors compared the results with the linear correlation proposed by Simonich and Bradshaw (1978) expressed by Eq. (3.1) and noted that reducing the proposed A=5 to A=2.8 gave a better match with their results. They also proposed the following correlation:

$$Nu_L = (0.094TI + 0.035)Re^{0.8}Pr^{1/3} \tag{3.7}$$

The lower increase in CHTC observed in Karava et al. (2012) when compared to Simonich and Bradshaw (1978) may be due to the fact that the TI range examined was much wider in Karava et al. (2012). In addition, Karava et al. (2012) positioned the leading edge of the plate at the beginning of the domain, where TKE decay is higher (Sarkar, 2018) and the percentage difference of TI from the inlet to the outlet is as much as 75%. In the cases investigated by Karava et al. (2012) the average free-stream TI to which the plate is subjected is much lower than the TI defined at the inlet and used in Eq. (3.7), which could lead to a lower increase of CHT with varying FST. Besides that, the influence on Nu_x of other parameters, such as integral length scale, was not investigated.

Other numerical studies did not focus on the comparison with previous correlations or the development of new expressions, but they reached the same overall conclusion that convective heat transfer is enhanced with increasing free-stream TI and that heat transfer is more sensitive than skin friction to variations in FST (Ivyer and Yavuzkurt, 1999; Kondjoyan et al., 2004; Péneau et al., 2004; Lioznov et al., 2012). Ivyer and Yavuzkurt (1999) examined free-stream turbulence levels of up to 25.7% but presented an over-prediction of more than 50% for local Stanton numbers when compared to results from Ames and Moffat (1990). Lioznov et al. (2012) reported a percentage increase of St_x of up to 13% for a *TI* of 9%, but their results were not compared with data from previous studies.

Péneau et al. (2004) only investigated flows in the laminar regime ($Re_x \leq 8x10^4$) and presented a St_x enhancement of up to 200% for a TI of 10%. A comparison between previous experimental and numerical studies discussed in this section is presented in Table 3.1. Note that the percentage increase of St_x is given by $\frac{St_x - St_{xo}}{St_{xo}} x100\%$. Additionally, some studies did not mention the range of L_u and this is indicated by 'N/A'. The experimental and numerical studies are indicated by 'Exp' and 'Num', respectively.

Table 3.1 – Main experimental and numerical studies on the effect of FST on CHTC

Authors	**Type of study**	**Re_x up to**	**Range of TI**	**Range of L_u**	**St_x percentage increase**
Dyban et al. (1977)	Exp	$2.0x10^4$	0.1-9%	N/A	0%
Junkhan and Sevory (1967)	Exp	$3.7x10^5$	0.4-8.3%	N/A	0%
Simonich and Bradshaw (1978)	Exp	$6.3x10^6$	0.03-7%	N/A	Up to 30%
Blair (1983)	Exp	$6.0x10^6$	0.25-7%	1-3 cm	Up to 20%
Ames and Moffat (1990)	Exp	$3.2x10^6$	0.1-17%	9-13 cm	Up to 35%
Maciejewski and Moffat (1992)	Exp	$1.0x10^6$	0.1-55%	8-25 cm	Up to 300%
Ivyer and Yavuzkurt (1999)	Num	$6.0x10^6$	0.1-25.7%	N/A	Up to 80%
Barrett and Hollingsworth (2003)	Exp	$1.0x10^6$	0.1-8%	1-3 cm	Up to 46%
Kondjoyan et al. (2004)	Exp	$1.3x10^5$	1-50%	2-10 cm	Up to 300%

Péneau et al. (2004)	Num	$7.0x10^4$	1-10%	2-14 cm	Up to 200%
Karava et al. (2012)	Num	$8.2x10^6$	0.1-30%	10 cm	Up to 80%
Lioznov et al. (2012)	Num	$3.0x10^6$	1.5-9%	N/A	Up to 13%

There is a large discrepancy between the quantitative effect of FST on CHTC observed in previous experimental and numerical studies. Additionally, the difference correlations proposed by previous studies and presented in Section 3.1.1 were not capable of predicting the effects of different parameters, such as *TI* and *Lu*, on convective heat transfer (Kondjoyan et al., 2002). The inconsistencies are related to the wide range of *TI* and Re_x, differences in turbulence generators and turbulence conditions of the incoming flow. Moreover, the streamwise decay of turbulence intensity was not examined by previous studies. Therefore, the present study employs CFD techniques to investigate the influence of key parameters (*TI*, *Lu*, Re_x or Re_L) on CHTC (local and total) and to develop a generalized dimensionless correlation for local and total CHTC taking into account those key parameters and the streamwise free-stream TKE decay. The numerical method used in the current work is presented next.

3.2 Numerical method

The problem is represented by the diagram below (Figure 3.2), where a free-stream with uniform velocity U_o, initial turbulence intensity TI_o, initial integral length scale L_{uo} and uniform temperature T_o approaches a flat plate of length L and constant temperature T_p on which a boundary layer of thickness $\delta(x)$ develops.

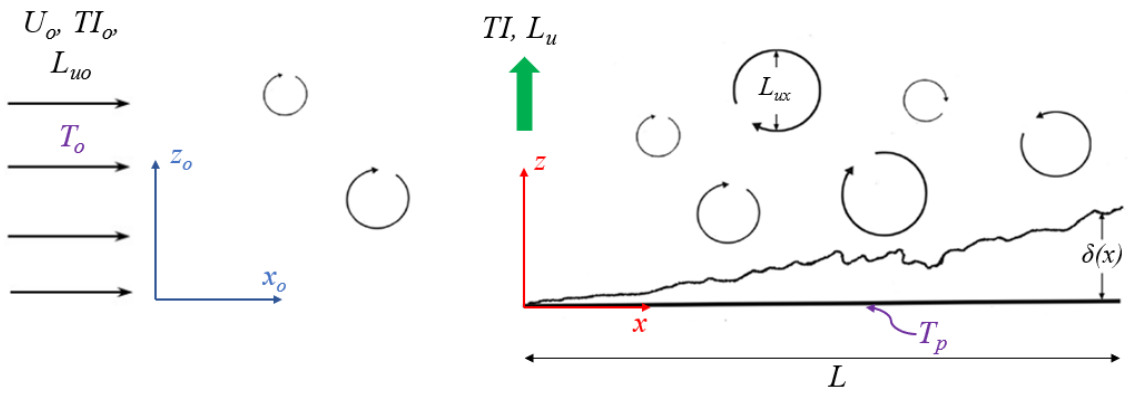

Figure 3.2 – Problem diagram for heated flat plate with main variables and coordinate system

3.2.1 Computational domain

The 3-D computational domain for this problem is presented in Figure 3.3. The domain dimensions are L_x = 4.0m, L_y = 0.5m and L_z = 0.5m. L_x was set as 4.0m because between x_o = 2.0m to x_o = 4.0m there is a nearly uniform turbulence region as mentioned before (Sarkar, 2018), so for most cases the plate leading edge is positioned at x_o = 2.0m. Furthermore, some cases were also analyzed with the leading edge of the plate located at x_o = 1.5m and x_o = 1.0m to investigate the effect of higher TKE decay rates on the turbulent boundary layer.

The other domain dimensions (L_y and L_z) were defined in such a way that the boundary conditions imposed at the walls, which will be presented later, would not affect the flat plate boundary layer. These dimensions are then analyzed with respect to the turbulent boundary layer thickness (δ_t), defined by the Eq. (1.3).

The turbulent boundary layer developed at the plate trailing edge is 35.2mm, so $L_y/\delta = L_z/2\delta$ = 14.2. These dimensions are large enough to avoid erroneous boundary layer profiles due to imposed wall boundary conditions (Kawai and Larsson, 2012; Mukha et al., 2018). Additionally, the plate has zero thickness, i.e., a thickness of a node unit, to avoid flow separation at the leading edge.

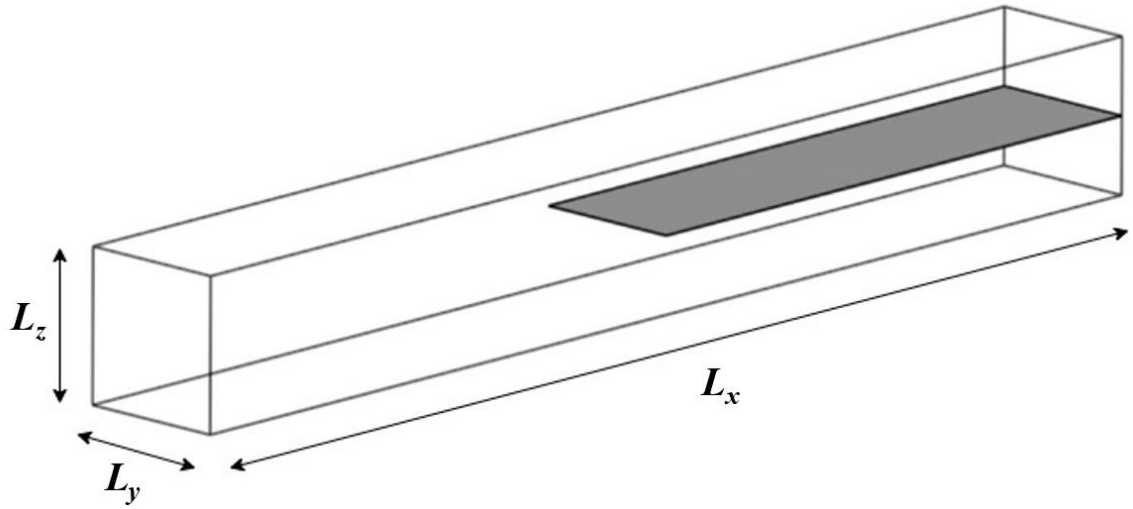

Figure 3.3 – 3D Computational domain

Since adding heat transfer to the problem increases the computational cost substantially, an investigation was performed to examine whether reducing the problem to a 2D domain would affect the results for heat transfer coefficients, skin friction or boundary layer development. The 2D domain used was the middle plane of the 3D domain perpendicular to the plate as shown in Figure 3.4.

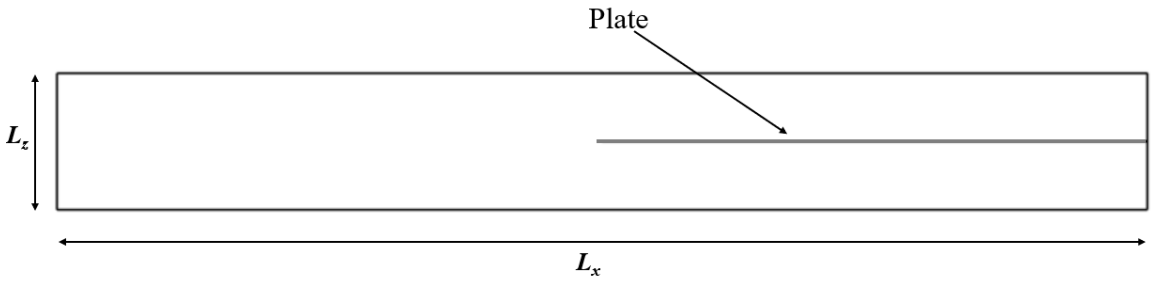

Figure 3.4 – 2D computational domain diagram

3.2.2 Grid generation

The meshes were created using ICEM CFD 19.1 and all of them are orthogonal hexahedral meshes since they are more suitable for unidirectional flow over a plane surface, because the grid lines should be perpendicular to the wall (Frank et al., 2007) and it produces a more precise numerical solution (Baker et al., 2019). The mesh topology is presented in presented in Figure 3.5.

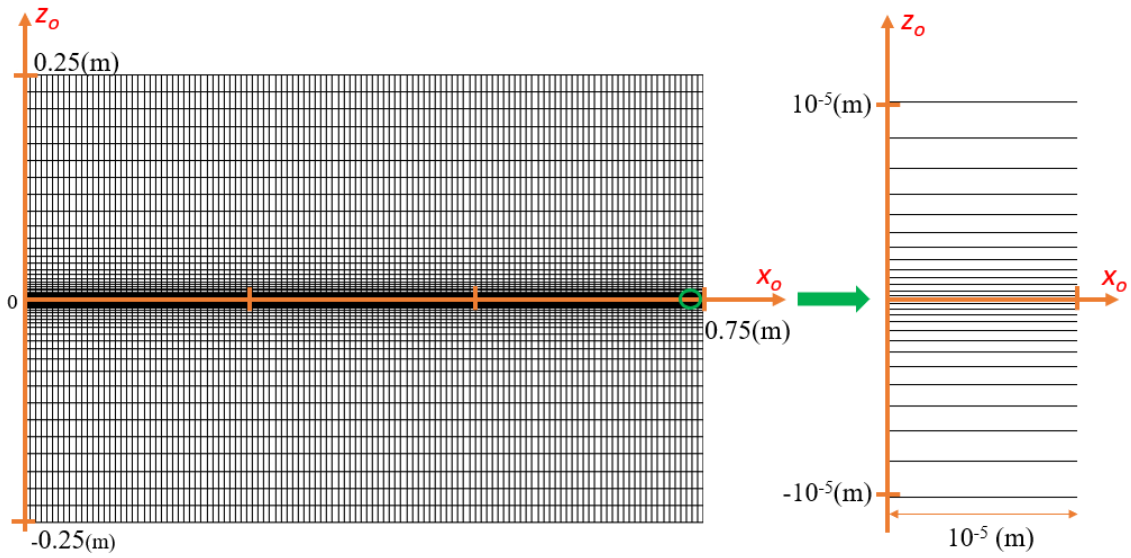

Figure 3.5 – Mesh topology

In the y-direction the mesh is equally spaced. Note that there is a better refinement near the plate, since the viscous region is resolved using the Low Reynolds Number Modelling (LRNM) approach as recommended by Blocken et al. (2009). This model resolves the viscosity-affected region including the viscous sub-layer but requires high grid resolution near the plate. This resolution is defined by the dimensionless wall distance $y+$ values, given by Eq. (3.8), and growth ratio.

$$y^+ = \frac{\rho u^* y_p}{\mu} \tag{3.8}$$

where u^* is the friction velocity and y_p is the distance from the first grid point to the wall. This value should be less than 1 to solve the near wall region and generate an appropriate LRNM grid (Blocken et al., 2009), so in this study $y^+ \approx 0.8$. This generates at least 20 points inside the whole boundary layer, which is desirable to compute the boundary layer region, including the viscous region (Versteeg and Malalasekera, 1995; Defraeye et al, 2010). Besides that, the growth ratio was defined as 1.2, which is the highest recommended value according to COST Guidelines (Franke et al, 2007). The grid in the other directions is equally spaced with Δx=0.0066m and Δy=0.0067m, which was sufficient to provide grid independent results, as will be presented later.

3.2.3 Methodology

3.2.3.1 Solver

All cases were studied using the commercial software FLUENT 19.1. The software was set for a 2-D domain and the option “double precision” was enabled for better accuracy (ANSYS, 2013). It was set for a 3-D domain just for the case used to compare and validate the 2-D cases. The general setup for the solver was pressure-based, since it is appropriate for incompressible flows (Chorin, 1968). This solver is based on the projection method, where the continuity (mass conservation) of the velocity field is resolved by pressure or pressure correction equations (Chorin, 1968). The pressure equation is obtained from the continuity and momentum equations so that the velocity field satisfies continuity when corrected by the pressure. Then the set of governing equations is solved for as many iterations as needed to achieve a converged solution.

3.2.3.2 Governing equations and turbulence model

The instantaneous conservation equations of mass and momentum can be expressed by Eq. (3.9) and Eq. (3.10) respectively.

$$\frac{\partial \rho}{\partial t} + \frac{\partial}{\partial x_i}(\rho u_i) = 0 \tag{3.9}$$

$$\frac{\partial}{\partial t}(\rho u_i) + \frac{\partial}{\partial x_j}\left(\rho u_i u_j\right) = -\frac{\partial p}{\partial x_i} + \frac{\partial}{\partial x_j}\left[\mu\left(\frac{\partial u_i}{\partial x_j} + \frac{\partial u_j}{\partial x_i}\right)\right] \tag{3.10}$$

where t is time, u_i is the instantaneous velocity, x_i is the axial coordinate and p is the pressure. These equations are computationally expensive to calculate directly because turbulence is characterized by fluctuating velocity fields. In order to consume less computational resources, the instantaneous governing equations can be time-averaged, and a modified set of equations obtained.

Thus, substituting a parameter ϕ by its mean value and a fluctuating component ($\phi = \bar{\phi} + \phi'$), we obtain the following equations for an incompressible, steady flow:

$$\frac{\partial U_i}{\partial x_i} = 0 \tag{3.11}$$

$$\frac{\partial}{\partial x_j}\left(\rho U_i U_j\right) = -\frac{\partial p}{\partial x_i} + \frac{\partial}{\partial x_j}\left[\mu\left(\frac{\partial U_i}{\partial x_j} + \frac{\partial U_j}{\partial x_i}\right)\right] + \frac{\partial}{\partial x_j}\left(-\rho\overline{u_i' u_j'}\right) \tag{3.12}$$

where U denote the mean velocity. These equations are commonly referred to as the Reynolds-Averaged Navier-Stokes (RANS) equations. They are almost equivalent to the instantaneous equations when the instantaneous velocity is substituted by its mean value. The only additional terms are the Reynolds stresses, $\tau_{ij} = -\rho\overline{u_i' u_j'}$, that represent the effects of turbulence on the flow. These unknown terms are then solved by additional equations, which are defined depending on the selected turbulence model.

This numerical work was conducted using the SST k-w model with Low-Re corrections since it can predict the correct decay of TKE (Sarkar, 2018) and the skin friction, as well as the integral parameters of turbulent boundary layers (Abdollazadeh et al., 2017).

3.2.3.2.1 Shear Stress Transport (SST) k-ω model

The Shear Stress Transport k-ω model was developed by Menter (1994) with the objective of combining the standard k-ω model near the wall, due to its accuracy and robustness in computing the viscous sub-layer, and the k-ε model at the free-stream (Launder and Spalding, 1974).

This is a two-equation model, one for the turbulent kinetic energy (k) and one for the dissipation rate (ω) expressed by Eq. (3.13) and Eq. (3.14) (Menter, 1994).

$$\frac{\partial}{\partial x_i}(\rho k u_i) = \frac{\partial}{\partial x_j}\left(\Gamma_k \frac{\partial k}{\partial x_j}\right) + G_k - Y_k \tag{3.13}$$

$$\frac{\partial}{\partial x_j}\left(\rho\omega u_j\right) = \frac{\partial}{\partial x_j}\left(\Gamma_\omega \frac{\partial \omega}{\partial x_j}\right) + G_\omega - Y_\omega + D_\omega \tag{3.14}$$

where G_k represents the production of turbulence kinetic energy, G_ω represents the generation of ω, and Γ_k and Γ_ω represent the effective diffusivity of k and ω, respectively, which are calculated by Eq. (3.15) and Eq. (3.16). Y_k and Y_ω represent the dissipation of k and ω due to turbulence, and D_w represents the cross-diffusion term.

$$\Gamma_\omega = \mu + \frac{\mu_t}{\sigma_\omega} \tag{3.15}$$

$$\Gamma_k = \mu + \frac{\mu_t}{\sigma_k} \tag{3.16}$$

where σ_k and σ_ω are the turbulent Prandtl numbers for k and ω, respectively.

The constants for this model are defined as (Menter, 1994):

$$\sigma_{k,1} = 1.176, \qquad \sigma_{\omega,1} = 2.0, \qquad \sigma_{k,2} = 1.0, \qquad \sigma_{\omega,2} = 1.168,$$

$$a_1 = 0.31, \qquad \beta_{i,1} = 0.075, \qquad \beta_{i,2} = 0.0828$$

3.2.3.2.2 Energy equation

The energy equation is given by Eq. (3.17):

$$\frac{\partial}{\partial x_j}(\rho U_i T) = \frac{\partial}{\partial x_j}\left(k_{eff}\nabla T\right) \tag{3.17}$$

where T is the temperature and k_{eff} is the effective thermal conductivity defined as:

$$k_{eff} = \frac{k_m}{C_p} + \frac{\mu_t}{Pr_t} \tag{3.18}$$

where k_m is the molecular thermal conductivity, C_p is the specific heat capacity and Pr_t is the turbulent Prandtl number. Although some numerical studies considered the properties of air constant (Lioznov et al., 2012; Péneau et al., 2004), it is known that the properties vary with temperature (Incropera et al., 2007). Accounting for these variations increases the computational cost but reproduces the correct physical behaviour. Therefore, a range of temperature from 290K to 320K was defined, since this interval includes the range of temperature analyzed in the current study, which will be presented later along with the boundary conditions. The values of different properties were extracted from air properties tables from Incropera et al. (2007) and a polynomial fit was performed. It was found that generally first-degree polynomials describe accurately the variations of properties with temperature (R^2 = 0.99 for all linear fits). The values of density (ρ, kg/m^3), dynamic viscosity (μ, kg/ms) and thermal conductivity (k_m, W/mK) were defined as follows:

$$\rho = 2.2207 - 0.0035T \tag{3.19}$$

$$\mu = 10^{-5}(0.4802 + 0.0046T) \quad (3.20)$$

$$k_m = 0.0037 + 0.00007T \quad (3.21)$$

The specific heat capacity for this range is constant (C_p = 1007 J/kgK).

3.2.3.3 Solution parameters

The solution method was set as SIMPLE pressure-velocity coupling since it is suitable for steady cases (Patankar et al, 1972). The second order spatial discretization scheme was selected for pressure, momentum and turbulence parameters (specific dissipation rate and turbulent kinetic energy) and energy, because it provides better accuracy (Barth and Jespersen, 1989). The gradients were computed using the least squares cell-based gradient evaluation since it is less expensive computationally and accurate for structured meshes. The convergence criteria were defined as 10^{-4} for all equations and the solution residuals observed were less than 10^{-8}.

3.2.4 Boundary conditions

The proper choice of boundary conditions is essential for correct development of the flow field, as well as for accurate representation of the influence of the surroundings. In this case, it is extremely important to define properly the inlet conditions. The incoming flow is uniform, and the inlet condition is defined by the velocity, turbulent kinetic energy and specific dissipation rate and temperature. The velocity is uniform and the different values will be presented later. The inlet temperature is constant and equal to 293K, since this is the normal condition of temperature defined by the National Institute of Standards and Technology (NIST) and a common reference temperature used in studies of photovoltaic panel systems (Palyvos, 2008).

The turbulent parameters at the inlet were calculated using desired predetermined values at the leading edge and the established decay of TKE expressed by Eq. (3.22) and Eq. (3.23) (Sarkar, 2018).

$$log(k') = \log(k'_o) - n_1 log\left(\frac{A_1(k'_o)^{0.5}(x_o - x_{vo})}{L_u} + 1\right) \quad (3.22)$$

$$log(k') = \log(k'_o) - n_2 log\left(\frac{A_2(k'_o)^{0.5}(x_o - x_{vo})}{L_{uo}} + 1\right) \quad (3.23)$$

where x_{vo} denotes the virtual origin, which is the streamwise distance from the grid origin where the turbulence is well-developed and nearly isotropic and homogeneous. In the current study, it is coincident with the origin of the numerical domain, i.e., x_{vo} = 0m. The value of x_o is be the position of the plate leading edge inside the domain where the turbulent parameters are defined beforehand. Note that k_o and L_{uo} indicate the values at the inlet, and the values of k and L_u at the leading edge are known. The constants in these equations are:

$$A_1 = 0.27;\ A_2 = 0.44;\ n_1 = 2.38;\ n_2 = 1.16$$

They were defined in a way that the expressions presented quantify the streamwise decay of homogeneous and isotropic turbulence. The values of ω are then obtained from the correlation involving k and L_u: $\omega = \frac{k^{0.5}}{\beta^*_\infty L_u}$

Sarkar (2018) also showed that for the correct free-stream TKE decay, the parameter β^*_∞ used in the turbulence model must be changed from the default value of 0.09 to 0.046.

Furthermore, the plate surface was set as no-slip, the outlet as a pressure-outlet and the other walls as symmetric, as represented in the diagram below. The symmetry condition is more appropriate since the pure-slip condition does not guarantee that the gradients of all parameters (especially turbulent kinetic energy and specific dissipation rate) are zero at the boundaries (Versteeg and Malalasekera, 1995). The plate temperature was set as constant and equal to 313K, since the temperature difference between the plate and the free-stream is set as 20K, which is an average value used in previous experiments (Blair, 1983; Ames and Moffat, 1990; Maciejewski and Moffat, 1992) and a common temperature difference used in studies of photovoltaic panel systems (Palyvos, 2008).

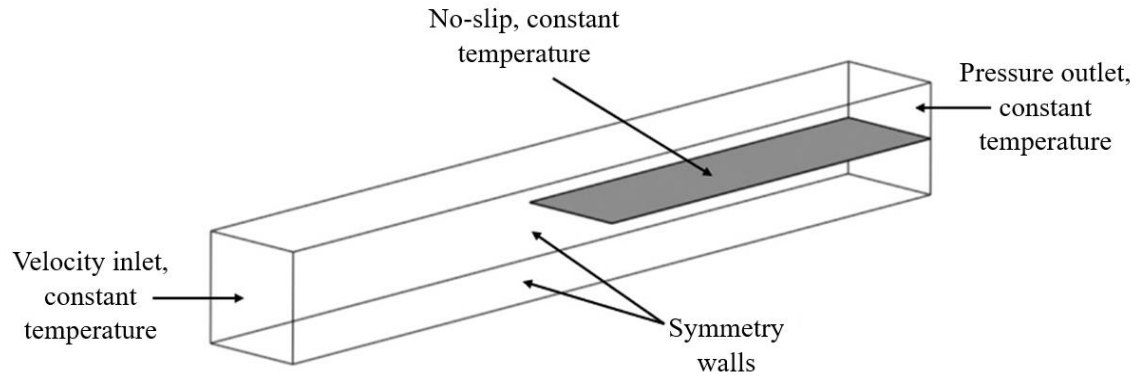

Figure 3.6 – 3D Numerical domain diagram with boundary conditions

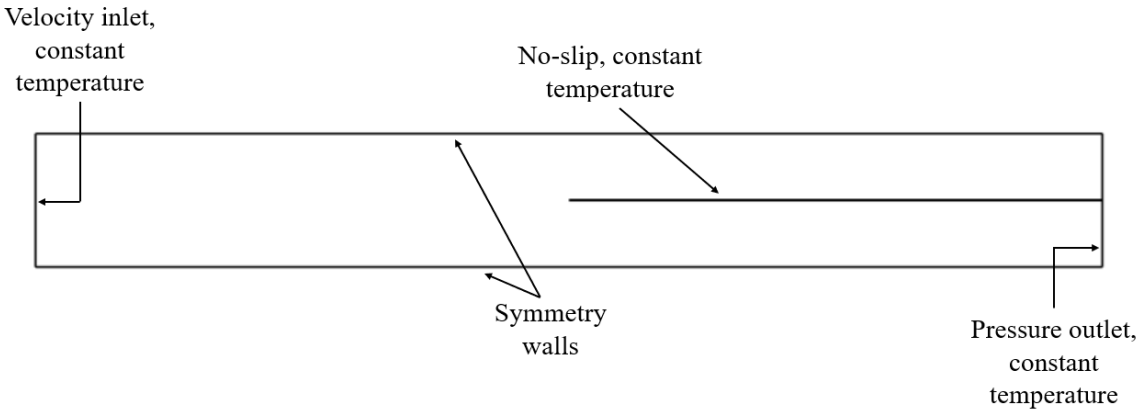

Figure 3.7 – 2D numerical domain diagram with boundary conditions

3.2.5 Validation of the 2D domain

The 2D domain was validated using the case with free-stream velocity of 40m/s and the highest *TI* examined in the current work (*TI* = 12.6% and L_u = 0.1m), since it would be the case in which the differences between the domains would be most noticeable. The local skin friction and local Nusselt number difference from the 2D to the 3D domain are below 0.2% and 0.5%, respectively, as shown in Figure 3.8 and Figure 3.9.

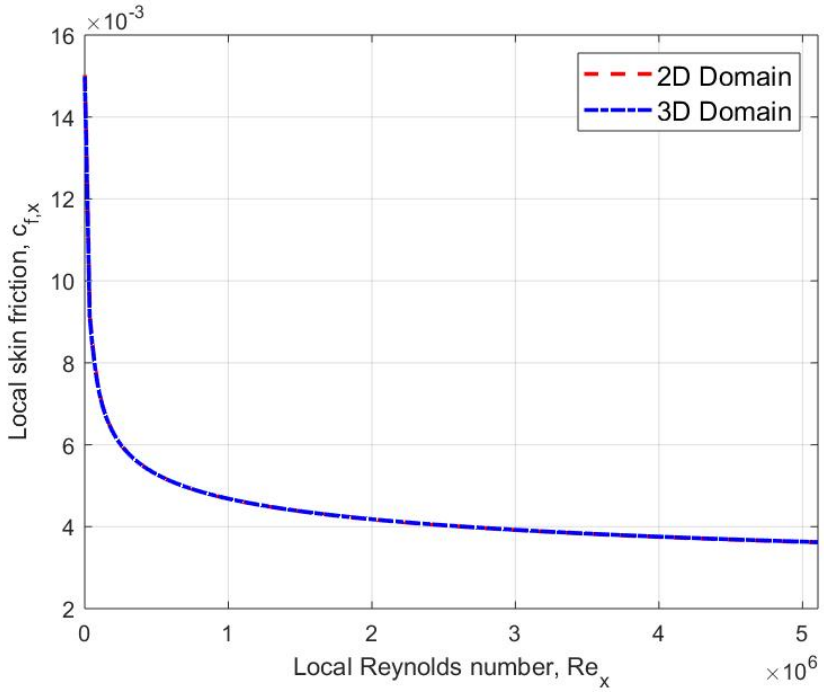

Figure 3.8 – Comparison between 2D and 3D domain results for local skin friction ($c_{f,x}$) with respect to local Reynolds number (Re_x)

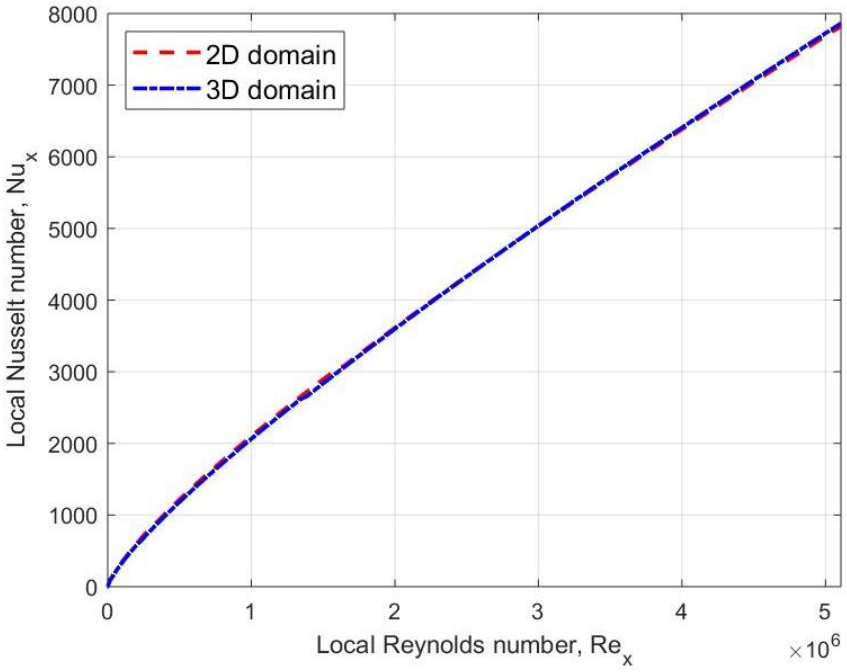

Figure 3.9 - Comparison between 2D and 3D domain results for local Nusselt number (Nu_x) with respect to local Reynolds number (Re_x)

The use of a 2D domain instead of a 3D domain for the heated cases would not cause significant differences for heat transfer coefficients. Moreover, the TI decay, which is an important factor in the current study, is within 0.1% from the 3D domain case, as shown in Figure 3.10.

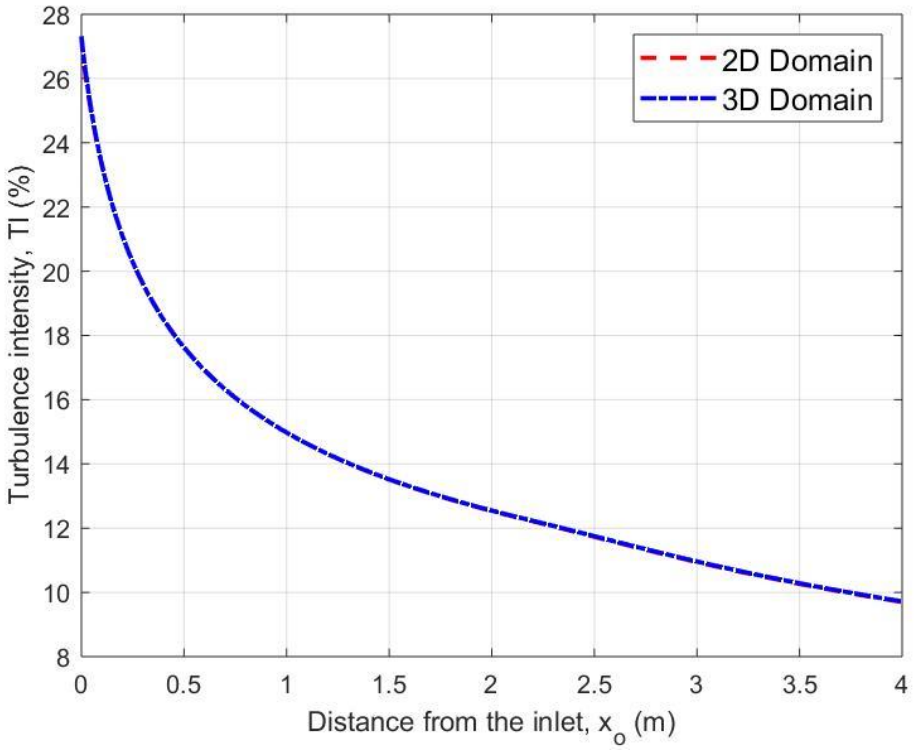

Figure 3.10 – Streamwise TI decay comparison between 2D and 3D domains for *TI* = 12.6% and L_u = 0.1m

Thus, the FST conditions applied in the 2D cases will be the same as the setups chosen for the 3D domain, with the addition of heat transfer. The BL development observed was also similar, with the BL thickness and momentum thickness for the 2D domain being within 0.1% and 0.5% from the results for the 3D domain, respectively, as presented below.

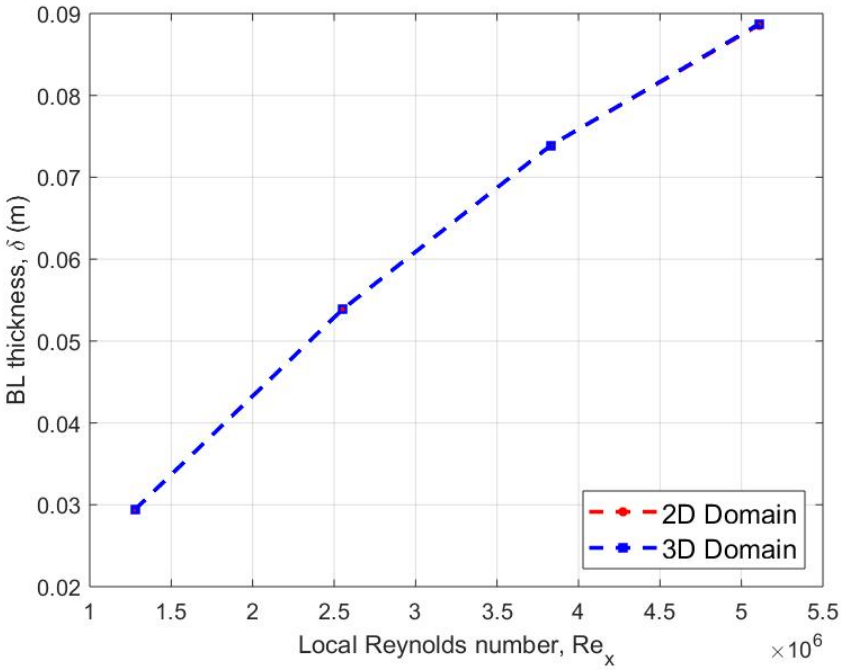

Figure 3.11 – Comparison between 2D and 3D domain results for BL thickness (δ) with respect to local Reynolds number (Re_x)

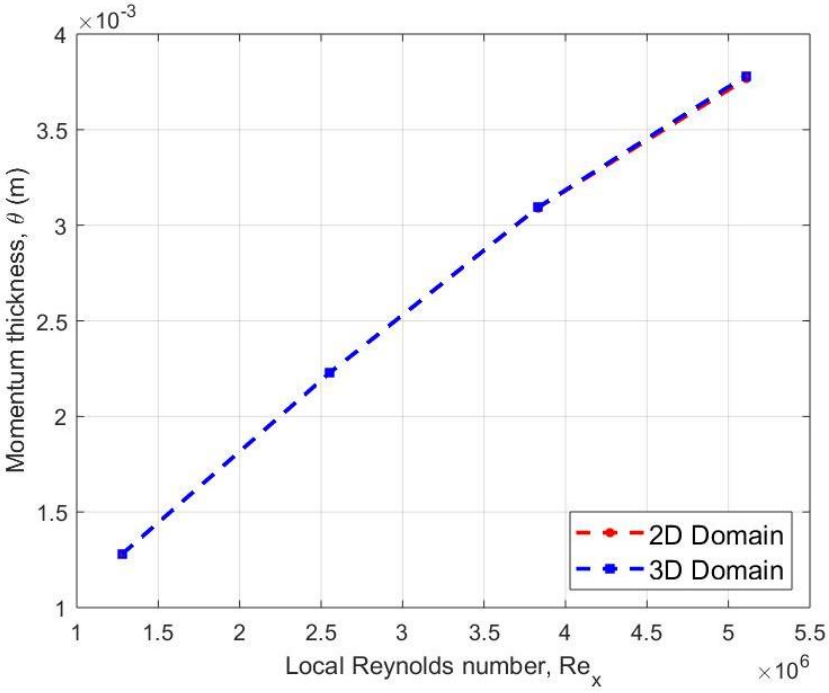

Figure 3.12 - Comparison between 2D and 3D domain results for momentum thickness (θ) with respect to local Reynolds number (Re_x)

Therefore, it is possible to conclude that using the 2D domain would provide similar results to those of the 3D domain.

3.2.6 Grid independence study

In order to ensure that the results are not affected by the chosen grid and that discretization errors are minimized, a study was conducted using three different meshes with 50,755 (M1), 76,231 (M2) and 122,868 (M3) nodes. Note that the refinement ratio between the grids is at least 1.5, as recommended by the COST guidelines (Frank et al., 2007). The results were validated by comparing the local Nusselt number, as well as the thermal boundary layer profile.

In these cases, the free-stream velocity was set as 40 m/s and the turbulence intensity was kept at a low value (TI_o = 0.1%, L_{uo} = 0.1m), which corresponds to TKE and specific dissipation rate values of 2.4×10^{-3} J/kg and 5.44 s^{-1} respectively, so that the flow field could be validated with respect to theoretical correlations. The comparison between the local Nusselt number values is presented in Figure 3.13 and the thermal profiles in Figure 3.14.

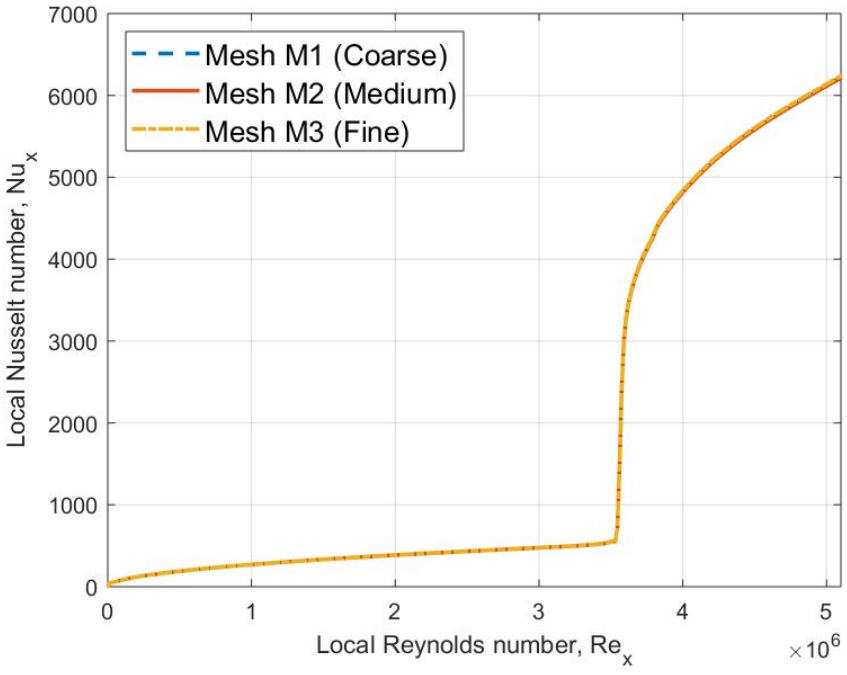

Figure 3.13 - Grid independence study – comparison between local Nusselt number results from meshes M1, M2 and M3

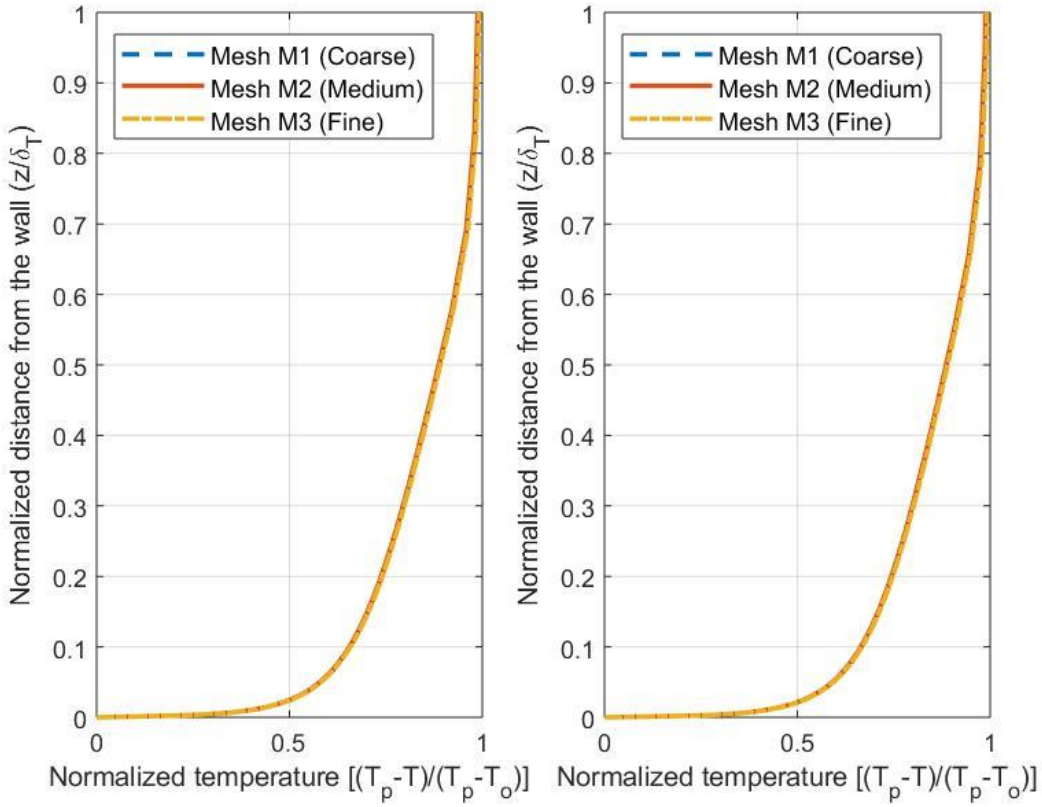

Figure 3.14 - Grid independence study – comparison between thermal profiles at the locations *x/L* = 0.75 (a) and *x/L* = 1.0 (b) from grids G1, G2 and G3

Where δ_T denotes the thermal boundary layer thickness, which is the distance *z* where the temperature *T* results in $\left[\left(T_p - T\right)/T_p - T_o\right] = 0.99$.

Both local Nusselt number and thermal profiles does not vary more than 1% from meshes M1 to M2 and M2 to M3. Thus, the results are grid independent and the medium mesh (M2) was used in the next cases. The validation of the flow field with theoretical correlations is presented next.

3.2.7 Validation of the flow field

The dimensionless correlations for local CHTC of laminar and turbulent boundary layers were expressed by Eq. (1.13) and Eq. (1.14), respectively. Figure 3.15 shows the

comparison of these correlations with the result obtained for the case with low turbulence (TI_o = 0.1%, L_{uo} = 0.1m).

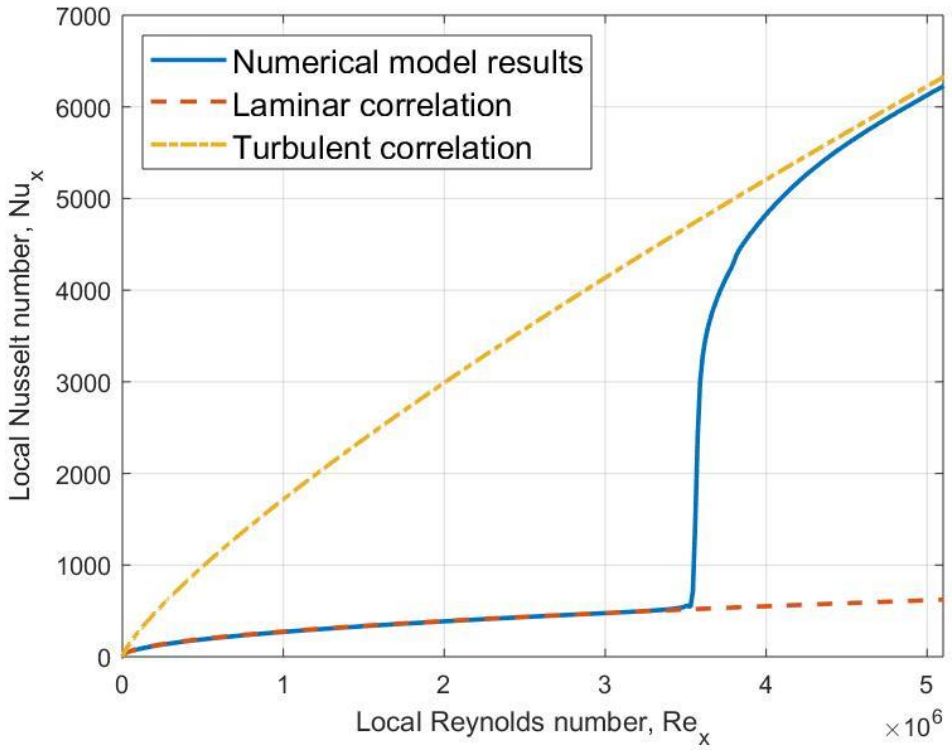

Figure 3.15 – Local Nusselt number validation with laminar and turbulent correlations with respect to local Reynolds number

Although transition is delayed, as presented before in Chapter 2 for the local skin friction validation, the model predicts the laminar part within 0.5% and the turbulent correlation is under predicted by 1.5%. Note that the theoretical turbulent correlation for Nu_x (refer to Eq. (1.14)) was derived for a flow with constant properties and Pr close to unity. Additionally, Eq. (1.14) assumes that the flow is fully turbulent and the mean velocity profile follows the one-seventh power law, but in this case (TI_o = 0.1%) the flow is not yet fully turbulent at the trailing edge of the plate, as shown in Section 2.2.6. Increasing the turbulence at the free-stream leads to earlier transition and the flow analyzed in the next cases will be fully turbulent, as will be presented in the next section.

One final validation to consider is the analysis of the importance of natural convection with respect to forced convection. This can be done by verifying the Richardson number, defined as (Nicholl, 1970):

$$Ri = \frac{Gr}{{Re_L}^2} \tag{3.24}$$

Where *Gr* is the Grashof number, given by Eq. (3.25) (Incropera et al., 2007):

$$Gr = \frac{g\beta(T_p - T_o)L^3}{\nu^2} \tag{3.25}$$

Where β is the volumetric thermal expansion of air, that can be calculated by $\beta = 1/T_o$, ν is the kinematic viscosity of air.

Richardson number express the influence of natural convection with respect to forced convection, i.e., the relative influence of buoyancy forces with respect to flow inertia (Nicholl, 1970). When *Ri* is less than 0.1, also known as 'critical value', natural convection is negligible. Considering the flow speed of 40m/s, *Ri* = 0.057, so the natural convection can be neglected and forced convection is dominant. The impact of different free-stream conditions on CHTC is examined next.

3.3 Analysis of different free-stream conditions

3.3.1 Effect of turbulence intensity

Various cases with different values of free-stream turbulence (FST) were analyzed. The free-stream velocity was defined as 40 m/s (Re_x up to 5.11×10^6) because most of the boundary layer developed on the plate would be turbulent and laminar-turbulent transition effects on the observed results would not be significant. Four different values of turbulence intensity at the leading edge (2.0%, 5.7%, 9.0% and 12.6%) were examined while keeping the integral length scale as L_u = 0.1m. These values were selected based on the TKE decay correlations presented before as Eq. (3.22) and Eq. (3.23) in such a way that the initial turbulence conditions at the inlet were still within the validity of these expressions ($TI \leq 30\%$). The inlet turbulence conditions are presented below, where the TKE and ω are normalized by U_o^2 and L_{uo}/U_o, respectively.

Table 3.2 – Inlet normalized turbulence conditions with varying leading edge TI values for U_o = 40m/s and L_u = 0.1m

TI at the leading edge (u'/U_o)	**TKE at the inlet (k_o/U_o^2)**	**ω at the inlet ($\omega_o L_{uo}/U_o$)**
2.0%	0.1×10^{-2}	0.44
5.7%	1.1×10^{-2}	1.89
9.0%	3.9×10^{-2}	4.34
12.6%	11.2×10^{-2}	9.23

T_p and T_o were kept as 313K and 293K, respectively. The comparison of local Nusselt number between these cases and the turbulent correlation, given by Eq. (1.14), is presented in Figure 3.16.

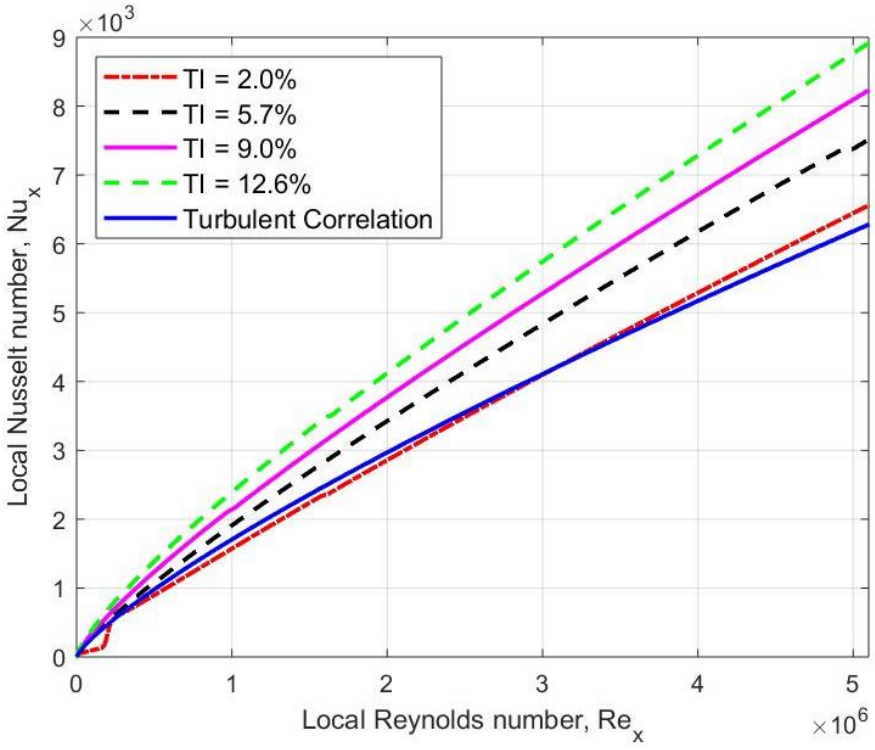

Figure 3.16 – Local Nusselt number (Nu_x) with respect to local Reynolds number (Re_x) for varying *TI* and comparison with turbulent correlation

The local Nusselt number increases with increasing free-stream TI, as noted by previous studies (Kondjoyan et al, 2002). Considering the results for *TI* = 2.0%, it is possible to observe that transition occurs close to the leading edge and the Nu_x value is within 5% of the turbulent correlation for Re_x up to $3x10^6$ ($x/L \approx 0.6$) and then surpasses it for $Re_x > 3.3x10^6$ ($x/L \approx 0.65$) by up to 6% for $Re_x = 5.1x10^6$. Additionally, the local Nusselt number is increased by 36% for *TI* = 12.6% when compared to *TI* = 2.0% at $Re_x = 5.1x10^6$. Note that the percentage increase of a quantity Q is given by the difference with respect to a reference value (Q_0) divided by Q_0, i.e., $\%increase = \frac{Q-Q_0}{Q_0} x100$. For the low turbulence case, the Nusselt number predicted by the numerical study is underpredicted with respect to the turbulent correlation, as was noted by Karava et al. (2012). Since the flow is already turbulent from $x/L = 0.25$ and to keep consistency with the considerations made in chapter 2, the analysis for local Nusselt number was conducted in the region from $x/L = 0.25$ to $x/L = 1$. The influence on Nu_x of other parameters, such as L_u, will be presented later.

Considering the total (or average) Nusselt number (Nu_L) of the plate using Eq. (3.26).

$$Nu_L = \frac{\bar{h}L}{k}, where\ \bar{h} = \frac{1}{0.75L}\int_{0.25L}^{L} \frac{q_x}{\Delta T} dx \tag{3.26}$$

The results obtained for the total Nusselt number are presented in Figure 3.17.

The increase in Nusselt number can be up to 42% when *TI* is increased from *TI* = 2.0% to *TI* = 12.6%. Considering the total Nusselt number empirical correlation for a fully turbulent boundary layer when *TI* = 0%, as presented by Eq. (1.18), the value of Nu_L for a case with no turbulence derived from the linear expression presented in Figure 3.17 is within 7% from what is predicted from Eq. (1.18). Next the effect of L_u on CHTC is examined.

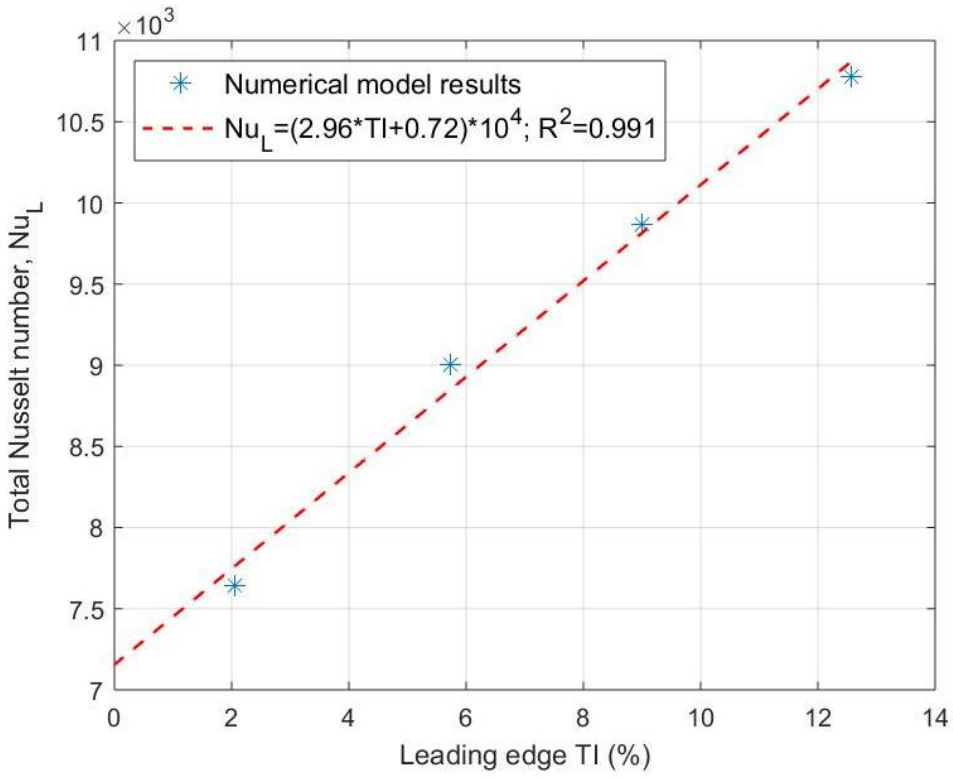

Figure 3.17 – Variation of total Nusselt number (Nu_L) with varying leading edge *TI* for Re_L = 5.1x10^6 and L_u = 0.1m

3.3.2 Effect of length scale

In order to analyze the effect of length scale on turbulent boundary layers, four different values of L_u were examined besides L_u = 0.10m, specifically L_u = 0.02m; 0.05m and 0.07m. As mentioned in Chapter 2, these values were defined knowing that the effect of free-stream turbulence was reported as being most significant when the length scale was of the same order of magnitude as the boundary layer (Hancock and Bradshaw, 1983). The length scale should also be large enough to perturb the boundary layer. In this study, the boundary layer thickness with no free-stream turbulence intensity is δ = 35.2mm at x/L = 1. Thus, most of the length scales analyzed here were greater than the BL thickness, except for L_u = 0.02m.

It is also important to observe that with a decreasing initial L_u, the TKE decays faster (see Eq. (3.22) and (3.23) and, therefore, higher values of TI need to be specified at the inlet until it is not feasible to attain the same leading edge TI as used in the cases with L_u = 0.1m.

For instance, in order to achieve TI = 9.0% at the leading edge with L_u = 0.05m, TI_o must be around 26% and it would not be feasible to achieve leading edge TI of 12.6%, because not even specifying TI_o of 80% would result in leading edge TI of 12.6%. Note also that the decay expressions (Eq. (2.15) and (2.16)) are valid for TI_o of up to 30%. The viable cases and conditions are then presented below.

Table 3.3 - Inlet normalized turbulence conditions with varying leading edge TI values for U_o = 40m/s and L_u = 0.02m

TI at the leading edge (u'/U_o)	**TKE at the inlet (k_o/U_o^2)**	**ω at the inlet ($\omega_o L_{uo}/U_o$)**
2.0%	$0.2\text{x}10^{-2}$	3.9
5.8%	$13.2\text{x}10^{-2}$	116.5

Table 3.4 - Inlet normalized turbulence conditions with varying leading edge TI values for U_o = 40m/s and L_u = 0.05m

TI at the leading edge (u'/U_o)	**TKE at the inlet (k_o/U_o^2)**	**ω at the inlet ($\omega_o L_{uo}/U_o$)**
2.1%	$0.1\text{x}10^{-2}$	0.8
5.7%	$2.1\text{x}10^{-2}$	5.2
9.1%	$10.2\text{x}10^{-2}$	18.1

Table 3.5 – Inlet normalized turbulence conditions with varying leading edge TI values for U_o = 40m/s and L_u = 0.07m

TI at the leading edge (u'/U_o)	**TKE at the inlet (k_o/U_o^2)**	**ω at the inlet ($\omega_o L_{uo}/U_o$)**
2.1%	0.1×10^{-2}	0.5
5.8%	1.5×10^{-2}	2.5
9.0%	5.9×10^{-2}	6.9
12.7%	20.1×10^{-2}	18.1

The comparison between local Nusselt number for varying L_u while keeping $TI \approx 2.0\%$ is presented in Figure 3.18. The turbulent correlation is given by Eq. (1.14).

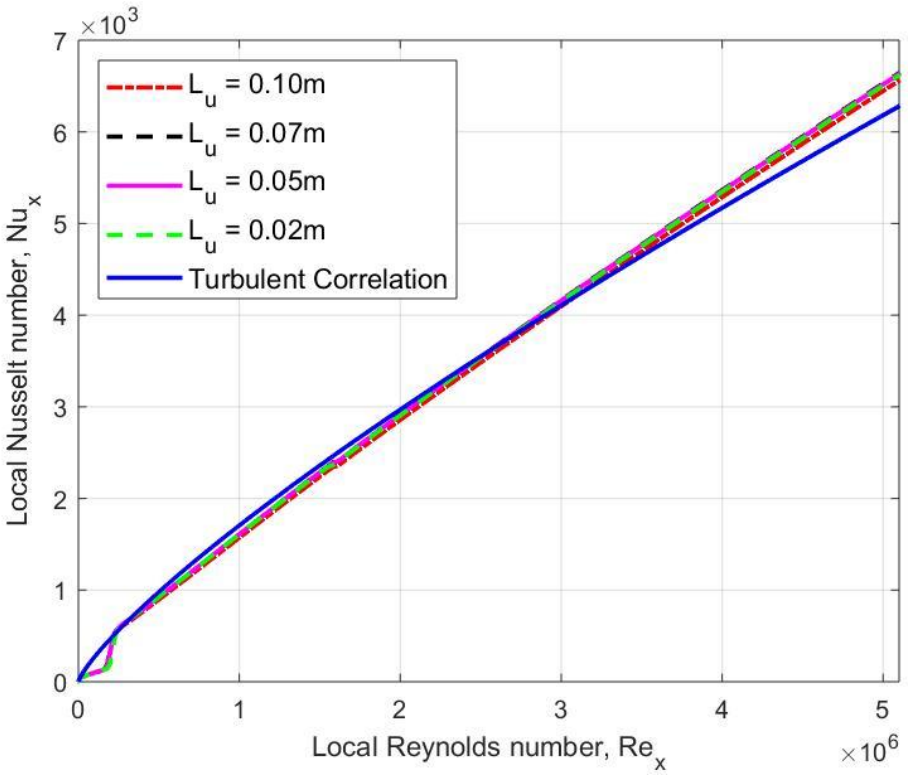

Figure 3.18 - Local Nusselt number (Nu_x) with respect to local Reynolds number (Re_x) for varying L_u with TI = 2.0% and comparison with turbulent correlation

It may be observed that the local Nusselt number was not greatly affected by the change in length scale. The increase in Nu_x was less than 1.3% for the different values of L_u compared to Nu_x for L_u = 0.1m when TI = 2.0%. For $TI \approx 5.7\%$, the difference of Nu_x between numerical cases was below 1.4% compared to the case with L_u = 0.1m, as shown in Figure 3.19.

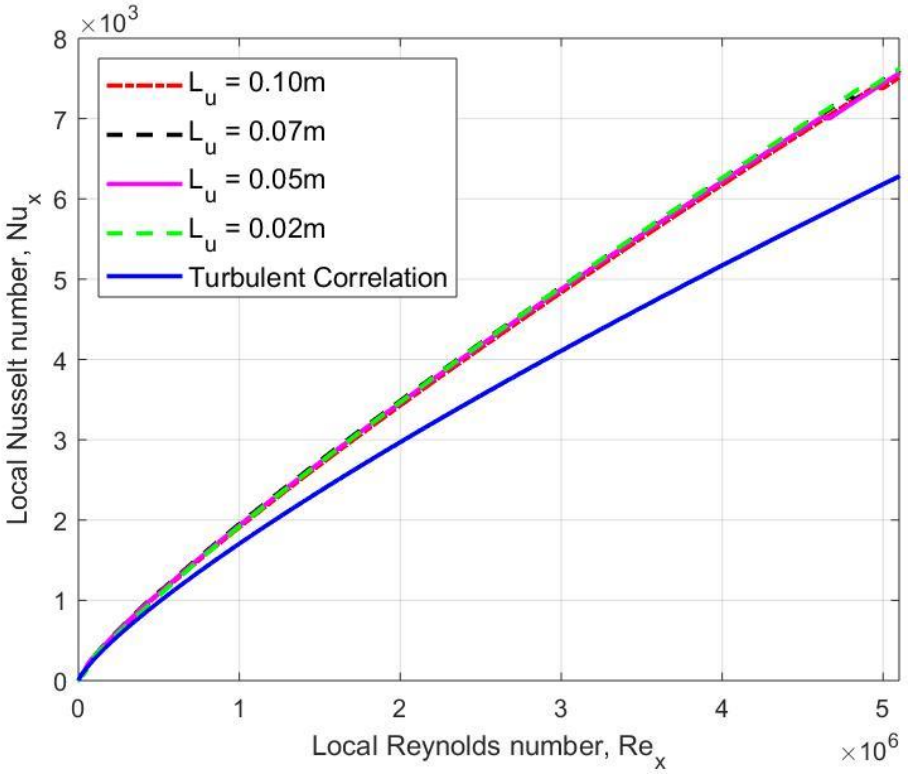

Figure 3.19 - Local Nusselt number (Nu_x) with respect to local Reynolds number (Re_x) for varying L_u with TI = 5.7% and comparison with turbulent correlation

For the cases with TI = 9.0% and TI = 12.6% the difference of Nu_x with varying L_u was below 0.5% when compared to the case with L_u = 0.1m. In the range of TI and L_u analyzed, the variation of L_u did not affect Nu_x by more than 1.3%. Regarding the total Nusselt number, Figure 3.20 shows the results for all cases with varying L_u.

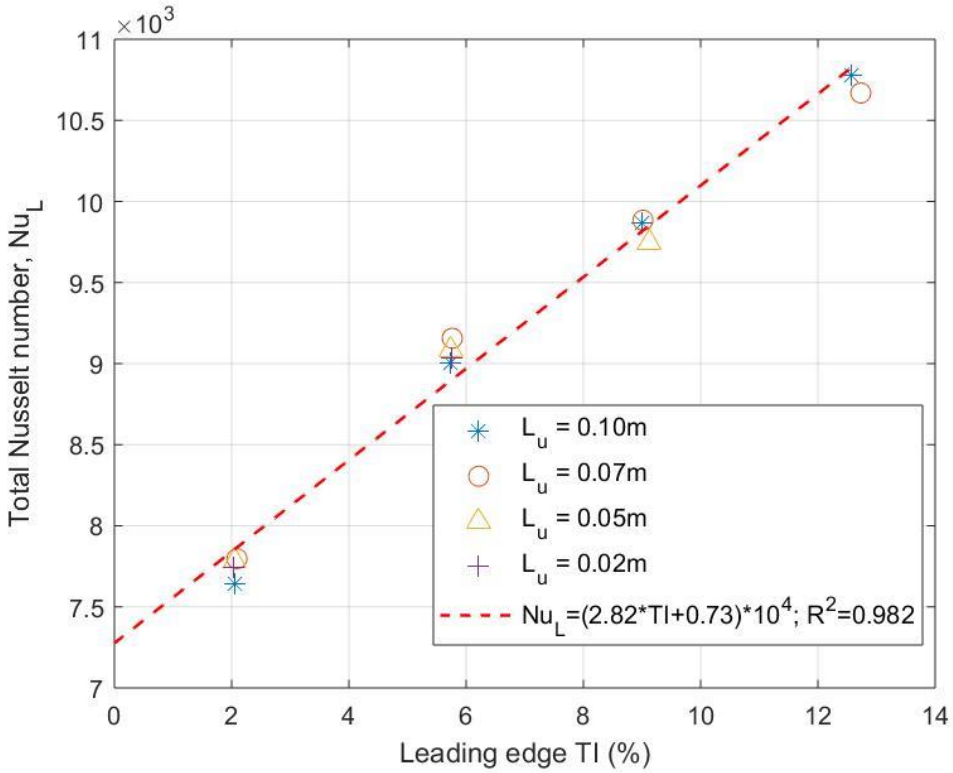

Figure 3.20 - Total Nusselt number (Nu_L) with respect to leading edge TI for varying L_u and Re_L = 5.1x10^6

The Nu_L predicted from the linear equation presented in Figure 3.20 for TI = 0% is within 5% of the empirical expression for a turbulent flow with no FST (refer to Eq. (1.18)). The percentage difference of total Nusselt number when changing the integral length scale to any given value while keeping the same TI is below 2.0%. The linear correlation derived from all cases is within 0.5% of the expression obtained for L_u = 0.1m. Therefore, no significant effect of length scale on CHTC was observed. As mentioned before in Section 3.1.1, the parameter proposed by Hancock and Bradshaw (1983) for the increase in local skin friction with FST was analyzed by Baskaran et al. (1989) and applied to the increase in St_x (refer to Eq. (3.2)), but there was a large scatter between their experimental results and the expression from Hancock and Bradshaw (1983). Furthermore, MacMullin et al. (1989) showed a large disparity between their experimental results and the expressions from Simonich and Bradshaw (1978) and Blair (1983). MacMullin et al. (1989) highlighted that the effect of L_u on St_x could not be concluded from their experimental data. Therefore,

there was no indication from previous studies that the inclusion of length scale on correlations for the increase in CHTC with FST improves the description of results from different studies (Baskaran et al., 1989; MacMullin et al., 1989; Kondjoyan et al., 2002) when compared to the simple linear relation presented by Simonich and Bradshaw (1978) (refer to Eq. (3.1)). Additionally, the effect of free-stream TKE decay and the different FST conditions at which the boundary layer starts to develop were not considered by previous works (Blair, 1983; Kondjoyan et al., 2002). Next different free-stream velocities are analyzed.

3.3.3 Effect of Reynolds number

With the aim of analyzing the effect of Reynolds number, two more values of free-stream velocity were examined: U_o = 60m/s and 80m/s (Re_x and Re_L up to 1.02×10^7). These values guarantee that the boundary layer will be fully turbulent while keeping the flow incompressible. The length scale was kept at L_u = 0.1m since it allows for a good range of TI. The conditions at the inlet were the same normalized conditions used for U_o = 40m/s and presented in Table 3.2. The local skin friction when TI = 2% for these different free-stream velocities is presented in Figure 3.21.

Considering the range of local Reynolds number common to all cases ($Re_x \leq 5.1 \times 10^6$), the local Nusselt number values are all within 0.5% from Nu_x for the case with U_o = 40m/s. This small variation of Nu_x was also observed for the other TI conditions, the cases with TI = 12.6% are presented in Figure 3.22.

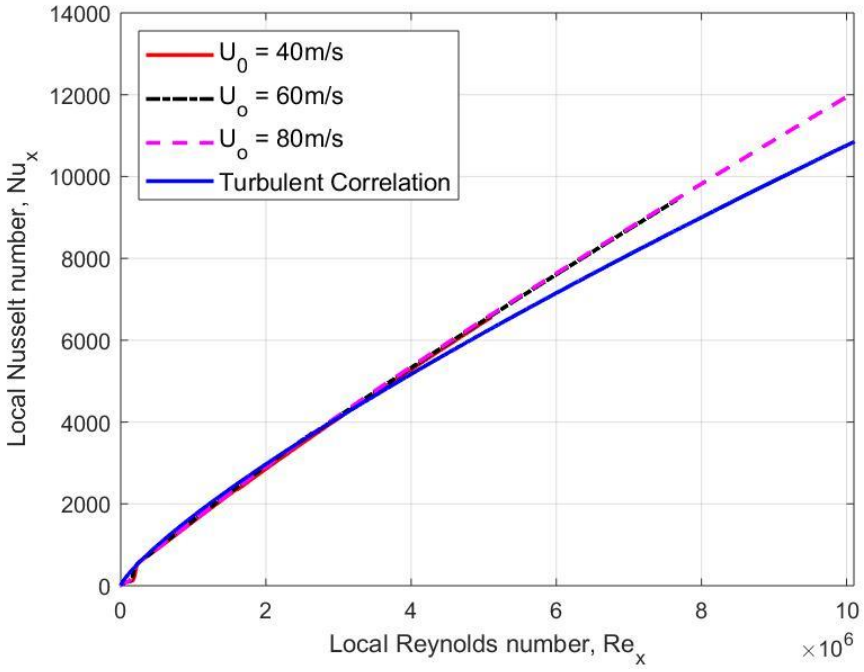

Figure 3.21 - Local Nusselt number (Nu_x) with respect to local Reynolds number (Re_x) for varying U_o with TI = 2.0% and comparison with turbulent correlation (Eq. (1.14))

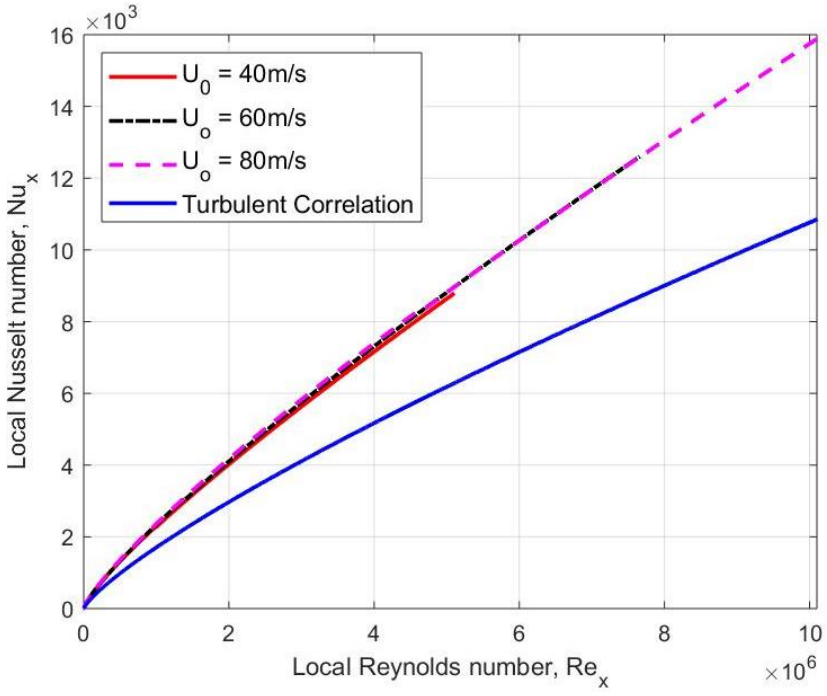

Figure 3.22 - Local Nusselt number (Nu_x) with respect to local Reynolds number (Re_x) for varying U_o with TI = 12.6% and comparison with turbulent correlation (Eq. (1.14))

The Nu_x values for the common range of Re_x ($Re_x \leq 5.1\text{x}10^6$) varies only up to 1% with respect to the case with U_o = 40m/s. As for the total Nusselt number, the results for the various cases with different U_o are presented in Figure 3.23.

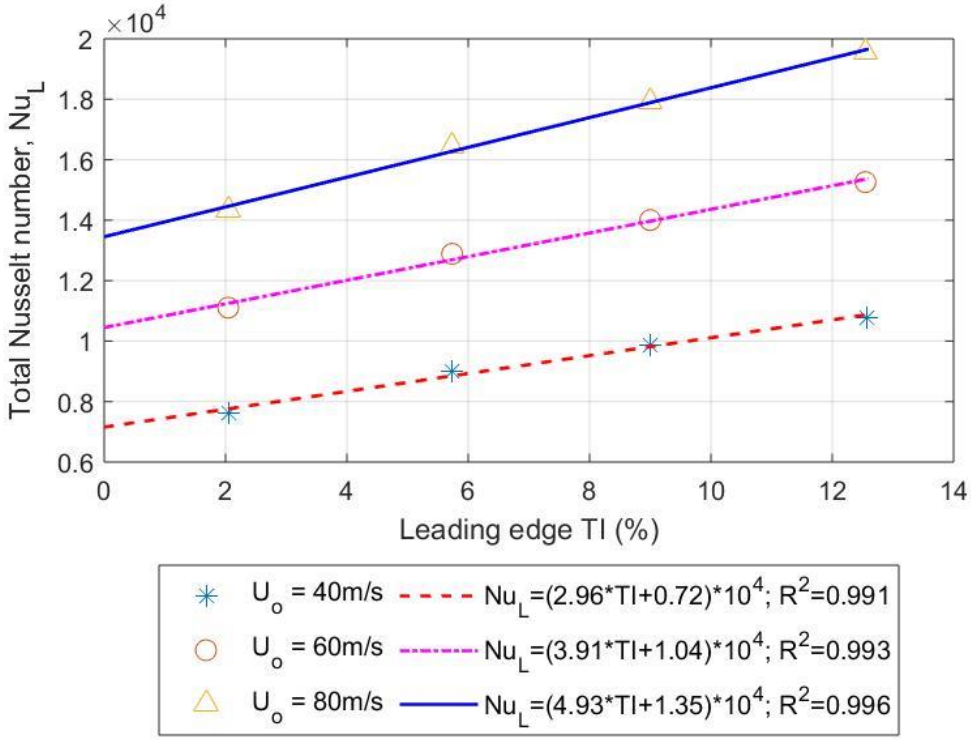

Figure 3.23 - Total Nusselt number (Nu_L) with respect to leading edge TI for varying U_o and respective linear fits

The increase in total Nusselt number are similar for the different free-stream velocities. The percentage increases for TI = 12.6%, compared to the value for TI = 2.0%, are 42%, 37% and 36% when U_o is equal to 40m/s, 60m/s and 80m/s, respectively. Furthermore, the linear expressions presented in Figure 3.23 for U_o = 40m/s, 60m/s or 80m/s for TI = 0% are within 7%, 2% and 1% of the expression for a turbulent flow with no FST (refer to Eq. (1.18)), respectively. Correlations for Nu_x and Nu_L that describe the increase in CHTC observed for all cases presented so far are evaluated next.

3.4 Development of correlations for CHTC

Taking the three different free-stream conditions analyzed, i.e., *TI*, L_u and Re_x (or Re_L) and assuming the following equations:

$$Nu_x = c_1 {Re_x}^{4/5}(1 + c_2 TI)\left(1 + {L_u}/{L_{uref}}\right)^{c_3} Pr^{1/3} \tag{3.27}$$

$$Nu_L = C_1 {Re_L}^{4/5}(1 + C_2 TI)\left(1 + {L_u}/{L_{uref}}\right)^{C_3} Pr^{1/3} \tag{3.28}$$

The exponents of Re_x (or Re_L) and Pr were kept as 4/5 and 1/3, respectively, in order to develop correlations consistent with the expressions of Nu_x and Nu_L for fully turbulent boundary layers with no FST (refer to Eq. (1.14) and Eq. (1.18)). Furthermore, the correlations were defined as linearly dependent with *TI*, as presented in Sections 3.3.1, 3.3.2 and 3.3.3. As noted before in Chapter 2 (Section 2.4), the dimension L_{uref} was defined as 0.1m and was chosen to nondimensionalize the L_u value in a way that it would not be necessary to know TBL characteristics such as BL thickness. Additionally, the L_{uref} value is the largest integral length scale examined in the current work and of the order of magnitude of the largest eddy analyzed in previous studies (Hancock and Bradshaw, 1983; Ames and Moffat, 1990; Karava et al., 2012).

The results for local Nusselt number were taken from $x/L = 0.25$ to $x/L = 1$, as discussed before in Section 3.3.1. There are more than 200 points in this region for each case and so an analysis was conducted to investigate the effect of considering a smaller number of points on the coefficient and exponents of Eq. (3.27). Two points ($x/L = 0.25$ and $x/L = 1$) were initially considered and then equally spaced points between those two were added for a resulting number of 4, 8, 16, 32, 64 and 128 points. The case with four different locations is shown in Figure 3.24.

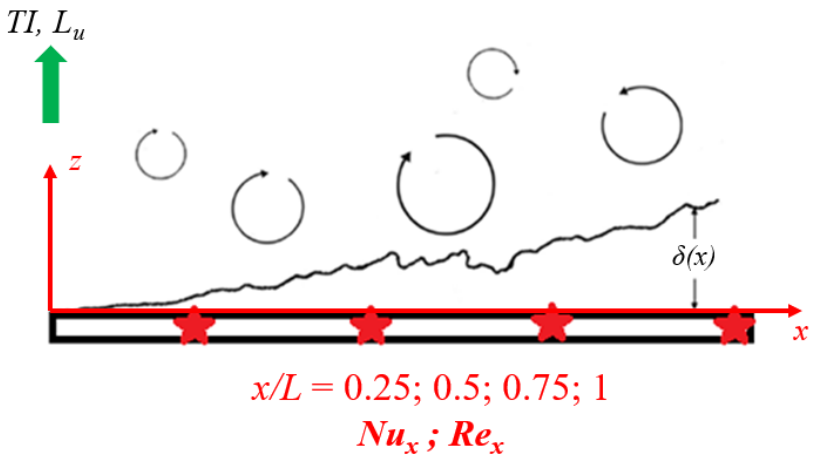

Figure 3.24 – Plate diagram with locations used to derive local Nusselt number correlations

The variation observed in the coefficient and exponents of Eq. (3.27) is presented in Figure 3.25.

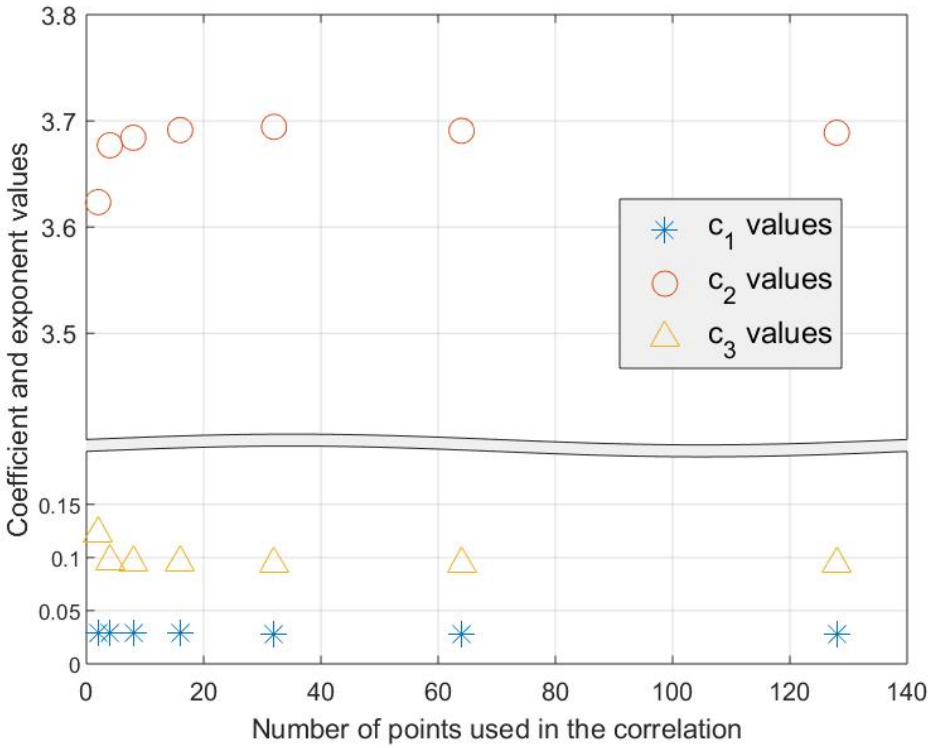

Figure 3.25 – Variation of coefficient and exponents values of Eq. (3.27) with respect to the number of points used in the correlation

The percentage difference between the calculated exponents and coefficients when the number of points is increased from 2 to 4 is up to 5%, but it is below 1% when the number of points is increased from 4 to any given value. Therefore, the correlations will be given considering the four locations presented in Figure 3.24.

Considering Eq. (3.27) and performing a non-linear regression, the results are c_1 = 0.029; c_2 = 3.677 and c_3= 0.096 (R^2 = 0.998). The comparison between the Nu_x values obtained from Eq. (3.27) and the numerical model results is shown in Figure 3.26.

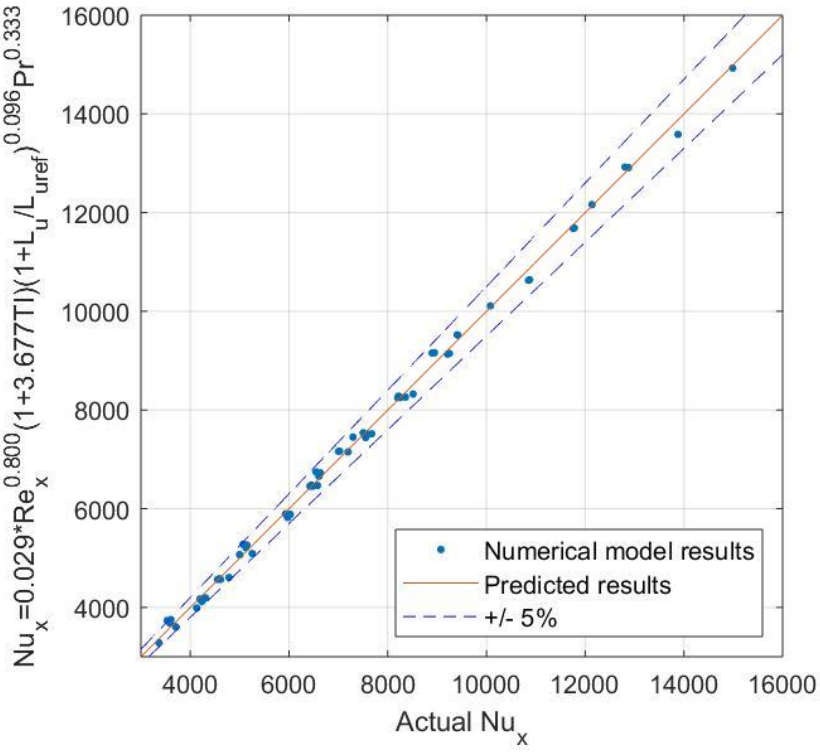

Figure 3.26 - Comparison of the local Nusselt number (Nu_x) values obtained from the predicted correlation with the numerical results from cases with varying U_o and leading edge *TI* and L_u

The numerical model results lie within ±5% of the derived correlation. This expression confirms that the influence of L_u is relatively small when compared to the other parameters. The parameter that has the greater effect on CHTC is turbulence intensity. Furthermore, if the results obtained from the derived correlation for the range of L_u examined in the current

study and for TI = 0% are compared with the expression for the local Nusselt number for turbulent flows with no FST (refer to Eq. (1.14)), the correlation derived in the current study predicts Nu_x within ±5%.

Considering Eq. (3.28), the resulting coefficient and exponents are C_1 = 0.035; C_2 = 3.729; C_3 = 0.097 (R^2 = 0.994). This expression represents most results from numerical cases within ±5% as shown below.

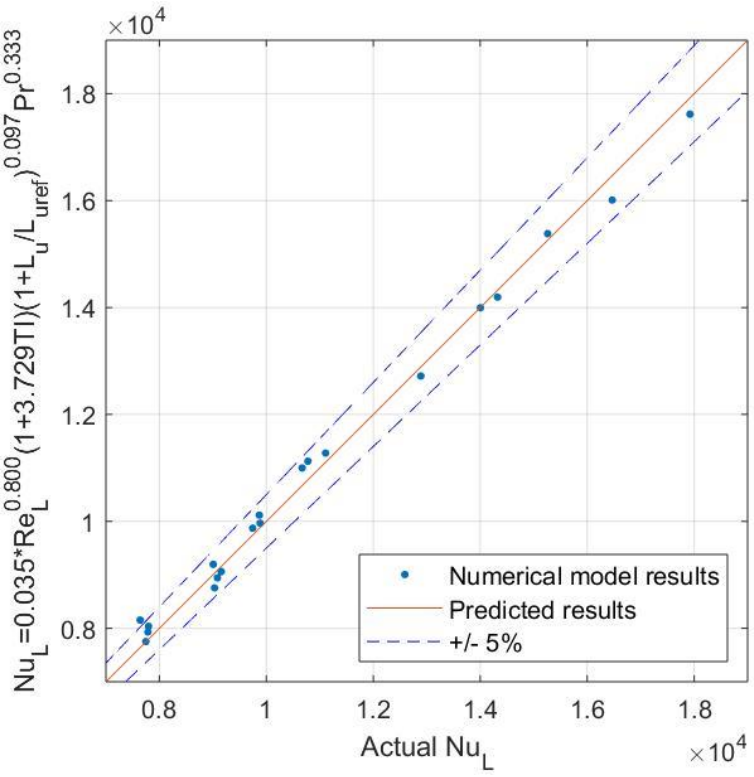

Figure 3.27 - Comparison of the total Nusselt number (Nu_L) values obtained from the predicted correlation with the numerical results from cases with varying U_o and leading edge TI and L_u

The Nu_L expression shows that the influence of TI and L_u on Nu_L is the same as the influence of the same parameters on Nu_x values, with the exponents of TI and L_u from the Nu_L correlation being within 1% of the exponents for these parameters from the Nu_x correlation. Additionally, considering the empirical correlation for the total Nusselt number for a fully turbulent flow with no FST (refer to Eq. (1.18)), the derived correlation presented in Figure

3.27 predicts the Nu_L for the range of L_u considered in the current study within 5% of the empirical correlation.

Other important correlations to obtain are for total Stanton number (St) and local Stanton number (St_x), since many studies present their heat transfer data in terms of this dimensionless parameter (Kondjoyan et al., 2002). Note that the Stanton number is given by the Nusselt number divided by the Reynolds and Prandtl numbers ($St = \frac{Nu_L}{Re_L\, Pr}$). Supposing that St and St_x follow similar correlations:

$$St_x = c_1 {Re_x}^{-1/5}(1 + c_2 TI)\left(1 + {L_u}/{L_{uref}}\right)^{c_3} Pr^{-2/3} \tag{3.29}$$

$$St = C_1 {Re_L}^{-1/5}(1 + C_2 TI)\left(1 + {L_u}/{L_{uref}}\right)^{C_3} Pr^{-2/3} \tag{3.30}$$

These expressions are consistent with the proposed correlations for Nu_x and Nu_L (refer to Eq. (3.27) and Eq. (3.28)). For Eq. (2.29), the resulting coefficient and exponents are: c_1 = 0.029; c_2 = 3.784; c_3 = 0.053 (R^2 = 0.979). For Eq. (3.30), the best fit is given by the following coefficient and exponents: C_1 = 0.035; C_2 = 3.805; C_3 = 0.048 (R^2 = 0.968).

The resulting correlations express most of the numerical model results for St_x and St within ±5%, as shown in Figure 3.28 and Figure 3.29, respectively.

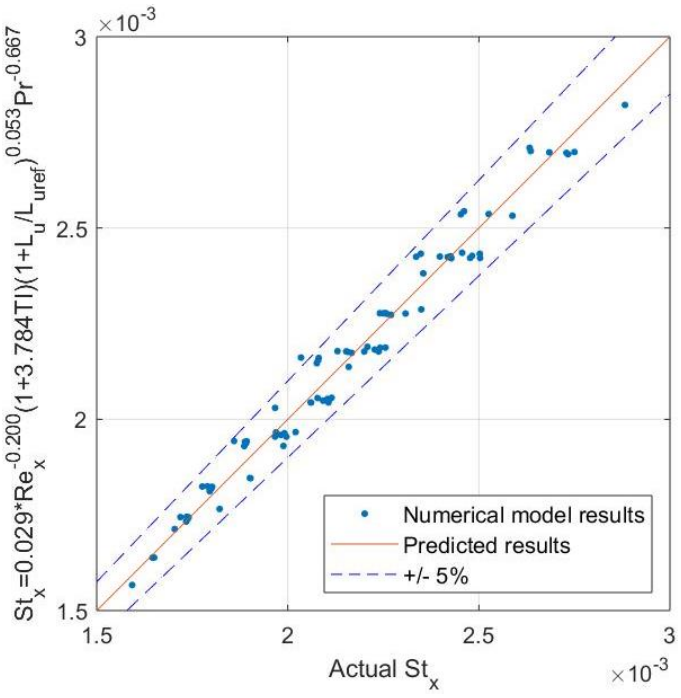

Figure 3.28 - Comparison of the local Stanton number (St_x) values obtained from the predicted correlation with the numerical results from cases with varying U_o, TI and L_u

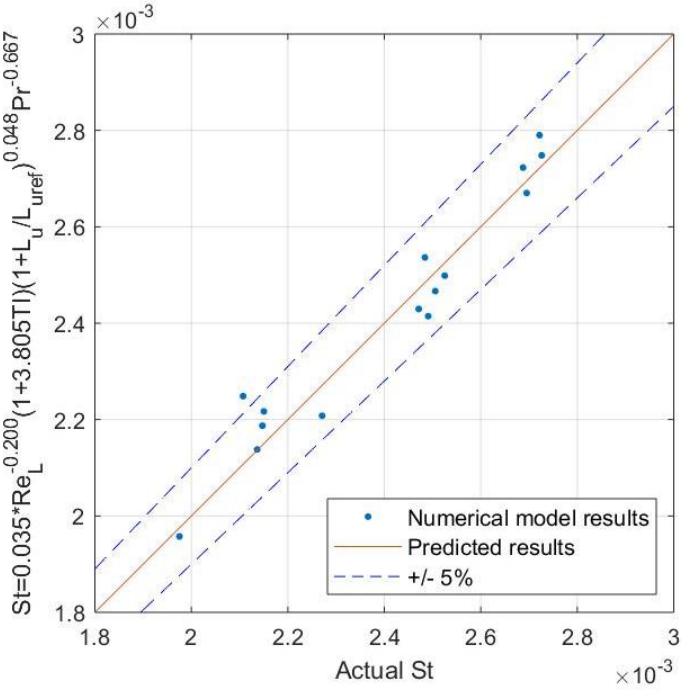

Figure 3.29 - Comparison of the total Stanton number (St) values obtained from the predicted correlation with the numerical results from cases with varying U_o, TI and L_u

Next, an investigation of whether the deduced expressions for Nu_x, Nu_L, St_x and St in terms of Re_x (or Re_L), TI and L_u are a good representation of the data from previous work is presented.

3.5 Comparison with previous studies

Since most studies present their data in terms of Stanton number, the local and total Stanton number correlations are analyzed and validated with previous studies first. One important aspect to mention is that, in order to compare the proposed expression with results from other works, the values of TI and L_u at the plate leading edge need to be estimated. For instance, Blair (1983) and Ames and Moffat (1990) present expressions for the turbulent kinetic energy decay in the test region and so it is possible to determine the plate leading edge TI. Besides that, the authors also present the growth of longitudinal length scale along the test section and so the parameter values used as inputs in the proposed correlations are consistent with those authors' experiments. As for the study from Barret and Hollingsworth (2003), it is possible to estimate the leading edge values because the plate location and TI and L_u at the beginning of the test section are known and the TKE decay correlations developed by Sarkar (2018) can be used. Karava et al. (2012) positioned the plate LE at the inlet of the numerical domain. Thus, Figure 3.30 shows the comparison of the proposed local Stanton number correlation with the results from previous studies.

The TI values from previous studies varies from 1.3% to 20%, the length scale range is from 0.01m to 0.13m and the Reynolds numbers considered vary from 5.0×10^5 to 8.2×10^6. Most values from previous works lie within ±10% of the proposed correlation. As already mentioned, the streamwise TKE decay is an important factor to be considered for the validation of the proposed expression.

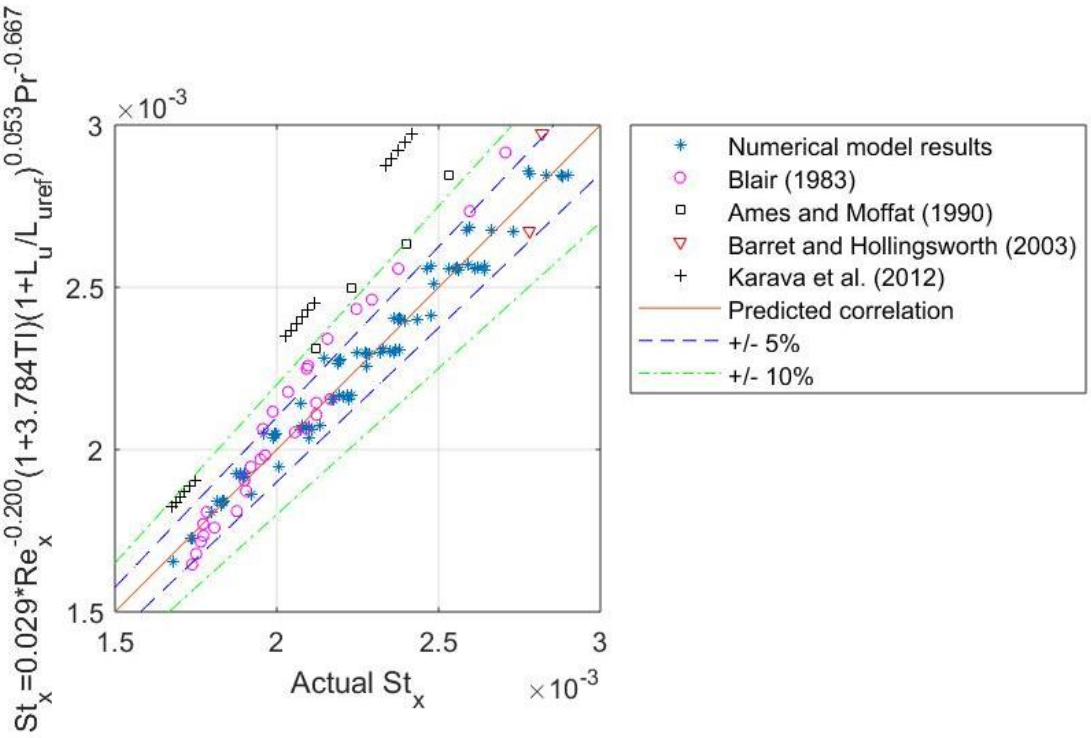

Figure 3.30 - Comparison between the estimated local Stanton number (St_x) values from previous studies and those predicted using the proposed correlation

Furthermore, the points that were not predicted by the correlation within 10% are mostly due to higher TKE decays. For instance, the results from Ames and Moffat (1990) that were predicted within 10% were taken for a case where *TI* = 16%, but with a TI percentage difference from the leading to the trailing edge of the plate of approximately 57%. For the other points that are within approximately 14% of the correlation, *TI* = 19% but the TI percentage difference is even higher and close to 96%. As for Karava et al. (2012), some points are within 10% of the correlation and others are within 25%. In these cases, *TI* is either 10% or 20% and the percentage difference of TI from the plate LE to the TE can be up to 70%. The greater disparity between the results from Karava et al. (2012) and the proposed correlation may be due to data being extracted by the authors only from x/L = 0.8 to x/L = 1 (Re_x starting from 6.6×10^6), where the TI is much lower than at the inlet, whereas the data from Ames and Moffat (1990) were taken along the plate starting from Reynolds numbers not much greater than transitional.

Additionally, Blair's experimental investigation only considered TI values of up to 7.7% and, although the percentage difference of TI could be up to 60%, the results are still within 10% of the correlation. A higher TKE decay leads to overpredicted values of St_x, since the correlation was developed assuming that the free-stream turbulence intensity does not vary by more than 25% in the plate region and, therefore, the predicted CHTC is higher. This seems to be more relevant for TI above 10%. Overall, it is possible to assume that the correlation provides a good prediction of local Stanton number with 10% accuracy when the plate is submitted to free-stream turbulence intensity levels that vary by up to 25% in the plate region.

Furthermore, the use of local free-stream turbulence intensity (TI_x) instead of the leading edge TI does not improve the scatter between the St_x values predicted by the proposed correlation and the data from previous studies, as shown in Figure 3.31.

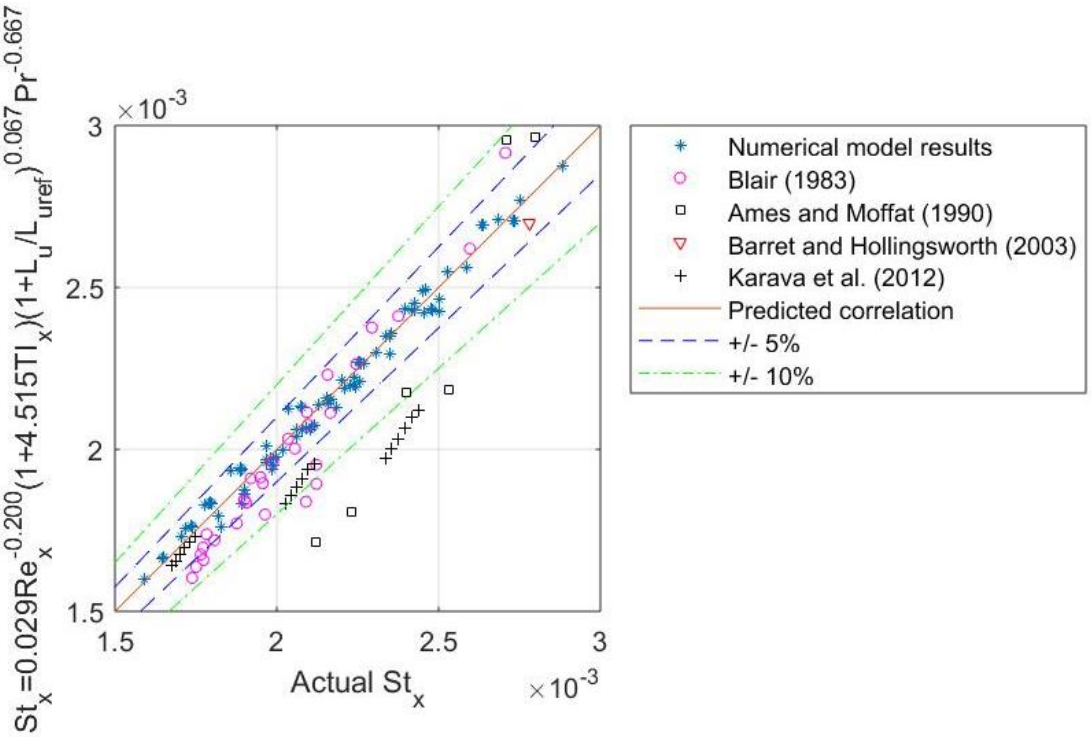

Figure 3.31 - Comparison between the estimated local Stanton number (St_x) values from previous studies and those predicted using the proposed correlation with local TI (TI_x)

The correlation using the local value of free-stream turbulence intensity underpredicts the St_x values from Ames and Moffat (1990) and Karava et al. (2012) by up to 20% and 17%, respectively. The St_x values were underpredicted because the local value of TI is much lower than the turbulence intensity at the leading edge (TI_x is around 30-40% of the leading edge TI), which indicates that the conditions at which the boundary layer starts to develop also influence the local Stanton number. If the leading edge TI in Eq. (3.29) is substituted by the average of the leading edge and trailing edge turbulence intensity values ($TI_{av} = (TI_{LE} + TI_{TE})/2$), most St_x values are predicted within ±5%, as shown in Figure 3.32.

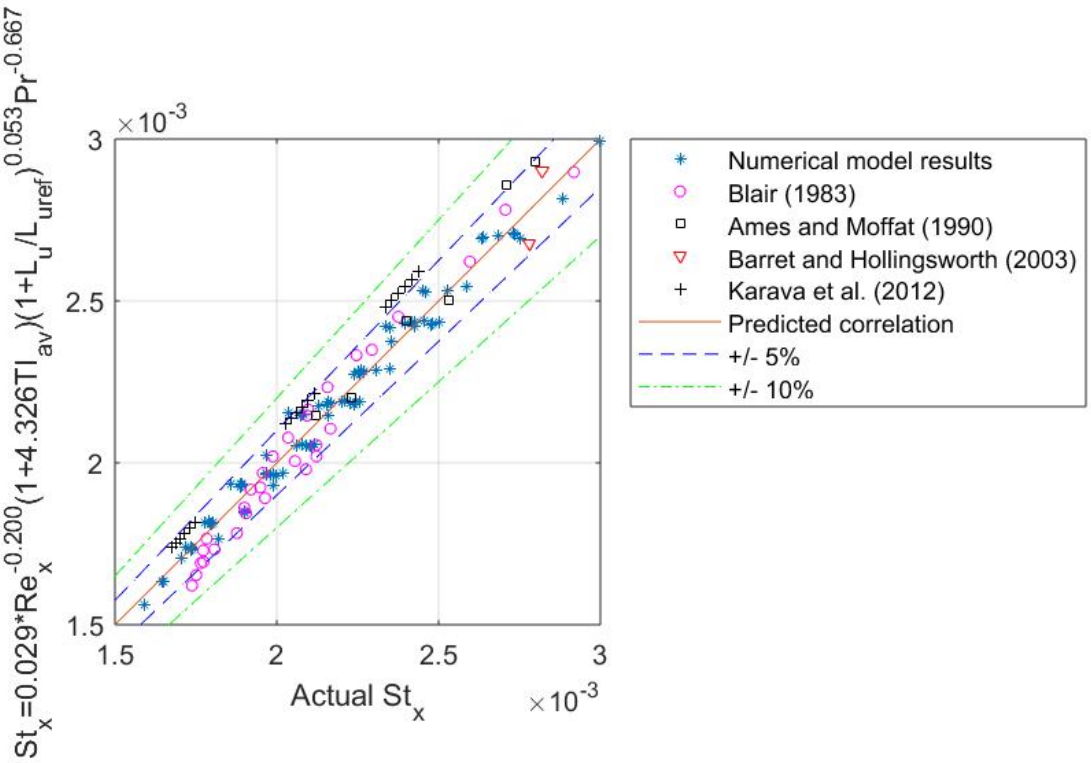

Figure 3.32 - Comparison between the estimated local Stanton number (St_x) values from previous studies and those predicted using the proposed correlation with average TI (TI_{av})

Therefore, the average value of turbulence intensity (TI_{av}) provides the best collapse of data from the current and previous studies and TI_{av} was used in the correlation for St.

Considering the total Stanton number, the experimental results from Barret and Hollingsworth (2003) were presented in one location at the plate and so were not included

in the validation. Blair (1983) and Ames and Moffat (1990) presented St_x values at four or more different locations downstream, therefore, it is possible to find the best curve that fits the St_x data. Considering a case with a given set of turbulence conditions (TI_{av} and L_u), the curve $St_x = A_1 x^{-0.2}$ (refer to Eq. (3.29)) was a good approximation ($R^2 > 0.95$ for all cases). Then an integral of this curve was performed from x = 0.5m to x = 2.0m because it was a common range when comparing the studies and it is consistent with the region used for the development of the *St* correlation. The comparison of the *St* values computed from the resulting expression and the values from previous studies estimated using the method presented is shown below.

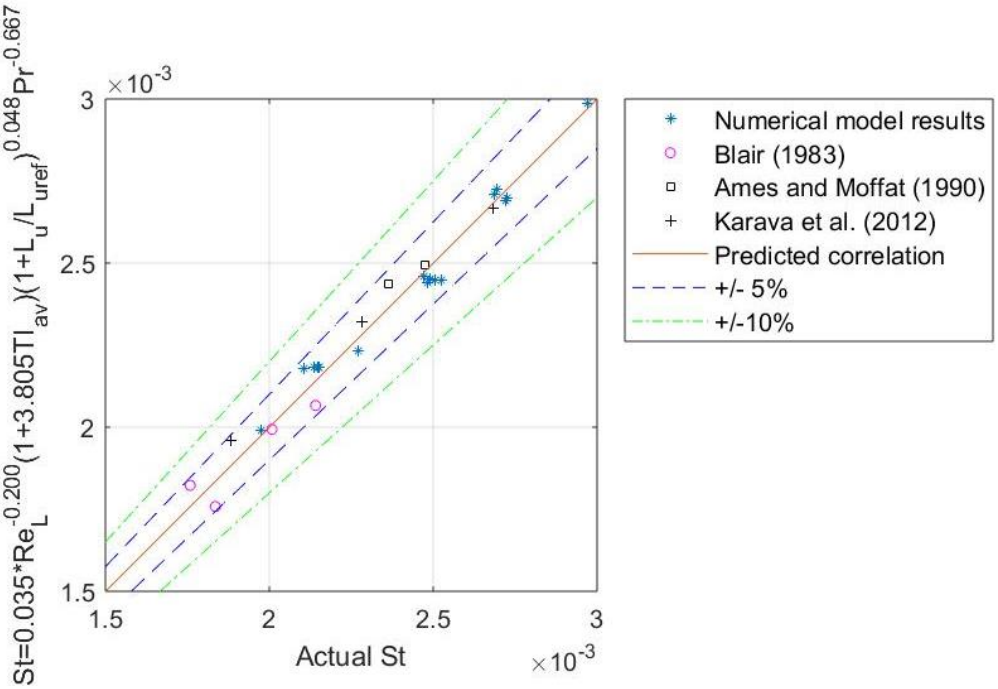

Figure 3.33 - Comparison between the estimated total Stanton number (*St*) values from previous studies and those predicted using the proposed correlation using TI_{av}

The proposed correlation predicts the values from those previous studies within ±5%. Therefore, the total *St* correlation provides a good estimate (within ±5%) of *St* for *TI* of up to 20% and fully turbulent boundary layers. Furthermore, the local and total Nusselt number correlations, when substituting *TI* by TI_{av} (refer to Eq. (3.27) and Eq. (3.28)), also predicts most results from the aforementioned studies within ±5%, as shown in Figure 3.34 and Figure 3.35.

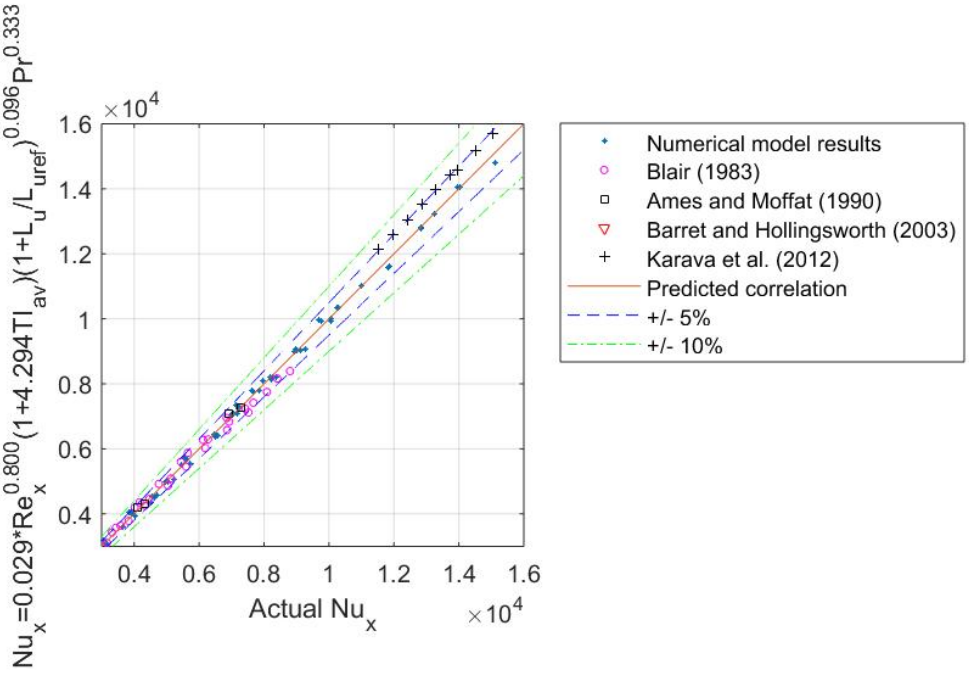

Figure 3.34 - Comparison between the estimated local Nusselt number (Nu_x) values from previous studies and those predicted using the proposed correlation with average TI (TI_{av})

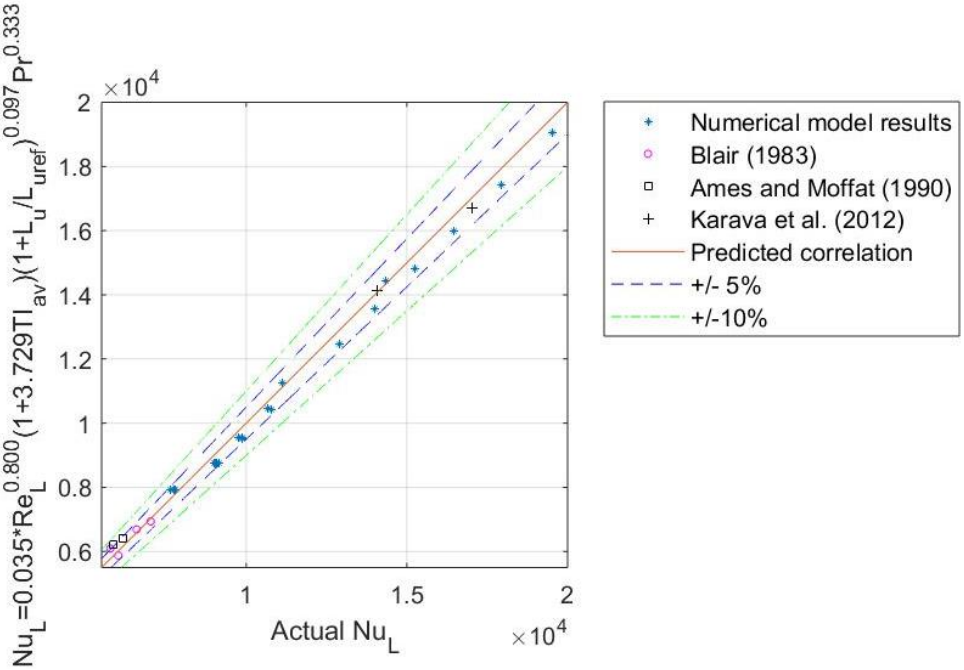

Figure 3.35 - Comparison between the estimated local Nusselt number (Nu_L) values from previous studies and those predicted using the proposed correlation with average TI (TI_{av})

Note that the Nusselt number (local and total) was estimated from the Stanton number multiplied by the Reynolds and Prandtl numbers, except for the data from Karava et al. (2012), which included the Nusselt number.

The proposed expressions for St_x, St, Nu_x and Nu_L do not show a significant effect of L_u on CHTC. The correlation from Blair (1983) showed a larger effect of L_u on CHTC than the proposed expressions in the current study, but Blair's (1983) equation (refer to Eq. (3.3)) did not describe the experimental results from other studies (Baskaran et al., 1989; MacMullin et al., 1989). Furthermore, the results from the current study do not correlate linearly with the *HB* parameter, as shown in Figure 3.36.

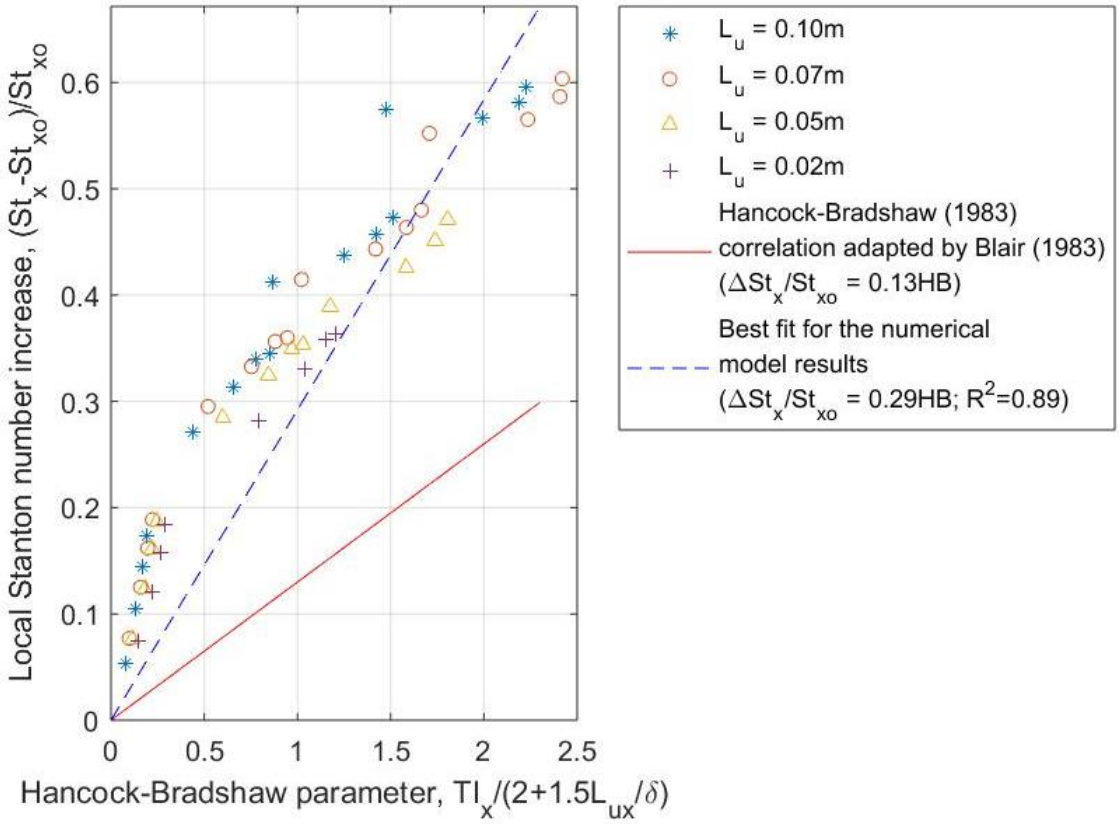

Figure 3.36 – Comparison between the local Stanton number increase and the correlating parameter proposed by Hancock and Bradshaw (1983) adapted by Blair (1983)

Note that the damping factor proposed by Blair (1983) is equal to 1 for the cases examined in the current study, since low Reynolds numbers cases are not considered (Re_θ>2000 for

all cases). Therefore, the correlating parameter from Blair (1983) is reduced to the Hancock and Bradshaw (1983) parameter (*HB*) (refer to Eq. (3.2)). A large scatter between the local Stanton number increase and the results predicted from Hancock and Bradshaw's (1983) expression adapted by Blair (1983) was also observed in previous works (Baskaran et al., 1989; MacMullin et al., 1989).

Additionally, the current numerical model results do not correlate linearly with the *TLR* parameter as proposed by the expression from Ames and Moffat (1990) (refer to Eq. (3.4)), as shown in Figure 3.37.

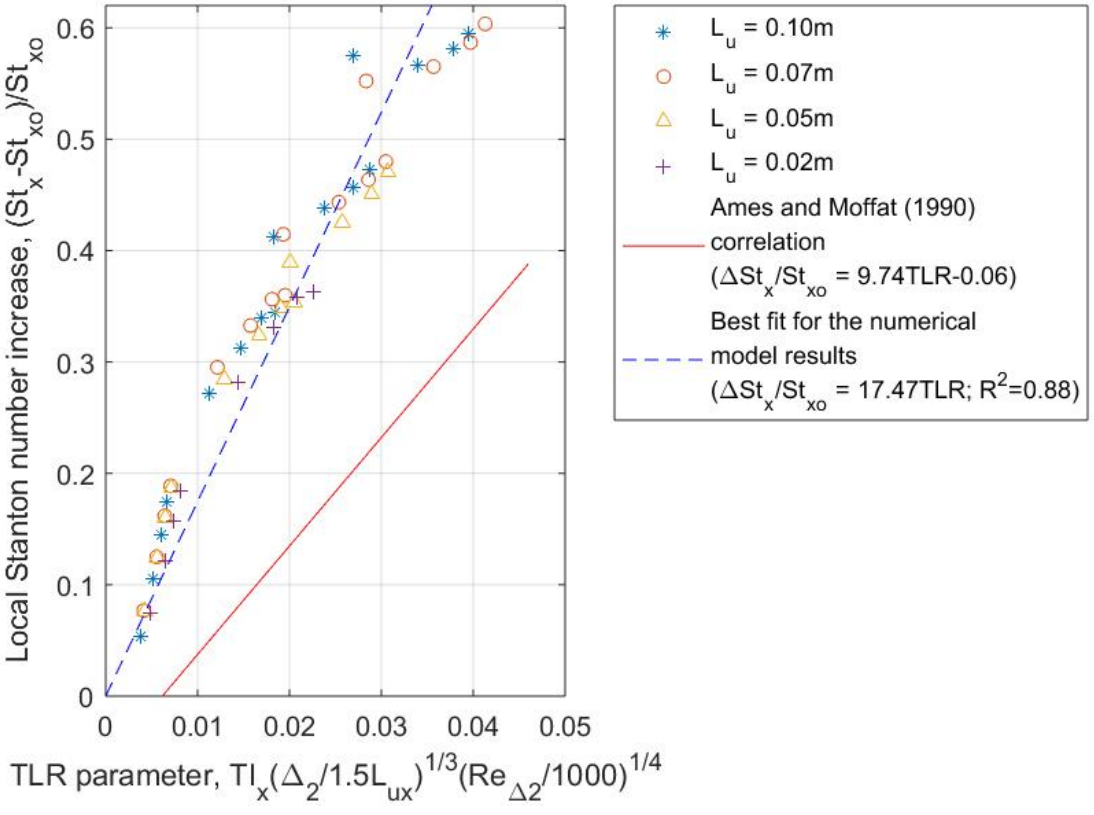

Figure 3.37 - Comparison between the local Stanton number increase and the correlating parameter from Ames and Moffat (1990)

Note that the proposed correlation from Ames and Moffat (1990) predicts a negative increase of local Stanton number for $TI = 0\%$ and the authors examined cases with $TI_x > 2\%$. The current numerical model results are underpredicted by up to 80% by Ames and

Moffat's (1990) expression. Additionally, the results from the current study lie within up to 30% of the best fit with respect to the *TLR* parameter presented in Figure 3.37. Barret and Hollingsworth (2003) also noted a large scatter between their results and the values predicted by Ames and Moffat's (1990) correlation. The differences observed between the local Stanton number increase and the values predicted by previous correlations may be influenced by various factors. For instance, the case with low turbulence using the current numerical model is not yet fully turbulent and the local Stanton number is underpredicted. Furthermore, as mentioned in Chapter 2, in cases from previous studies where TI_x>5%, the free-stream turbulence in the plate region varied by as much as 96%, e.g., TI_x values of 5% in studies from Hancock and Bradhsaw (1983), Blair (1983) and Ames and Moffat (1990) were attained in cases where TI_{dif} was 57%, 60% and 96%, respectively.

The local Stanton number increase with respect to TI_x and the comparison with the linear expression proposed by Simonich and Bradshaw (1978) (refer to Eq. (3.1)) are shown in Figure 3.38. The current numerical model results lie within up to 40% of the best linear fit.

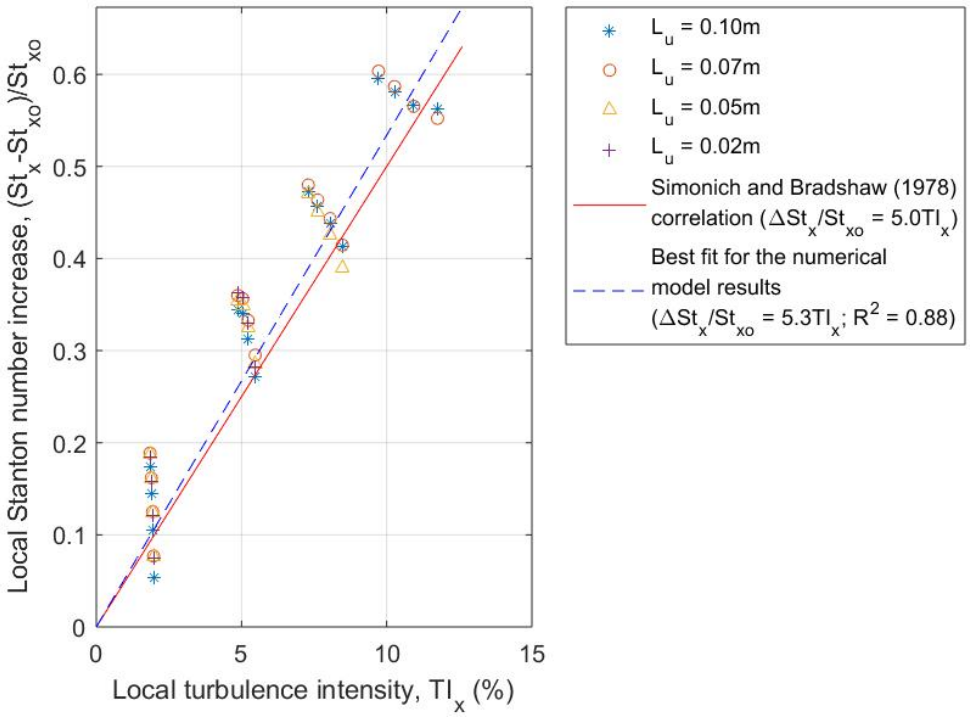

Figure 3.38 - Comparison between the local Stanton number increase and the expression from Simonich and Bradhsaw (1978)

The total Stanton number increase follows a linear relationship with respect to the leading edge TI, as shown in Figure 3.39, although the increase for $TI \approx 12\%$ is overpredicted by 14%. Note that Simonich and Bradshaw's (1978) expression referred to local Stanton number increase and the linear relation was with respect to local turbulence intensity.

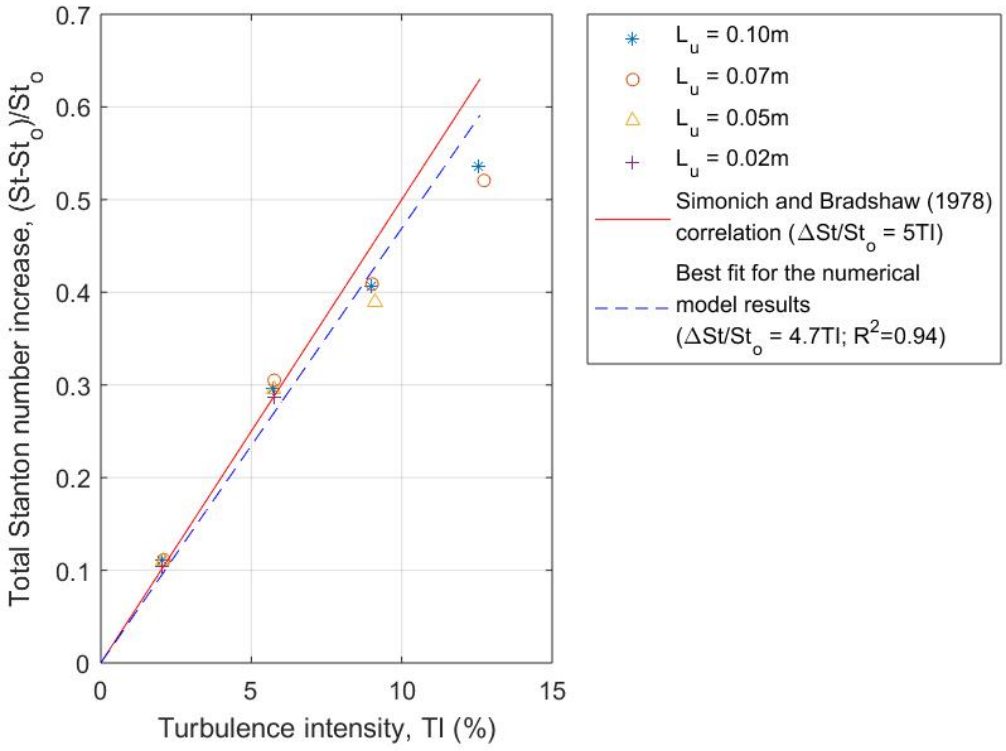

Figure 3.39 - Comparison between the local Stanton number increase and the expression from Simonich and Bradshaw (1978)

Both local and total Stanton number increase are higher than the local skin friction increase presented in Section 2.5 for *TI* of up to 9.0%, which is consistent with the results observed in previous studies (Blair, 1983; Kondjoyan et al., 2002). For *TI* = 9.0%, the increase with respect to a case with no FST of St_x and *St* is up to 48% and 41%, respectively, while the increase of $c_{f,x}$ and C_f is up to 34% and 33%, respectively. However, when *TI* is raised from 9.0% to 12.6%, the increase of St_x and *St* is up to 13% and 12%, respectively, while the increase of $c_{f,x}$ and C_f is up to 17% and 16%, respectively. A lower enhancement of St_x when compared to $c_{f,x}$ increase was observed by previous works for *TI* above 10% and up to 15% (MacMullin et al., 1989; Kondjoyan et al., 2002). Maciejewski and Moffat (1992)

showed a large disparity between their experimental results and the expression from Simonich and Bradshaw (1978) applied to local Stanton number increase (refer to Eq. (3.1)) for *TI* between 20% and 55% and the authors did not present local skin friction coefficients. It would be useful to examine cases with *TI* above 12.6% to analyze the trend of St_x increase with respect to *TI* and to the $c_{f,x}$ increase.

Having examined the effect of different parameters (*TI*, L_u and Re_x or Re_L on local and total CHTC, as well as the correlations for Nu_x, Nu_L, St_x, *St* derived from the results from the current study and validated with data from previous works, the next section summarized the main findings and conclusions from the present investigation.

3.6 Summary and conclusions

3.6.1 Summary

The overall results from the numerical study presented in this chapter can be summarized as follows:

- The SST k-ω model with Low-Re correction was suitable for the prediction of convective heat transfer coefficients for fully turbulent BL regions, although it does not predict accurately the laminar-turbulent transition. This model also provided correct TKE decay when modified as recommended by Sarkar (2018). This is then the most suitable model for this problem once it is focused on turbulent boundary layers and the influence on CHTC of different turbulence conditions in the free-stream.

- The local Nusselt numbers for a free-stream with low turbulence agree well with the theoretical correlation (refer to Eq. (1.14)), with an underprediction of 1.5% and, therefore, the numerical model is a good representation of a heated flat plate case.

- Local and total Nusselt (and Stanton) numbers are influenced by flow conditions, e.g., Re_x or Re_L, *TI* and L_u. These parameters were chosen for the development of

correlations that could predict the value of CHTC for different free-stream conditions.

- Heat transfer enhancement is observed with increasing *TI*, as reported by previous studies as well (Kondjoyan et al., 2002). The effect of L_u on CHTC is less significant when compared to the other parameters.

- The following correlations were derived:

$$Nu_x = 0.029{Re_x}^{0.800}(1 + 4.294TI_{av})\left(1 + {L_u}/{L_{uref}}\right)^{0.096} Pr^{0.333}$$

$$Nu_L = 0.035{Re_L}^{0.800}(1 + 3.729TI_{av})\left(1 + {L_u}/{L_{uref}}\right)^{0.097} Pr^{0.333}$$

$$St_x = 0.029{Re_x}^{-0.200}(1 + 4.326TI_{av})\left(1 + {L_u}/{L_{uref}}\right)^{0.053} Pr^{-0.667}$$

$$St = 0.035{Re_L}^{-0.200}(1 + 3.805TI_{av})\left(1 + {L_u}/{L_{uref}}\right)^{0.048} Pr^{-0.667}$$

  These expressions were examined for Re_x and Re_L of up to 1.0×10^7, integral length scales (L_u) varying from 0.01m to 0.13m and *TI* from 0.1% to 20%. The use of the average value of the leading edge and trailing edge free-stream turbulence intensity (TI_{av}) provided a better collapse of the data than the use of the leading edge value (*TI*) or the local value (TI_x).

- The derived expressions are valid for fully turbulent flows and predict the values of Nu_x, Nu_L, St_x and *St* within ±5% for the conditions mentioned above. The expressions may be applied when the percentage difference of free-stream turbulence intensity between the LE and TE of the plate vary by up to 96%.

3.6.2 Conclusions

A numerical model was implemented for the evaluation of the influence of free-stream turbulence on forced convective heat transfer from flat plate turbulent boundary layers. The simulations were performed using the SST k-ω turbulence model with Low-Re correction,

because it provides a good prediction of CHTC (Blocken et al., 2009) and TKE decay (Sarkar, 2018). The CHTC of the turbulent boundary layer was then validated with empirical correlations for a case with no free-stream turbulence.

Various numerical studies were examined with different FST conditions. It was possible to investigate cases with a plate leading edge *TI* range of 0.1 – 12.6%, L_u from 0.02m to 0.10m, Re_x of up to 1.07×10^7 and Re_L from 5.1×10^6 to 1.0×10^7. These parameters were then included in correlations for Nu_x and Nu_L, as well as St_x and St, that were validated with previous studies. This provided new insights into the effect of different free-stream conditions on convective heat transfer, specially with respect to the influence on CHTC of the TKE decay and turbulence conditions at which the boundary layer starts to develop.

It was demonstrated that the TKE decay in the plate region is an important factor to be considered in the validity of correlations. The current study was focused on regions where free-stream turbulence intensity varied only by 25% at most, but previous studies used to validate the proposed correlations presented percentage differences of TI of up to 96%. This TI difference seems to be more significant for higher initial TI values ($TI > 10\%$). Despite its limitations, the derived correlations are a good tool for convective heat transfer coefficient prediction, since they do not depend on the knowledge of boundary layer characteristics such as displacement, momentum or enthalpy thicknesses.

The next chapter will then present a summary of all analysis performed in the current study and recommendation for future works.

References

Abdollahzadeh, M., Esmaeilpour, M., Vizinho, R., Younesi, A. and Pàscoa, J. (2017) Assessment of RANS turbulence models for numerical study of laminar-turbulent transition in convection heat transfer. International Journal of Heat and Mass Transfer, 115(PB), pp. 1288–1308.

Ames, F.E. and Moffat, R.J. (1990) Heat transfer with high intensity, large scale turbulence: the flat plate turbulent boundary layer and the cylindrical stagnation point, Report No. HMT-44, Department of Mechanical Engineering, Stanford University, CA, USA.

ANSYS, Inc. (2013) ANSYS Fluent Theory Guide. Canonsburg, PA, USA, pp. 1-814.

Baker, N., Kelly, G. and O'Sullivan, P.D. (2019) A grid convergence index study of mesh style effect on the accuracy of the numerical results for an indoor airflow profile. International Journal of Ventilation, 19(4), pp. 300-314.

Barrett, M. J. and Hollingsworth, D. K. (2003) Heat transfer in turbulent boundary layers subjected to free-stream turbulence - Part I: Experimental results. Journal of Turbomachinery, 125(2), pp. 232–241.

Barrett, M. J. and Hollingsworth, D. K. (2003) Heat transfer in turbulent boundary layers subjected to free-stream turbulence - Part II: Analysis and correlation. Journal of Turbomachinery, 125(2), pp. 242–251.

Barth, T. J. and Jespersen, D. C. (1989) The design and application of upwind schemes on unstructured meshes. Proceedings of the 27th Aerospace Sciences Meeting, Reno, NV, USA, AAIA paper 89-0366, pp. 1-12.

Baskaran, V., Abdellatif, O. E. and Bradshaw, P. (1989) Effects of free-stream turbulence on turbulent boundary layers with convective heat transfer. Proceedings of the 7th Symposium on Turbulent Shear Flows, Stanford, CA, USA, pp. 20.1.1-20.1.6.

Blair, M. F. (1983a) Influence of free-stream turbulence on turbulent boundary layer heat transfer and mean profile development, Part I - Experimental data. Journal of Heat Transfer, 105(1), pp. 33–40.

Blair, M. F. (1983b) Influence of free-stream turbulence on turbulent boundary layer heat transfer and mean profile development, Part II - Analysis of results. Journal of Heat Transfer, 105(1), pp. 41–47.

Blocken, B., Defraeye, T., Derome, D. and Carmeliet, J. (2009) High-resolution CFD simulations for forced convective heat transfer coefficients at the facade of a low-rise building. Building and Environment, 44(12), pp. 2396–2412.

Chorin, A. J. (1968) Numerical solution of Navier-Stokes equations. Mathematics of Computation, 22(104), pp. 745–762.

Defraeye, T., Blocken, B. and Carmeliet, J. (2010) CFD analysis of convective heat transfer at the surfaces of a cube immersed in a turbulent boundary layer. International Journal of Heat and Mass Transfer, 53(1-3), pp. 297-308.

Franke, J., Hellsten, A., Schlünzen, H. and Carissimo, B. (2007) Best practice guideline for the CFD simulation of flows in the urban environment, COST action 732. Quality Assurance and Improvement of Microscale Meteorological Models. Hamburg, Germany.

Hancock, P. E. and Bradshaw, P. (1983) The effect of free-stream turbulence on turbulent boundary layers. Journal of Fluids Engineering, 105(3), pp. 284–289.

Incropera, F. P., Dewitt, D. P., Bergman, T. L. and Lavine, A. S. (2007) Fundamentals of Heat and Mass Transfer. New York, NY, USA: John Wiley & Sons, 6th edition, pp. 377-516.

Ivyer, G. R. and Yavuzkurt, S. (1999) Comparison of low Reynolds number k–ε models in simulation of momentum and heat transport under high free stream turbulence. International Journal of Heat and Mass Transfer, 42(4), pp. 723-737.

Junkhan, G. H. and Serovy, G. K. (1967) Effects of free-stream turbulence and pressure gradient on flat-plate boundary-layer velocity profiles and on heat transfer. Journal of Heat Transfer, 89(2), pp. 169–175.

Karava, P., Jubayer, C., and Savory, E. (2011) Numerical modelling of forced convective heat transfer from the inclined windward roof of an isolated low-rise building with application to photovoltaic/thermal systems. Applied Thermal Engineering, 31(11), pp. 1950–1963.

Karava, P., Jubayer, C., Savory, E., and Li, S. (2012). Effect of incident flow conditions on convective heat transfer from the inclined windward roof of a low-rise building with application to photovoltaic-thermal systems. Journal of Wind Engineering and Industrial Aerodynamics, 104-106, pp. 428–438.

Kawai, S. and Larsson, J. (2012) Wall-modeling in large eddy simulation: Length scales, grid resolution, and accuracy. Physics of Fluids, 24(1), 015105.

Kestin, J., Maeder, P. F. and Wang, H. E. (1961) Influence of turbulence on the transfer of heat from plates with and without a pressure gradient. International Journal of Heat and Mass Transfer, 3(2), pp. 133–154.

Kondjoyan, A., Péneau, F. and Boisson, H. (2002) Effect of high free stream turbulence on heat transfer between plates and air flows: A review of existing experimental results. International Journal of Thermal Sciences, 41(1), pp. 1–16.

Launder, B. E. and Spalding, D. B. (1974) The numerical computation of turbulent flows. Computer Methods in Applied Mechanics and Engineering, 3(2), pp. 269-289.

Lioznov, G. L., Lushchik, V. G., Makarova, M. S. and Yakubenko, A. E. (2012) Freestream turbulence effect on flow and heat transfer in the flat-plate boundary layer. Fluid Dynamics, 47(5), pp. 590–592.

Lopez, M. and Keith Walters, D. (2016) A recommended correction to the kT−kL−ω transition-sensitive Eddy-Viscosity model. Journal of Fluids Engineering, 139(2), 024501.

Maciejewski, P. K. and Moffat, R. J. (1992) Heat transfer with very high free-stream turbulence: Part I - Experimental data. Journal of Heat Transfer, 114(4), pp. 827–833.

Maciejewski, P. K. and Moffat, R. J. (1992) Heat transfer with very high freestream turbulence: Part II - Analysis of the results. Journal of Heat Transfer, 114(4), pp. 834–839.

MacMullin, R., Elrod, W., and Rivir, R. (1989) Free-stream turbulence from a circular wall jet on a flat plate heat transfer and boundary layer flow. Journal of Turbomachinery, 111(1), pp. 78–86.

Menter, F. R. (1994) Two-equation eddy-viscosity turbulence models for engineering applications. AIAA Journal, 32(8), pp. 1598–1605.

Mukha, T., Johansson, M. E. and Liefvendahl, M. (2018) Effect of wall-stress model and mesh-cell topology on the predictive accuracy of LES for wall-bounded flows. Proceedings of the 7th European Conference on Computational Fluid Dynamics (ECFD 7), Glasgow, UK.

Neale, A., Derome, D., Blocken, B. and Carmeliet, J. (2006) CFD calculation of convective heat transfer coefficients and validation - Part II: Turbulent flow. Proceedings of the IEA Annex 41 meeting, Kyoto, Japan.

Nicholl, C. I. H. (1970) Some dynamical effects on a turbulent boundary layer. Journal of Fluid Mechanics, 40(2), pp. 361–384.

Palyvos, J. A. (2008) A survey of wind convection coefficient correlations for building envelope energy systems' modeling. Applied Thermal Engineering, 28(8–9), pp. 801–808.

Patankar, S. V, Spalding, D. B. and Road, E. (1972) A calculation procedure for heat, mass and momentum transfer in three-dimensional parabolic flows. International Journal of Heat and Mass Transfer, 15(10), pp. 1787–1806.

Péneau, F., Boisson, H., Kondjoyan, A. and Djilali, N. (2004) Structure of a flat plate boundary layer subjected to free-stream turbulence. International Journal of Computational Fluid Dynamics, 18(2), pp. 175–188.

Pope, S. B. (2000) Turbulent flows. Cambridge, UK: Cambridge University Press, pp. 1-385.

Sarkar, D. (2018) A numerical tool for predicting the spatial decay of freestream turbulence. MESc Thesis, Electronic Thesis and Dissertation Repository, The University of Western Ontario, London, Canada. 5331.

Simonich, J. C. and Bradshaw, P. (1978) Effect of free-stream turbulence on heat transfer through a turbulent boundary layer. Journal of Heat Transfer, 100(4), pp. 671–677.

Versteeg, H. K. and Malalasekera, W. (1995) An introduction to computational fluid dynamics - The finite volume method. Harlow, England: Pearson Education Ltd, 1st edition, pp. 1-205.

Chapter 4

4 Conclusions

This Chapter presents the conclusions and contribution of the present work in section 4.1 and the recommendations for future works in section 4.2.

4.1 Conclusions and contributions

Various numerical simulations using CFD models were examined in the current study to evaluate the effect of free-stream turbulence (FST) on flat plate boundary layers. The main objective of this thesis was to evaluate the influence of difference free-stream conditions (*TI*, L_u and Re_x or Re_L) on turbulent boundary layers (TBL), mainly on skin friction and convective heat transfer coefficients (local and total). Additionally, another aim was to develop generalized dimensionless correlations for local and total skin friction and CHTC taking into account those different free-stream conditions and the free-stream turbulence intensity decay along the plate region. The main conclusions can be summarized as follows:

- The steady RANS simulations showed that the Shear Stress Transport (SST) k-ω turbulence model with low-Re number correction is the most appropriate for predicting skin friction and CHTC of turbulent boundary layers along with the proper turbulent kinetic energy (TKE) decay, although this turbulence model predicts a delayed laminar-turbulent transition.

- The turbulence intensity (*TI*) is the parameter that influences the most both skin friction and CHTC. Total skin friction and CHT coefficients can increase by up to 41% when *TI* is increased from 2.0% to 12.6%. The range of length scale analyzed in this study did not show a great influence on skin friction and CHT coefficients, both parameters varied only by up to 2% for different values of L_u (L_u = 0.02m; 0.05m; 0.07m or 0.1m) while keeping the same *TI*. The enhancement of skin friction and CHT coefficients were similar for different free-stream velocities (40m/s, 60m/s or 80m/s) when *TI* is increased from 2.0% to 12.6%.

- The turbulent boundary layer thickness and momentum thickness are also influenced by different FST conditions. The TBL thickness and momentum thickness increase by 218% and 22%, respectively, when *TI* is increased from 2.0% to 12.6%. Additionally, both quantities vary less than 1% when L_u is varied (L_u = 0.02m; 0.05m; 0.07m or 0.1m) for a constant *TI*, even for *TI* of up to 12.6%.

- Dimensionless correlations that quantify the effect of different FST parameters (*TI*, L_u and Re_x or Re_L) on local and total skin friction and CHT coefficients as well as momentum thickness were developed and validated with data from previous studies. The analysis showed that the values of $c_{f,x}$, Nu_x, St_x, C_f, Nu_L and *St* can be predicted within ±5% using the correlations with TI_{av} for *TI* of up to 19% if the plate is subjected to FST where the free-stream TI vary by up to 96% from the leading to the trailing edge of the plate. In addition, the correlation for momentum thickness can predict θ to within ±10% if the plate is subjected to *TI* of up to 13% and variations of free-stream TI from the plate LE to the TE of up to 60%.

- The current research demonstrated the importance of the streamwise TKE decay in the plate region and the free-stream turbulence conditions at which the boundary layer starts to develop. It is known that TI decays with distance from the inlet or turbulence generator and the value at the plate leading edge can be much lower than the TI specified at the beginning of the domain. Secondly, free-stream TI continues to decay in the plate region and it was verified that the percentage difference of TI between the leading and trailing edge is an important factor to be considered in the validity of correlations. The best fit of the dimensionless correlations was achieved when the average of the leading edge and trailing edge TI values was considered.

Therefore, the study contributed with simple tools for predicting the local and total skin friction and CHT coefficients as well as momentum thickness if the FST conditions are known and the plate is subjected to relatively uniform turbulence conditions. The predictions of those different parameters can be performed without the knowledge of the boundary layer development since they do not depend on parameters like boundary layer thickness.

4.2 Recommendations

Some recommendations can be provided for future studies as follows:

- In the current research, the focus was on fully turbulent boundary layers and high Reynolds numbers (from $1.3x10^6$ to $1.0x10^7$). It would be useful to investigate the effect of FST on boundary layers with lower Reynolds numbers, in the laminar region or even involving laminar-turbulent transition in order to evaluate correlations for skin friction and CHT coefficients for these regimes, as well as the importance of free-stream TKE decay in these cases.

- Additionally, the present work was also focused on developing correlations for cases where the plate was positioned in regions of almost uniform turbulence conditions, although the correlations were validated with previous experimental data where the percentage difference of turbulence intensity from the leading to the trailing edge of the plate was up to 96%. Therefore, cases with *TI* of up to 12.6% and with free-stream TI percentage difference in the plate region of up to 25% were examined, but it is useful to analyze cases with higher values of leading edge *TI* and free-stream TKE decay rates in the plate region.

- Direct Numerical Simulations (DNS) could also be performed to analyze detailed turbulence statistics and the structure of a turbulent boundary layer subjected to almost uniform FST conditions. Such investigations would help to deepen the knowledge of the dynamic mechanisms behind the interaction between the boundary layer and the free-stream.

Curriculum Vitae

Name:	Ivian Carolina Alfaia de Magalhaes
Post-secondary Education and Degrees:	Military Institute of Engineering Rio de Janeiro, Brazil 2008-2012 B.E. The University of Western Ontario London, Ontario, Canada 2018-Present M.E.Sc.
Honours and Awards:	Western Engineering Scholarship 2018-2020
Related Work Experience	Teaching Assistant The University of Western Ontario 2019-2020 Research Assistant The University of Western Ontario 2018-2020

Public presentation:

Magalhaes, I. and Savory, E. (2019). Effect of free-stream turbulence on turbulent boundary layers from flat plates. Joint Canadian Society for Mechanical Engineering and CFD Society of Canada International Congress (CSME-CFDSC Congress 2019). June 2-5 2019. London, ON, Canada.